Liquid crystalline elastomers as stimuli-responsive microactuators

Dissertation zur Erlangung des Grades

Doktor der Naturwissenschaften

im Promotionsfach Chemie

am Fachbereich Chemie, Pharmazie und Geowissenschaften

der Johannes Gutenberg-Universität Mainz

vorgelegt von

Eva-Kristina Fleischmann

geboren in Wiesbaden

Mainz 2013

Die vorliegende Arbeit wurde unter der Betreuung von [redacted] in der Zeit von Januar 2010 bis März 2013 am Institut für organische Chemie der Johannes Gutenberg-Universität in Mainz durchgeführt.

Dekan: [redacted]

1. Berichterstatter: [redacted]

2. Berichterstatter: [redacted]

Tag der mündlichen Prüfung: 29.04.2013

Contents

Abstract

Liquid crystalline elastomers (LCEs) are known to perform a reversible change of shape upon the phase transition from the semi-ordered liquid crystalline state to the chaotic isotropic state. This unique behavior of these "artificial muscles" arises from the self-organizing properties of liquid crystals (mesogens) in combination with the entropy-elasticity of the slightly crosslinked elastomer network. In this work, micrometer-sized LCE actuators are fabricated in a microfluidic setup. The microtubular shear flow provides for a uniform orientation of the mesogens during the crosslinking, a perquisite for obtaining actuating LCE samples. The scope of this work was to design different actuator geometries and to broaden the applicability of the microfluidic device for different types of liquid crystalline mesogens, ranging from side-chain to main-chain systems, as well as monomer and polymer precursors. For example, the thiol-ene "click" mechanism was used for the polymerization and crosslinking of main-chain LCE actuators. The main focus was, however, placed on acrylate monomers and polymers with LC side chains. A LC polymer precursor, comprising mesogenic and crosslinkable side-chains was synthesized. Used in combination with an LC monomer, the polymeric crosslinker promoted a stable LC phase, which allowed the mixture to be isothermally handled in the microfluidic reactor. If processed without the additional LC components, the polymer precursor yielded actuating fibers. A suitable co-flowing continuous phase facilitates the formation of a liquid jet and lowers the tendency for drop formation. By modification of the microfluidic device, it was further possible to prepare core-shell particles, comprised of an LCE shell and filled with an isotropic liquid. In analogy to the heart, a hollow muscle, the elastomer shell expels the inner liquid core upon its contraction. The feasibility of the core-shell particles as micropumps was demonstrated. In general, the synthesized LCE microactuators may be utilized as active components in micromechanical and lab-on-chip systems.

Zusammenfassung

Bei flüssigkristallinen Elastomeren wird der Übergang von der flüssigkristallinen in die isotrope Phase begleitet von einer makroskopischen, reversiblen Formänderung. Dieses einzigartige Verhalten der auch als „künstliche Muskeln“ bekannten Materialien entsteht durch die Kombination aus der Entropie-Elastizität des Elastomers und der Selbstorganisation der flüssigkristallinen Einheiten. In der vorliegenden Arbeit wurden Aktoren im Mikromaßstab aus flüssigkristallinen Elastomeren in einem mikrofluidischen Reaktor hergestellt. Die Scherströmung innerhalb der Mikroschläuche bewirkt eine einheitliche Orientierung der flüssigkristallinen Moleküle (Mesogene). Diese makroskopische Vorzugsrichtung der Mesogene ist ausschlaggebend für den Erhalt formändernder Elastomere und wird anschließend durch Photo-Vernetzung eingefroren. Die mikrofluidische Apparatur wurde dahingehend weiterentwickelt, dass sie für die Verarbeitung von monomeren und polymeren Ausgangsverbindungen sowie der Herstellung von Haupt- und Seitenketten-Elastomeren Anwendung findet. Zum Beispiel konnte die Thiol-En-Reaktion zur Erzeugung von Hauptkettenelastomeren genutzt werden. Der Schwerpunkt dieser Arbeit lag jedoch auf der Verarbeitung von Seitenketten-Systemen. Ein vernetzbares flüssigkristallines Seitenketten-Polymer wurde synthetisiert, welches in Kombination mit einem flüssigkristallinen Monomer zu einer Stabilisierung der flüssigkristallinen Phase beitrug. Dadurch konnte die Mischung unter isothermen Bedingungen im Mikroreaktor verarbeitet werden. Durch eine geeignete Wahl der kontinuierlichen Phase im Reaktor wurde die Tendenz zur Tropfenbildung unterdrückt, so dass aus dem Mikrojet des reinen Polymers kontrahierende Fasern herstellt werden konnten. Durch eine Modifikation des Mikroreaktors wurden Kern-Schale-Partikel erhalten, deren Elastomer-Schale mit einem flüssigen Kern gefüllt war. Nach Erzeugung eines Ventils in der Elastomer-Schale konnten diese Partikel den flüssigen Kern wie ein künstliches Herz reversibel einsaugen und ausstoßen. Die erzeugten Mikroaktoren aus flüssigkristallinen Elastomeren eignen sich als Bauteile zur Erzeugung mechanischer Bewegung in mikroelektromechanischen und sogenannten „lab-on-chip“ Systemen.

Abbreviations

η	viscosity
2θ	scattering angle
ρ	density
σ	interfacial tension
Å	Angstrom (unit)
AAO	anodic aluminium oxide
a.u.	arbitrary unit
AIBN	azoisobutyronitril
ATRP	atom transfer radical polymerization
br	broad (NMR spectroscopy)
°C	degree Celsius
Ca	capillary number
$CDCl_3$	deuterated chloroform
CNT	carbon nanotubes
Cr	crystalline phase
cSt	centistokes
d	diameter
DSC	differential scanning calorimetry
eq.	equivalent
FLCE	ferroelectric liquid crystalline elastomers
GBDA	glyoxal bis(diallyl acetal)
GPC	gel permeation chromatography
h	hours
HDDA	hexanedioldiacrylate
I	intensity
I(χ)	azimuthal intensity distribution (WAXS)

ID	inner diameter
Iso	isotropic phase
l	length
LC	liquid crystal
LCE	liquid crystalline elastomer
LCP	liquid crystalline polymer
LMW	low molecular weight
LSCE	liquid single crystal elastomer
μm	micrometer
MEMS	microelectromechanical system
MHz	megahertz
M_n	number average molar mass
mol%	mol percent
mPa	megapascal
n	director
N	nematic mesophase
nl	nanoliter
nm	nanometer
NMR	nuclear magnetic resonance
OD	outer diameter
PDI	polydispersity index
PDMS	polydimethylsiloxane
PETMP	pentaerythritol tetrakis(3-mercaptopropionate)
POM	polarized optical microscopy
ppm	parts per million
PTFE	polytetrafluoroethylene
R	radius of gyration
RAFT	reversible addition fragmentation chain-transfer
Re	Reynolds number

RT	room temperature
s	second
S	order parameter
SANS	small angle neutron scattering
Sm	smectic mesophase
SMA	shape memory alloys
T	temperature
$T_{Cr,N}$	crystalline-nematic phase transition temperature
$T_{N,Iso}$	nematic-isotropic phase transition temperature
UV	ultraviolet
WAXS	wide-angle X-ray scattering
We	Weber number
wt.%	weight percent

1 Introduction

1.1 Fundamentals of liquid crystals

Since their first observation by botanist Friedrich Reinitzer in the late 19th century, liquid crystals have attracted the attention of chemists and physicists alike.[1–3] With their ability to self-organize into mesoscopic structures, so-called mesophases, they belong to the topical field of soft matter.[4] These mesophases represent an intermediate state between the "classical" crystalline and isotropic liquid phases and their macroscopic behavior is defined by the molecular properties of their constituents, the mesogens. The premise for the formation of a liquid crystalline phase, which combines crystalline order with the mobility of fluids, is the shape anisotropy of these mesogens. We distinguish between calamitic (rod-like), discotic[5] (disc-like), sandic[6] (board-like) and banana-shaped mesogens[7] (Figure 1.1A). While a rigid core - often consisting of aromatic rings - induces structural order, flexible parts (e.g. alkyl chains) provide for the necessary mobility within the liquid crystalline phase. Typical molecular building blocks and typical phase sequences are presented in Figure 1.1. It should be noted that not only organic compounds, but also anisotropic inorganic nanoparticles form liquid crystalline phases.[8] The necessary mobility for the stiff particles can be provided by a polymer coating resulting in organic-inorganic hybrid materials with potential applications in the field of opto-electronics.

One further distinguishes between thermotropic and lyotropic liquid crystals. This terminology defines the conditions under which a mesophase forms. While thermotropic liquid crystals form mesophases within a certain temperature range without the help of any additive, the formation of lyotropic mesophases requires the aid of a solvent either to provide the necessary fluidity and mobility or to form the anisotropic superstructures. Owing to the amphiphilicity of lyotropic liquid crystals they are capable of forming phases different from those of thermotropic LCs.[9]

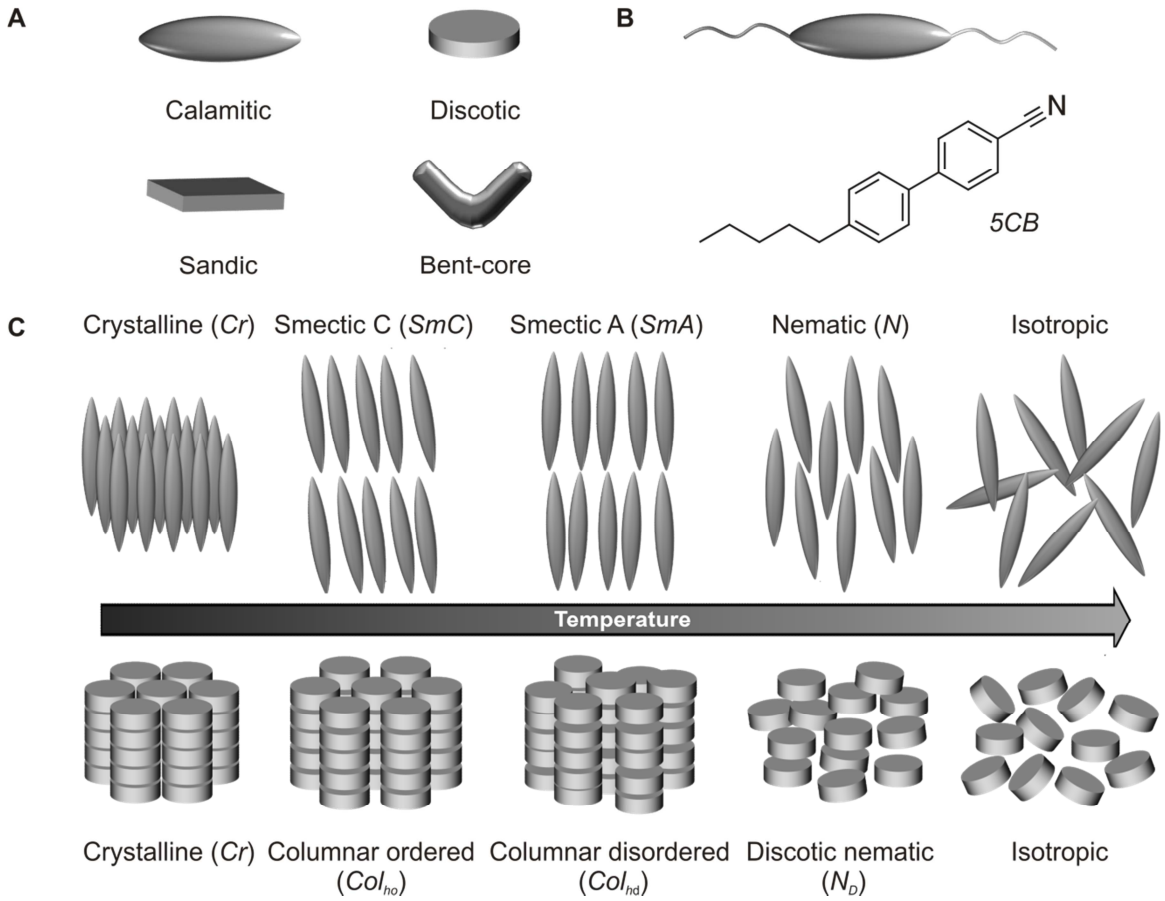

Figure 1.1: ***A*** *Shape anisotropic cores of liquid crystalline molecules.* ***B*** *Top: Schematic representation of a common class of liquid crystalline molecule consisting of a rigid rod-shaped core with flexible side-chains. Bottom: Chemical structure of 4-cyano-4'-pentylbiphenyl (5CB), one of the best known representatives of this class of liquid crystals.* ***C*** *Mesomorphism in thermotropic calamitics and discotics. Calamitic LCs preferably self-assemble in layers, while discotics stack into columnar structures. With increasing temperature the molecular order decreases until all order is lost in the isotropic melt.*

Concerning thermotropic mesogens, the liquid crystalline order is lost in the isotropic melt due to the thermal motion of the molecules. On cooling the mesogens spontaneously self-organize and adopt a long-range orientational order until a well-ordered crystalline phase is formed at lower temperatures. The mesogens may exhibit several LC phases at different temperatures, distinguishable by the degree of order of the mesogens (Figure 1.1C) The *nematic* phase is the least ordered mesophase and usually found at the highest temperatures. It is marked by a long-range orientational order of the mesogens, meaning that their only alignment is along one common axis. Additional positional order of calamitic mesogens first appears at lower temperatures within layered *smectic* phases. Here, the long axis of the mesogens aligns along the layer normal

in a *smectic A* phase, while they are slightly tilted to the layer normal in a *smectic C* phase. Additional smectic phases with an improved packing within the layers can exist at even lower temperatures. In comparison, discotic mesogens exhibit positional order by stacking into different types of columnar structures (see Figure 1.1C).[10] The degree of orientational order of the mesogens is described by a dimensionless unit vector, termed the director n. It is quantified as order parameter $S = \langle \frac{3\cos^2\theta - 1}{2} \rangle$. S is obtained by averaging the angle Θ between the molecular symmetry axis of the mesogens (long axis for calamitic mesogens, short axis for discotics) and the local director over all molecules in a small, but macroscopic volume. For an isotropic liquid, the random distribution of angles Θ yields an order parameter of S = 0. On the other hand, S = 1 for a perfectly aligned crystalline state. Typical values from 0.3 to 0.8 are found for calamitic nematic and smectic phases.

The possibility for a smooth transition between a crystalline and an isotropic phase in a step-wise fashion[2,3,11] establishes liquid crystals as a tool-kit for a variety of applications, which require well-ordered packing over large distances. Sharp grain boundaries, often found in polycrystalline samples, are not present in a liquid crystalline phase due to the ability of the director to continuously change its orientation within the sample. Bending the director of a liquid crystalline phase requires only little energy and defects are more easily tolerated. Thus, liquid crystalline phases allow many packing motives, which would not be compatible with a regular crystalline lattice.[12] In combination with the ⊚-conjugated core of the mesogens, this recommends liquid crystals as active materials for the design of organic semiconducting devices.

Due to the cooperative behavior of the mesogens (parallel orientation of their long axis), liquid crystalline phases are very sensitive to external fields.[13] They interact as a collective and the effect of switching the director in an applied electric field is many orders of magnitude larger compared to an isotropic liquid, where only the dipole moments of individual molecules interact with the electric field (Kerr effect). In combination with their optical properties (birefringence), liquid crystals can be used to switch the transmittance of polarized light (see especially chapter 2 and 6 in Ref. [3]). This effect is exploited for the fabrication of opto-electric displays and forms an integral part in today's display technology.[14]

Compared to crystalline materials, liquid crystals are not only more tolerant towards structural defects but can also host other non-mesogenic units. This allows the synthesis of liquid crystalline polymers (LCP) and elastomers (LCE), which combine shape-anisotropic mesogens with flexible isotropic polymer chains. In combination with the entropy elasticity of an elastomer network, this gives rise to a stimuli-responsive behavior in slightly crosslinked LCE networks.

1.2 Liquid crystalline order in networks: Liquid crystalline elastomers

In 1969 Pierre de Gennes was pondering the question, which benefit might come from the combination of liquid crystals and polymers, imagining an analogue to glass with enhanced elastic properties.[15] It took a couple of years and some experiments before he proposed a unique feature of such a material: the use of liquid crystalline elastomers (LCEs) as artificial muscles[16]. These would create macroscopic motion and force due to processes on a microscopic scale and surpass the response times of by then known pH-responsive polymer networks.[17]

The underlying principle is that the mesogens act as an anisotropic solvent for the isotropic polymer chains. In an isotropic solvent an undisturbed ideal polymer chain will adopt a spherical random coil conformation with an angle-independent, i.e. isotropic radius of gyration.[18] If the polymer is, on the other hand, mixed with liquid crystals, they will impose their anisotropy on the polymer chain, forcing it into a conformation, where the radius of gyration changes with respect to the director orientation.[19] This distortion may lead to a prolate or oblate chain conformation (Figure 1.2A). In a prolate conformation the long axis of the polymer coil coincides with the director ($l_{\parallel} > l_{\perp}$), while it is perpendicular in an oblate conformation ($l_{\parallel} < l_{\perp}$). The mesogens only influence the polymer conformation, as long as they are in their liquid crystalline phase. Upon the phase transition into the isotropic phase, where the order parameter of the mesogens equals zero, the polymer chain is free to revert back to its unperturbed spherical conformation.[20]

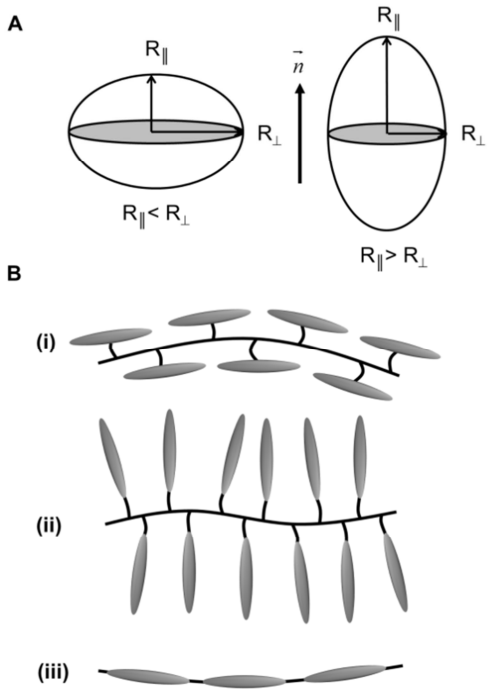

Figure 1.2: A *Prolate and oblate conformation of the polymer chain due to the liquid crystals acting as anisotropic solvent The radius of gyration R changes with respect to the director orientation n.* ***B*** *Scheme of (i) side-on, (ii) end-on side-chain and (iii) main-chain polymers.*

The reversible phase transition between the mesophase and the isotropic phase of the liquid crystal makes this polymer chain deformation a fully reversible process, which can be exploited for applications such as stimuli-responsive actuators.[21,22] In combination with the elastic reset force of a crosslinked elastomer network this unique feature can be converted into macroscopic "artificial muscles". Several characteristics of an elastomer network have to be considered, namely the type of LC polymers, crosslinking strategies of the LC polymers, sample preparation and the mode of actuation-triggering. This will be discussed in the following paragraphs, chiefly engaging in LC elastomers made from calamitic (rod-like) mesogens.

1.2.1 Liquid crystalline polymers

As implied above, the influence of the mesogens on the polymer conformation is strongly dependent on the manner of interaction and is considerably stronger if the mesogens are linked to the polymer via chemical bonds.[23,24] The length of the spacer

dictates the influence of the mesogens on the polymer chain conformation.[25] Longer spacers weaken the coupling between mesogen and polymer, while short spacers increase the shape anisotropy of the polymer chain. Additionally, the position of the spacer with regard to the mesogens influences the chain anisotropy[26] and consequently the shape-changing properties. Using flexible alkyl chains as spacers, the mesogens can be attached in a side-on or end-on manner to the polymer chain (Figure 1.2B) and are generally classified as side-chain polymers. Side-on systems promote an orientation of the polymer chain along the director while two conflicting forces affect the conformation of an end-on polymer. For these comb-like polymers the anisotropy of the liquid crystal moieties acts along the director field while it simultaneously forces the polymer backbone in a plane perpendicular to it. In such cases, oblate conformations of the polymer chain have been found by small angle neutron scattering (SANS) measurements.[27] Consequently, end-on polymers show a weaker chain extension along the director compared to side-on polymers and therefore the corresponding elastomer exhibit weaker contractions upon the isotropic phase transition.[28]

Considering that laterally attached mesogens with short spacers induce a stronger anisotropy of the polymer chain, polymers with mesogens directly integrated into their backbone should show the strongest anisotropy. This has indeed been found for so-called main-chain polymers.[24,29] Main-chain LCEs strongly contract on losing their liquid crystalline order in the isotropic phase with reported relative length changes of up to 500%.[30]

1.2.2 Liquid crystalline elastomers

Highly crosslinked networks of LC polymer chains (thermosets) permanently lock-in the liquid crystalline order of the mesogens. Here the mesogens lack the flexibility to rearrange upon the transition to the disordered isotropic phase and the LC order is preserved even above T_{NI}.[31] These dense and highly ordered systems are useless for any actuator application, but exhibit unique optical properties which makes them useful as retarder foils for LC displays, wherein they further improve the color contrast or the viewing angle.[32] It is essential to

increase the flexibility of the mesogens to enable efficient actuation. Slightly crosslinked LCE samples with elastic moduli of several megapascals (MPa)[33] have to be prepared, with crosslinking being accomplished in two ways: either via the formation of covalent bonds or via physical interactions between the polymer chains.

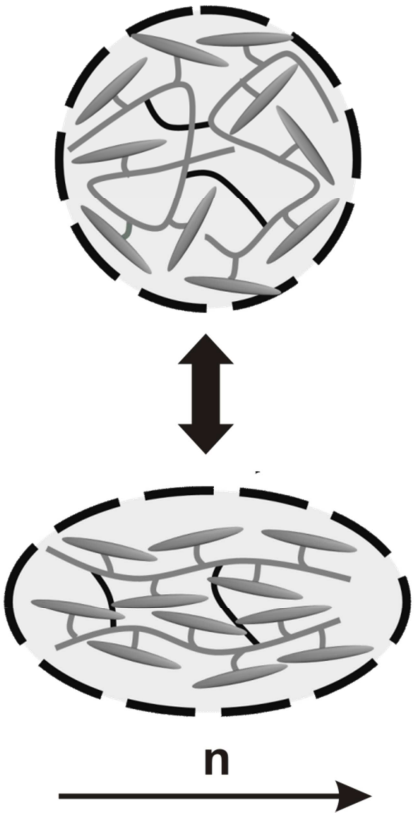

Figure 1.3: *The microscopic loss of order upon the nematic-isotropic phase transition results in a reversible macroscopic shape-change of the slightly crosslinked elastomer.*

Supramolecular architectures of LC actuators and sensors can be realized with hydrogen-bonding mesogens.[34] A very nice example was recently provided by the Ikeda group. A free-standing film of a LC elastomer could be realized by mixing a hydrogen-bond donating LC polymer with a low-molecular weight (LMW) crosslinker, which acts as hydrogen-bond acceptor.[35] Additionally incorporated azobenzenes provided for isothermal switching with UV light. In another example of physical crosslinking, ionic interactions were used to create a weakly crosslinked polymer network by performing an oxidation-reduction reaction on an redox-active LC copolymer.[36]

It is, however, more common to covalently crosslink the LC polymer chains. A large variety of synthetic methods have been developed over the past 20 years, the main difference being that polymerization and crosslinking are either conducted simultaneously or consecutively.

Simultaneous polymerization and crosslinking allows a conventional bi-functional LMW crosslinker to be used. The crosslinker can either be mesogenic[37] or isotropic[38,39], since the liquid crystalline phase is relatively stable towards non-mesogenic impurities. Side-chain elastomers could be realized with polymerizable groups such as acrylates[38] and methacrylates[40] attached to the mesogen. A main-chain elastomer was accomplished by thiol-ene coupling.[41,42]

If crosslinking is done in a consecutive step, the polymer precursor is synthesized from mesogenic units and contains either crosslinkable groups or functional groups, which may further react with a crosslinkable LMW component. Polymer precursors with incorporated crosslinkable groups are advantageous for in-bulk preparations of LC elastomers since no additional component is needed for crosslinking. The photo-reactive group benzophenone, for example, can already be linked to mesogenic units before polymerization and afterwards crosslink upon irradiation with UV light.[43] Crosslinkable groups (i.e. acrylate, vinyl) can further be introduced in a consecutive polymer functionalization and easily be crosslinked in a second step by thermal or photo-chemical initiation.[44,45]. Hydroxyl group-containing LC polymer chains can be converted with bis-isocyanates to yield an elastomer network.[46,47] Elastomers from azide-terminated telechelic side-group LC polymers could be realized by click-chemistry, crosslinking the LC polymer with a LMW triacetylene species.[48]

All the systems described so far are assembled from “classical” carbon-based organic molecules, whether in a step-wise fashion or in a one-pot reaction. A different synthetic route is based on polymers with a polysiloxane backbone. An LC polymer is obtained via platinum-catalyzed addition of the vinyl-substituted mesogenic units to the Si-H bond of a siloxane precursor polymer.[49] The ease to choose from a variety of mesogens makes this a modular system, where LC polymers with different compositions and architectures are accessible. Crosslinking can easily be accomplished either during functionalization of the polymer backbone using divinyls[22] or in a consecutive step.[50] It

was this method developed and improved by Finkelmann and co-workers which put actuating LCEs into practice and made it relatively easy to produce macroscopic actuating LCE films.

1.2.3 Preparation of LCEs and their use as active devices

While the contraction or expansion of a film is a macroscopic process, it results from the microscopic reorientation of the mesogens and the attached polymer chains. Although liquid crystals self-assemble in the nematic or smectic phase, the director does not align uniformly throughout the sample. Without an external directing force, poly-domains form, with the director being randomly distributed in the elastomer network. When, however, such an external force is applied during crosslinking, the mesogens and hence the polymer chains align along one preferred direction and form a mono-domain sample. In the latter case the loss of orientation in the isotropic phase results in a directed macroscopic shape change of the sample.

Fine-tuning the above-described hydrosilylation synthesis, liquid single crystal elastomers (LSCE), highly ordered LC networks, could be obtained via a two-step crosslinking procedure.[22] Polysiloxane and a judicious mixture of mesogens and crosslinker carrying vinyl as well as methacroyl groups are converted to a weakly crosslinked film. This film is firm enough to be mechanically stretched. This stretching force provides for a uniform orientation of the polymer chains. In a second step, unreacted methacryloyl groups are further converted to yield a fully functional monodomain actuator. A film made with this technique could be incorporated into a microfluidic chip to act as a flow-regulating valve, expanding normal to the director upon the phase transition and thus sealing the microfluidic channel (Figure 1.4A).[51]

The procedure of mechanical stretching can however not be adopted to processing reactive LMW mesogens or for the fabrication of micro- and nanoscopic samples. The fabrication of small samples with different geometries is of particular interest for future applications of LCEs as active components in microscopic devices.[52] For LMW mesogens, surface forces are commonly exploited to induce a uniform orientation of the director. The interaction between surface and mesogens may promote a planar (parallel

to the surface) or homeotropic (normal to the surface) alignment. A uniform director orientation may simply be induced by micro-scratches through rubbing of the substrate with cloth. Planar aligned free-standing films could be produced with polyimide-coated substrates.[38,39,53] Surface interactions could also be utilized for the fabrication of nano-actuators made from a main-chain polyester via a mini-emulsion process.[54] The mesogens' rigid cores of benzene rings generate diamagnetism, and can then be aligned with a magnetic field.[45,55] This feature allowed Keller and co-workers to create actuating LCE micro-pillars via a soft-molding process, in a magnetic field (Figure 1.4B).[42,56]

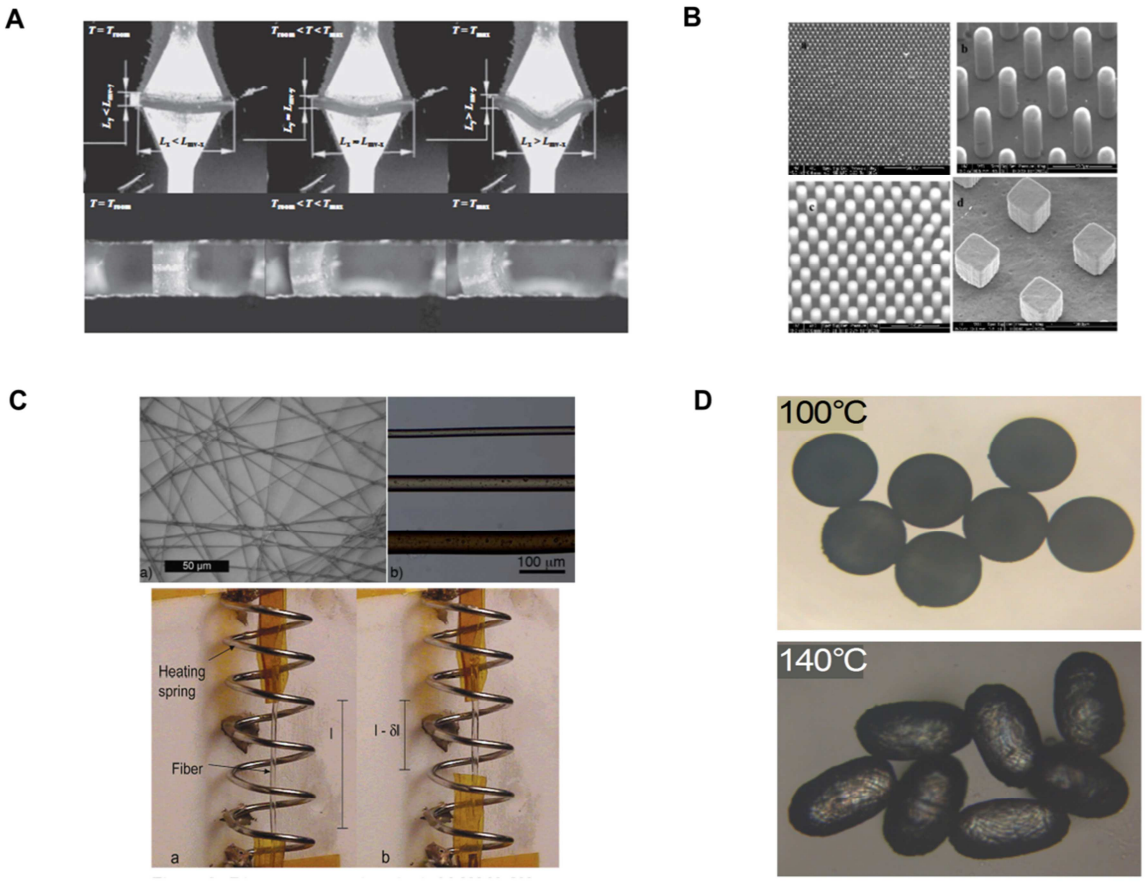

Figure 1.4: ***A*** *An LCE film acts as a flow-regulating valve inside a microfluidic chip. The fluid is allowed to flow while the LCE film is in its glassy-nematic state. When heating the LCE film above the nematic-isotropic transition temperature with a copper circuit, the film expands thus closing the valve and blocking the fluid flow.*[51] ***B*** *The melt of a reactive mesogen is molded inside a PDMS stamp and subsequently polymerized to give LCE micro-pillars.*[56] ***C*** *Top: Continuous fibers produced in a microfluidic device.*[57] *Bottom: A fiber drawn from a reactive monomer melt lifts a 200 mg weight.*[47] ***D*** *A microfluidic device can be used to prepare bulk particles, which elongate when heated to the isotropic phase.*[58]

The director orientation can also be influenced by spatial confinement. Yang et al. used a softlithographic method to prepare a LCE film with a columnar topography. Since the diameter of the columns is below the characteristic uniform domain size, the elastomer film adopts a monodomain conformation inside the columns.[59] Similarly, nanoporous anodized aluminium oxide (AAO) templates provide one-dimensional confinement and were used as molds to synthesize wired-shaped nano-LCEs.[60] Such patterned nano- and microstructures created by soft- and photolithography[61] can be used as stimuli-responsive surfaces for micromechanical devices. The flow field within microfluidic tubing can also induce a preferred orientation in co-flowing LC droplets. These droplets are prepared within a T-junction and then subjected to shear flow in a thin capillary. The imposed orientation of the mesogens is then permanently fixed by UV-initiated crosslinking. LCE particles with varying shapes are accessible at different flow rates.[58,62]

In addition to the so far described sample geometries of films, patterned surfaces and particles it is also possible to create highly ordered LCE fibers (Figure 1.4C). By simply drawing fibers from a reacting melt of a side-chain polymer and crosslinker with tweezers, the LC polymer spontaneously orients along the fiber axis (d ~ 300 μm).[47] The above-mentioned microfluidic procedure is also applicable for the preparation of fibers from a crosslinkable main-chain polymer. The fibers created via this wet-spinning process were of a regular thickness between 20 - 50 μm, depending on the chosen flow rates, and could lift a weight three orders of magnitude higher than their own mass.[57] Even thinner fibres of only several microns in diameter are accessible by electro-spinning.[63] The resulting fleece-like sample, a chaotic cluster of fibers on top of each other, makes it, however, difficult to extract single fibers for a characterization of their individual properties.

1.2.4 Stimuli-responsive LCEs: Not only temperature dependent

As already mentioned, the phase transition of thermotropic liquid crystals is triggered by a change in temperature. This most-common actuation was exploited for most of the LCEs presented so far. Admittedly, when integrating LCEs in an active device, it is not advantageous to heat the whole device. Efforts have been made to induce the desired

shape change by local heating of the LC-elastomer. Incorporating carbon black allows electro-thermal heating of the now conductive LCE with an electric current.[64] Similarly, the introduction of iron oxide particles into the elastomer allows inductive heating with an applied alternating magnetic field.[65] It is also possible to dope LCEs with carbon nanotubes (CNT). They efficiently absorb visible and infra-red light, convert it into local heat and thus induce the phase transition.[66] The difficulty of producing a stable and homogeneous suspension of CNTs in a liquid crystalline matrix can be overcome by using a liquid crystalline polymer surfactant containing pyrene anchoring groups.[67] It could be shown that CNT concentrations below 1% are sufficient for a pronounced actuation of an LCE sample and that the presence of the dispersed CNT does not significantly affect the LC order or the internal structure of the elastomer.[68] A nematic elastomer in the shape of a cantilever made from such LC-CNT composites exhibited a bending motion on local heating with a laser diode at 660 nm.[69] By creating an elaborate moulding process Camargo and co-workers processed an LCE-CNT film to give a poly-domain sample with mono-domain regions (Figure 1.5). These mono-domain regions are shaped like blisters and contract on irradiation with red light. They could successfully integrate these films into a display, where the localized actuation of the mono-domain blisters turns into an active Braille alphabet.[70,71]

Liquid crystals can also be responsive to electric fields, if they possess a ferroelectric phase.[72] The electromechanical response is in this case due to the strong macroscopic polarization of the chiral smectic C* phase of the elastomer.[73] For recent summarizations of these ferroelectric liquid crystalline elastomers (FLCEs) we refer to Ref. [74] and [75].

Alternatively an isothermal phase transition can be induced by incorporating azo-groups into the mesogenic structures, often in the form of azobenzene moieties (Figure 1.6).[76] The *trans*-configuration of the azo-group stabilizes the liquid crystalline alignment of rod-like mesogens. Upon irradiation with UV light at the π-π^* absorption band (~360 nm) the photoisomerization for the *trans* to the *cis* configuration of the azobenzene destabilizes the mesophase. The now bent (or kinklike) molecules act as isotropic impurities, which lower the nematic order parameter.[77] This reduces the nematic-isotropic transition temperature to such a degree, that an isothermal isotropization

becomes possible. A macroscopic shape change of LCEs can be induced at ambient temperatures upon irradiation. The *trans-cis* isomerization can either be reversed by irradiation with visible light (< 470 nm, equivalent to the n-π* absorption) or by thermal activation.[78]

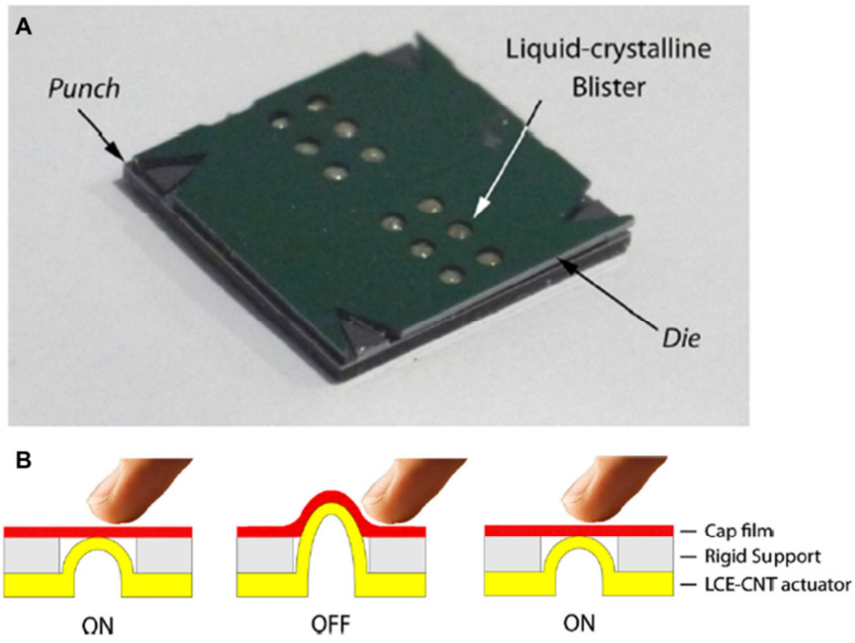

Figure 1.5: A *A stretched LCE-CNT film gets stamped between punch mould and die mould. Also visible are the mono-domain blisters.*[71] ***B*** *Dynamic Braille dots: The LCE-CNT blister contracts upon irradiation with a light source and becomes unreadable. It recovers its original shape once the light source is turned off.*[71]

A problem of the azo-chromophores is their high absorption coefficient. The concentration of azo-chromophores (above 5%) necessary to achieve a strong shift of the phase transition temperature, entails a high optical density at the surface. Illumination of the sample creates a concentration gradient of the *cis* isomers away from the surface, and this gradient results in a bending motion of the LCE films towards the light source.[39,79] The bending motion creates little stress and cannot be used to lift "heavy" cargo, but it is very impressive to view. For monodomain samples the bending axis is normal to the director. The Ikeda group could further develop the potential of such film, by making a polydomain LCE film and controlling its bending direction with linear polarized light. Even though the macroscopic orientation of the director was randomly distributed over

the whole film, a bending motion parallel to the direction of light polarization was observed.[80]

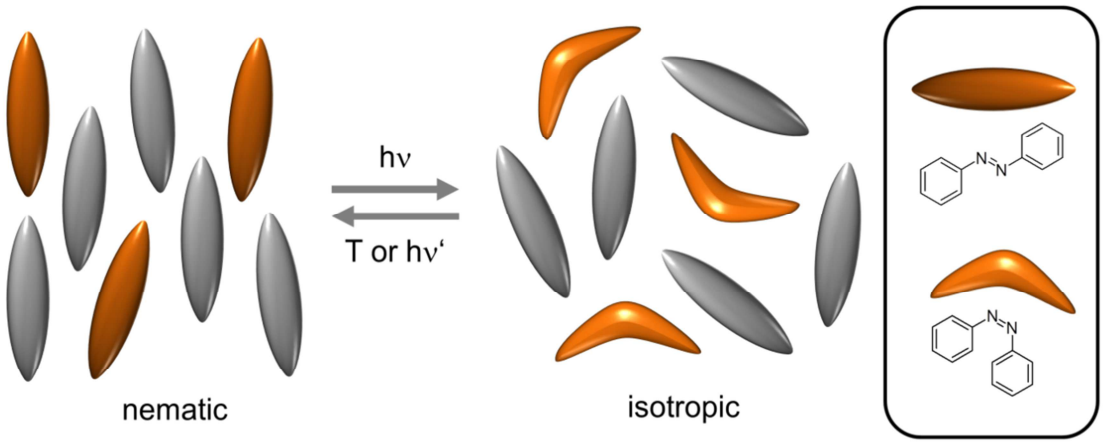

Figure 1.6: *Azobenzene moieties switch from* trans *to the* cis *state upon irradiation with UV light. The kink-like molecules lower the order parameter of the nematic phase, causing an isothermal shift to the isotropic state. The reversibility of this process allows to specifically initiate the shape change of such an LC elastomer by UV irradiation.*

Irradiation of a cantilever-shaped sample causes an in-plane bending motion of the cantilever towards the light source, as long as the director is oriented along the long axis of the cantilever. Once the director orientation is rotated with respect to the sample's long axis, an out-of-plane twisting motion can be observed due to a shear gradient and contraction along the diagonal of the cantilever.[82] The bending of the photoactive LCEs can further be improved by creating splayed or twisted instead of just planar alignments of the mesogens.[83] The deposition with an ink-jet printer allows different LC materials to be arranged in cantilever-like shape, one sensitive to UV light, the other to visible light. Thus a cilia-like motion can be induced by addressing the different components with their respective wavelength of light (Figure 1.7A).[37]

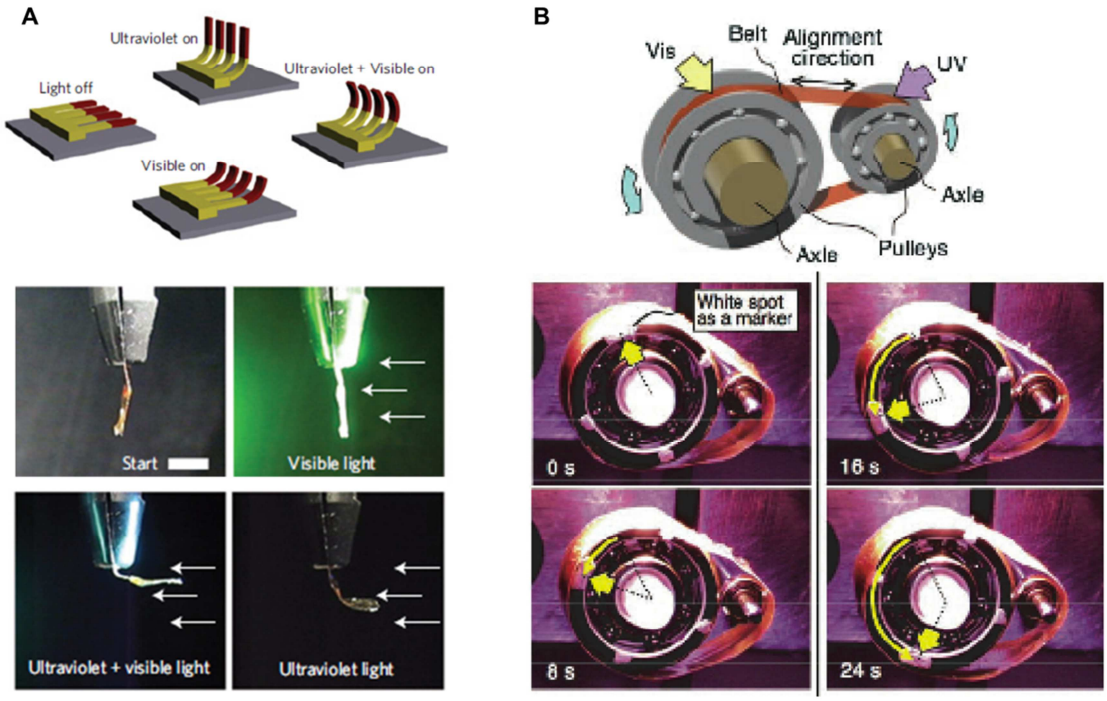

Figure 1.7: A *Schematic representation and real-life image of a cantilever-like two–component LCE producing asymmetric cilia-like motion depending on the light source.*[37] ***B*** *Top: Scheme of a motor laminated with a photo-responsive LCE film. Bottom: By simultaneous irradiation with UV and visible light, the plastic motor is propelled by a bending-unbending movement of the LCE film.*[81]

Instead of covalently linking the azo moiety to the elastomer, Palffy-Muhoray and co-workers created LC elastomer network with an azo-dye simply dispersed in it. When floating on water the material was found to swim into the darker regions, i.e. away from the irradiating light source as a result of exchanging momentum between water and the sample upon its bending motion.[84] A light-driven plastic motor was realized by wrapping a photoactive LCE film around two pulleys and illuminating the film with UV light and visible light from two opposing sides. The resulting contraction on one and expansion on the other side results in a rolling motion of the film, which propels the two pulleys (Figure 1.7B).[81] The same concept and material could also be used for mimicking the three-dimensional movements of an inchworm walk and a robotic arm motion.[85]

In recent years we could observe a significant progress in the fabrication of LCEs, creating elaborate shapes that are capable of performing complex motions. Particularly,

the possibility to manufacture micro- and nano-sized LCEs allows their integration into lab-on-chip systems. These advances will fuel the transition from fundamental research to competitive commercial applications.

1.3 References

[1] T. J. Sluckin, D. A. Dunmur, H. Stegemeyer, *Crystals that flow. Classic papers from the history of liquid crystals*, Taylor & Francis, London, **2004**.

[2] D. Demus, J. Goodby, G. W. Gray, H.-W. Spiess, V. Vill, *Handbook of Liquid Crystals Set*, Wiley-VCH Verlag GmbH, Weinheim, **1998**.

[3] H. Stegemeyer (Ed.) *Topics in physical chemistry*, *Vol. 3*, Steinkopff, Darmstadt, **1994**.

[4] P.-G. de Gennes, *Angew. Chem. Int. Ed.* **1992**, *31*, 842.

[5] S. Chandrasekhar, B. K. Sadashiva, K. A. Suresh, *Pramana* **1977**, *9*, 471.

[6] O. Herrmann-Schönherr, J. H. Wendorff, H. Ringsdorf, P. Tschirner, *Makromol. Chem. Rapid Commun.* **1986**, *7*, 791.

[7] T. Niori, T. Sekine, J. Watanabe, T. Furukawa, H. Takezoe, *J. Mater. Chem.* **1996**, *6*, 1231.

[8] J.-C. P. Gabriel, P. Davidson, *Adv. Mater.* **2000**, *12*, 9. b) P. Davidson, J.-C. P. Gabriel, *Curr. Opin. Colloid Interface Sci.* **2005**, *9*, 377.

[9] A. G. Petrov, *The lyotropic state of matter*. *Molecular physics and living matter physics*, Gordon & Breach, Amsterdam, **1999**.

[10] C. Destrade, P. Foucher, H. Gasparoux, N. H. Tinh, A. M. Levelut, J. Malthete, *Mol. Cryst. Liq. Cryst.* **1984**, *106*, 121.

[11] G. W. Gray, J. W. G. Goodby, *Smectic liquid crystals*. *Textures and structures*, L. Hill, Glasgow; Distributed by Heyden, Philadelphia, **1984**.

[12] C. Tschierske, *J. Mater. Chem.* **2001**, *11*, 2647. b) C. Tschierske, *Chem. Soc. Rev.* **2007**, *36*, 1930.

[13] G. H. Heilmeier, *Appl. Phys. Lett.* **1968**, *13*, 91.

[14] E. Lueder, *Liquid crystal displays*. *Addressing schemes and electro-optical effects*, Wiley, Chichester, West Sussex, U.K, Hoboken, NJ, **2010**.

[15] P.-G. de Gennes, *Phys. Lett. A* **1969**, *28*, 725.

[16] a) P.-G. de Gennes, *C. R. Acad. Sci. II B* **1997**, *324*, 343. b) P.-G. de Gennes, *C. R. Acad. Sci. Ser. B* **1975**, *281*, 101.

[17] A. Katchalsky, *Experientia* **1949**, *5*, 319.

[18] P. Flory, *Statistical mechanics of chain molecules*, Hanser Gardner, **1989**.

[19] H. Mattoussi, R. Ober, M. Veyssie, H. Finkelmann, *Europhys. Lett.* **1986**, *2*, 233.

[20] a) P.-G. de Gennes in *Materials science and technology series* (Eds.: A. Ciferri, W. R. Krigbaum, R. B. Meyer), Academic Press, New York, **1982**. b) A. Ciferri (Ed.) *Liquid crystallinity in polymers*. *Principles and fundamental properties*, VCH, New York, **1991**.

[21] a) R. Zentel, *Angew. Chem.* **1989**, *101*, 1437. b) C. Ohm, M. Brehmer, R. Zentel, *Adv. Mater.* **2010**, *22*, 3366. c) W. H. de Jeu, M. Brehmer (Eds.) *Advances in polymer science "Liquid Crystal Elastomers: Materials and Application"*, Springer, Berlin, **2012**.

[22] J. Küpfer, H. Finkelmann, *Makromol. Chem. Rapid Commun.* **1991**, *12*, 717.

[23] a) A. M. Donald, A. H. Windle, S. Hanna, *Liquid crystalline polymers*, Cambridge Univ. Press, Cambridge, **2006**. b) C. Boeffel, H. W. Spiess, B. Hisgen, H. Ringsdorf, H. Ohm, R. G. Kirste, *Makromol. Chem. Rapid Commun.* **1986**, *7*, 777. c) H. Finkelmann, *Angew. Chem. Int. Ed.* **1987**, *26*, 816.

[24] R. Zentel in *Topics in physical chemistry*, *Vol. 3* (Ed.: H. Stegemeyer), Steinkopff, Darmstadt, **1994**.

[25] a) W. Kaufhold, H. Finkelmann, H. R. Brand, *Makromol. Chem.* **1991**, *192*, 2555. b) H. Finkelmann, H. Ringsdorf, J. H. Wendorff, *Makromol. Chem.* **1978**, *179*, 273. c) N. Leroux, P. Keller, M. F. Achard, L. Noirez, F. Hardouin, *J. Phys. II France* **1993**, *3*, 1289.

[26] M. Warner, K. P. Gelling, T. A. Vilgis, *J. Chem. Phys.* **1988**, *88*, 4008.

[27] a) R. G. Kirste, H. G. Ohm, *Makromol. Chem. Rapid Commun.* **1985**, *6*, 179. b) P. Keller, B. Carvalho, J. Cotton, M. Lambert, F. Moussa, G. Pépy, *J. Phyique Lett.* **1985**, *46*, 1065.

[28] F. Moussa, J. Cotton, F. Hardouin, P. Keller, M. Lambert, G. Pépy, M. Mauzac, H. Richard, *J. Phys. France* **1987**, *48*, 1079.

[29] F. Hardouin, G. Sigaud, M. F. Achard, A. Brulet, J. P. Cotton, D. Y. Yoon, V. Percec, M. Kawasumi, *Macromolecules* **1995**, *28*, 5427.

[30] S. V. Ahir, A. R. Tajbakhsh, E. M. Terentjev, *Adv. Funct. Mater.* **2006**, *16*, 556.

[31] a) L. Strzelecki, L. Liebert, *Bull. Soc. Chim.* **1973**, 597. b) S. N. Bhadani, D. G. Gray, *Mol. Cryst. Liq. Cryst.* **1984**, *102*, 255.

[32] D. J. Broer, G. P. Crawford, S. Žumer, *Cross-linked liquid crystalline systems. From rigid polymer networks to elastomers*, CRC Press, Boca Raton, **2011**.

[33] a) P. Martinoty, P. Stein, H. Finkelmann, H. Pleiner, H. R. Brand, *Eur. Phys. J. E* **2004**, *14*, 311. b) T. Pakula, R. Zentel, *Makromol. Chem.* **1991**, *192*, 2401. c) R. Zentel, J. Wu, *Makromol. Chem.* **1986**, *187*, 1727.

[34] D. J. Broer, C. M. W. Bastiaansen, M. G. Debije, A. P. H. J. Schenning, *Angew. Chem. Int. Ed.* **2012**, *51*, 7102.

[35] J.-I. Mamiya, A. Yoshitake, M. Kondo, Y. Yu, T. Ikeda, *J. Mater. Chem.* **2008**, *18*, 63.

[36] A. Wiesemann, R. Zentel, T. Pakula, *Polymer* **1992**, *33*, 5315.

[37] C. L. van Oosten, C. W. M. Bastiaansen, D. J. Broer, *Nat. Mater.* **2009**, *8*, 677.

[38] D. L. Thomsen, P. Keller, J. Naciri, R. Pink, H. Jeon, D. Shenoy, B. R. Ratna, *Macromolecules* **2001**, *34*, 5868.

[39] T. Ikeda, M. Nakano, Y. Yu, O. Tsutsumi, A. Kanazawa, *Adv. Mater.* **2003**, *15*, 201.

[40] M.-H. Li, P. Auroy, P. Keller, *Liq. Cryst.* **2000**, *27*, 1497.

[41] H. T. A. Wilderbeek, M. G. M. van der Meer, M. A. G. Jansen, L. Nelissen, H. R. Fischer, J. J. G. S. van Es, C. W. M. Bastiaansen, J. Lub, D. J. Broer, *Liq. Cryst.* **2003**, *30*, 93.

[42] A. Buguin, M.-H. Li, P. Silberzan, B. Ladoux, P. Keller, *J. Am. Chem. Soc.* **2006**, *128*, 1088.

[43] a) P. Beyer, E. M. Terentjev, R. Zentel, *Macromol. Rapid Commun.* **2007**, *28*, 1485. b) A. Komp, J. Rühe, H. Finkelmann, *Macromol. Rapid Commun.* **2005**, *26*, 813.
[44] a) P. Beyer, L. Braun, R. Zentel, *Macromol. Chem. Phys.* **2007**, *208*, 2439.b) M. Brehmer, R. Zentel, *Mol. Cryst. Liq. Crys. A* **1994**, *243*, 353.
[45] M.-H. Li, P. Keller, J. Yang, P.-A. Albouy, *Adv. Mater.* **2004**, *16*, 1922.
[46] R. Zentel, M. Benalia, *Makromol. Chem.* **1987**, *188*, 665.
[47] J. Naciri, A. Srinivasan, H. Jeon, N. Nikolov, P. Keller, B. R. Ratna, *Macromolecules* **2003**, *36*, 8499.
[48] Y. Xia, R. Verduzco, R. H. Grubbs, J. A. Kornfield, *J. Am. Chem. Soc.* **2008**, *130*, 1735.
[49] H. Finkelmann, G. Rehage, *Makromol. Chem. Rapid Commun.* **1980**, *1*, 31.
[50] R. Zentel, G. F. Schmidt, J. Meyer, M. Benalia, *Liq. Cryst.* **1987**, *2*, 651.
[51] A. Sánchez-Ferrer, T. Fischl, M. Stubenrauch, A. Albrecht, H. Wurmus, M. Hoffmann, H. Finkelmann, *Adv. Mater.* **2011**, *23*, 4526.
[52] H. Yang, G. Ye, X. Wang, P. Keller, *Soft Matter* **2011**, *7*, 815.
[53] K. Urayama, S. Honda, T. Takigawa, *Macromolecules* **2005**, *38*, 3574.
[54] S. Haseloh, C. Ohm, F. Smallwood, R. Zentel, *Macromol. Rapid Commun.* **2011**, *32*, 88.
[55] a) M.-H. Li, P. Keller, P.-A. Albouy, *Macromolecules* **2003**, *36*, 2284. b) H. Hirschmann, P. M. S. Roberts, F. J. Davis, W. Guo, C. D. Hasson, G. R. Mitchell, *Polymer* **2001**, *42*, 7063.
[56] H. Yang, A. Buguin, J.-M. Taulemesse, K. Kaneko, S. Méry, A. Bergeret, P. Keller, *J. Am. Chem. Soc* **2009**, *131*, 15000.
[57] C. Ohm, M. Morys, F. R. Forst, L. Braun, A. Eremin, C. Serra, R. Stannarius, R. Zentel, *Soft Matter* **2011**, *7*, 3730.
[58] C. Ohm, C. Serra, R. Zentel, *Adv. Mater.* **2009**, *21*, 4859.
[59] Z. Yang, G. A. Herd, S. M. Clarke, A. R. Tajbakhsh, E. M. Terentjev, W. T. S. Huck, *J. Am. Chem. Soc.* **2006**, *128*, 1074.
[60] C. Ohm, N. Haberkorn, P. Theato, R. Zentel, *Small* **2011**, *7*, 194.
[61] A. L. Elias, K. D. Harris, C. W. M. Bastiaansen, D. J. Broer, M. J. Brett, *J. Mater. Chem.* **2006**, *16*, 2903.
[62] a) C. Ohm, E.-K. Fleischmann, I. Kraus, C. Serra, R. Zentel, *Adv. Funct. Mater.* **2010**, *20*, 4314. b) C. Ohm, N. Kapernaum, D. Nonnenmacher, F. Giesselmann, C. Serra, R. Zentel, *J. Am. Chem. Soc.* **2011**, *133*, 5305.
[63] S. Krause, R. Dersch, J. H. Wendorff, H. Finkelmann, *Macromol. Rapid Commun.* **2007**, *28*, 2062.
[64] M. Chambers, H. Finkelmann, M. Remškar, A. Sánchez-Ferrer, B. Zalar, S. Žumer, *J. Mater. Chem.* **2009**, *19*, 1524.
[65] A. Kaiser, M. Winkler, S. Krause, H. Finkelmann, A. M. Schmidt, *J. Mater. Chem.* **2009**, *19*, 538.
[66] L. Yang, K. Setyowati, A. Li, S. Gong, J. Chen, *Adv. Mater.* **2008**, *20*, 2271.

[67] a) Y. Ji, Y. Y. Huang, R. Rungsawang, E. M. Terentjev, *Adv. Mater.* **2010**, *22*, 3436. b) Y. Ji, Y. Y. Huang, E. M. Terentjev, *Langmuir* **2011**, *27*, 13254.

[68] J. E. Marshall, Y. Ji, N. Torras, K. Zinoviev, E. M. Terentjev, *Soft Matter* **2012**, *8*, 1570.

[69] N. Torras, K. E. Zinoviev, J. E. Marshall, E. M. Terentjev, J. Esteve, *Appl. Phys. Lett.* **2011**, *99*, 254102.

[70] C. J. Camargo, H. Campanella, J. E. Marshall, N. Torras, K. Zinoviev, E. M. Terentjev, J. Esteve, *Macromol. Rapid Commun.* **2011**, *32*, 1953.

[71] C. J. Camargo, H. Campanella, J. E. Marshall, N. Torras, K. Zinoviev, E. M. Terentjev, J. Esteve, J. Micromech. Microeng. **2012**, *22*, 075009.

[72] W. Lehmann, H. Skupin, C. Tolksdorf, E. Gebhard, R. Zentel, P. Kruger, M. Losche, F. Kremer, *Nature* **2001**, *410*, 447.

[73] a) E. Gebhard, R. Zentel, *Macromol. Chem. Phys.* **2000**, *201*, 902. b) E. Gebhard, R. Zentel, *Macromol. Chem. Phys.* **2000**, *201*, 911.

[74] S. T. Lagerwall, *Ferroelectric and Antiferroelectric Liquid Crystals*, Wiley-VCH Verlag GmbH, Weinheim, **1999**.

[75] M. Brehmer, R. Zentel, *Ferroelectric Liquid Crystalline Elastomers. Encyclopedia Of Polymer Science and Technology*, Wiley-VCH Verlag GmbH, Weinheim **2011**.

[76] a) S. Tazuke, S. Kurihara, T. Ikeda, *Chem. Lett.* **1987**, 911. b) Y. Yu, T. Ikeda, *Angew. Chem. Int. Edit.* **2006**, *45*, 5416.

[77] T. Ikeda, O. Tsutsumi, *Science* **1995**, *268*, 1873.

[78] a) H. Finkelmann, E. Nishikawa, G. Pereira, M. Warner, *Phys. Rev. Lett.* **2001**, *87*. b) P. Hogan, A. Tajbakhsh, E. Terentjev, *Phys. Rev. E* **2002**, *65*. c) J. Cviklinski, A. Tajbakhsh, E. Terentjev, *Eur. Phys. J. E* **2002**, *9*, 427. d) M. Warner, E. Terentjev, *Macromol. Symp.* **2003**, *200*, 81. e) M.-H. Li, P. Keller, B. Li, X. Wang, M. Brunet, *Adv. Mater.* **2003**, *15*, 569. f) T. Öge, R. Zentel, *Macromol. Chem. Phys.* **1996**, *197*, 1805.

[79] Y. Yu, M. Nakano, A. Shishido, T. Shiono, T. Ikeda, *Chem. Mater.* **2004**, *16*, 1637.

[80] Y. Yu, M. Nakano, T. Ikeda, *Nature* **2003**, *425*, 145.

[81] M. Yamada, M. Kondo, J.-I. Mamiya, Y. Yu, M. Kinoshita, C. J. Barrett, T. Ikeda, *Angew. Chem. Int. Ed.* **2008**, *47*, 4986.

[82] K. M. Lee, M. L. Smith, H. Koerner, N. Tabiryan, R. A. Vaia, T. J. Bunning, T. J. White, *Adv. Funct. Mater.* **2011**, *21*, 2913.

[83] C. L. van Oosten, K. D. Harris, C. W. M. Bastiaansen, D. J. Broer, *Eur. Phys. J. E* **2007**, *23*, 329.

[84] M. Camacho-Lopez, H. Finkelmann, P. Palffy-Muhoray, M. Shelley, *Nat. Mater.* **2004**, *3*, 307.

[85] M. Yamada, M. Kondo, R. Miyasato, Y. Naka, J.-I. Mamiya, M. Kinoshita, A. Shishido, Y. Yu, C. J. Barrett, T. Ikeda, *J. Mater. Chem.* **2008**, *19*, 60.

2 Results and Discussion

This thesis focuses on the micro-structuring of liquid crystalline elastomers (LCEs) and their development as possible active components in micromechanical devices. Micrometer sized LCE samples are prepared in a microfluidic system. The shear-flow present in the microtubings induces a preferred orientation of the mesogens inside the monomer droplets, which is then locked up by photo-initiated crosslinking. This processing step is mandatory for obtaining reversibly shape-changing LCE actuators and could be established in previous works. The objectives here were to expand the synthesis of LCEs in a microfluidic setup for different types of actuator architectures (bulk particles, core-shell particles and fibers) and to customize it for different types of elastomer chemistry (mesogens of the side-chain and main-chain type, acrylate monomers, and thiol-ene click chemistry). By judiciously controlling the microfluidic parameters such as flow rates, temperature, crosslinking density, and the degree of confinement, microactuators with optimized properties were produced. These microactuators and their corresponding monomer/polymer precursors were tested with regard to, inter alia, their actuating behavior, director field configuration and rheological properties.

2.1 Micropumps from liquid crystalline core-shell elastomers

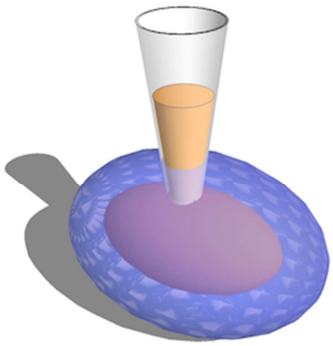

Figure 2.1: *Repeated heating and cooling of a LC elastomer shell causes its liquid core to be reversibly expelled.*

Many recent developments in the field of liquid crystalline elastomers focus on the fabrication of microactuators. This is a direct result from the advances made in microelectromechanical and lab-on-chip technologies. However, the preparation of miniature-sized active components by conventional lithographic techniques is costly and time-consuming and elaborate three-dimensional structures are only accessible by multi-layered 2D components.

As a more cost-efficient solution, liquid crystalline elastomers may be used as active components to induce mechanical motion. However, their miniaturization is still associated with major challenges and the predominant shapes of LCE microactuators are that of micro-rods and micro-spheres. In this work we were able to modify the microfluidic device such that core-shell systems could be obtained in a double-emulsion process. The continuous nature of the microfluidic process enables the production of a large number of samples within a short period of time. The shell consists of an elastomer comprised of a nematic side-chain mesogen and is filled with a liquid core of isotropic glycerol. Detailed analysis of the core-shell particles by X-ray studies revealed a bipolar alignment of the director in the elastomer shell, which results from the flow-profile within the particles prior to crosslinking. Due to the uniform orientation of the mesogens, the particles exhibit a directed change of shape when heated above the nematic-isotropic phase transition of the elastomer. Once an outlet is created in the elastomer shell, the shape change of the LC shell leads to a volume compression of the

glycerol core, which allows the fluid to be pumped out of the particle. Once the particle is cooled below the phase transition temperature, the elastomer shell reverts back to its original shape and the liquid is sucked back into the particle. The pumping motion of the elastomer is fully reversible and recommends the core-shell systems as one-piece micropumps which may be integrated into micro-meter sized fluid systems.

Chapter 3.1:

E.-K. Fleischmann‡, H.-L. Liang‡, J. Lagerwall, R. Zentel, *Proc. of SPIE* **2012**, *8279*, 82790M-1.

Chapter 3.2:

E.-K. Fleischmann‡, H.-L. Liang‡, N. Kapernaum, F. Giesselmann, J. Lagerwall, R. Zentel *Nat. Commun.* **2012**, *3*, 1178.

‡ These authors contributed equally.

2.2 Synthesis of a liquid crystalline polymer crosslinker and its application in customized microactuators

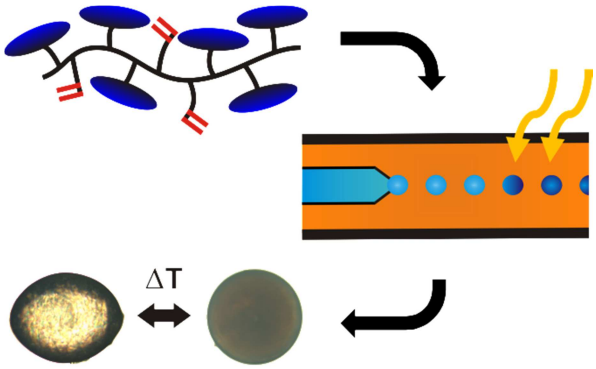

Figure 2.2: *Synthesis of a liquid-crystalline polymer crosslinker designed for the preparation of liquid crystalline elastomers and its application in a microfluidic device. The resulting microactuators show a thermally triggered reversible shape change.*

LC monomers are commonly crosslinked with isotropic low molecular weight (LMW) crosslinkers such as hexanedioldiacrylate to form an LC elastomer network. Just as other impurities, the isotropic crosslinkers destabilize the liquid crystalline phase of the LC monomer. This often results in the formation of a monotropic mesophase, i.e. the

liquid crystalline phase only appears when the isotropic melt is cooled down. For the purpose of obtaining actuating samples with a preferred orientation of the director, the LCE has to be crosslinked within the temperature range of the ordered mesophase. When preparing LCEs from a monotropic monomer mixture in the microfluidic device, a sophisticated temperature-controlled environment becomes necessary. Droplet formation has to be conducted in the isotropic phase and crosslinking below the melting point of the monomer/crosslinker mixture. This inconvenience can be overcome by using a liquid crystalline crosslinker, which promotes the formation of a stable enantiotropic mesophase.

A polymeric liquid crystalline crosslinker **CrP** was designed, comprised of a mesogenic side-chain monomer **M1** and the isotropic monomer 4-hydroxybutylacrylate (**M2**), and copolymerized in a controlled radical polymerization using a chain-transfer agent (RAFT polymerization). **M2** was further converted in a post-polymerization reaction with acryloyl chloride, yielding crosslinkable acrylic groups. Several polymer crosslinkers **CrP** were synthesized and the crosslinking characteristics were adjusted by varying the ratio of mesogenic and non-mesogenic units **M1** and **M2**. The polymeric crosslinking agents exhibited a nematic mesophase, as long as the amount of incorporated 4-hydroxybutylacrylate did not exceed 50 mol%. Used in the preparation of soft LCE actuators, the crosslinking agents **CrP** ensured an entantiotropic LC phase of the LC monomer, which allowed macroscopically oriented LCE particles to be isothermally prepared and processed in the microfluidic device. By adjusting the crosslinking density with a suitable crosslinker polymer **CrP**, particles with different mechanical properties could be obtained. While mechanically robust particles require a high degree of crosslinks, the shape change can be increased by using a polymer producing a low crosslinking density.

The admixture of the polymer crosslinker increased the viscosity of the monomer mixture and as a consequence thereof reduced the Reynolds number *Re*. Compared to low molecular weight crosslinkers this further promotes laminar flow conditions in the microfluidic device. Measurements of the interfacial tension also revealed that the isotropic crosslinker hexanedioldiacrylate diffuses into the continuous phase silicone oil

during the fabrication process, an unwanted process that is not observed for the polymer crosslinkers.

Chapter 3.3:

E.-K. Fleischmann, C. Ohm, C. Serra, R. Zentel *Macromol. Chem. Phys.* **2012**, *213*, 1871.

2.3 Liquid crystalline side-chain elastomer fibers with large amplitude contractions

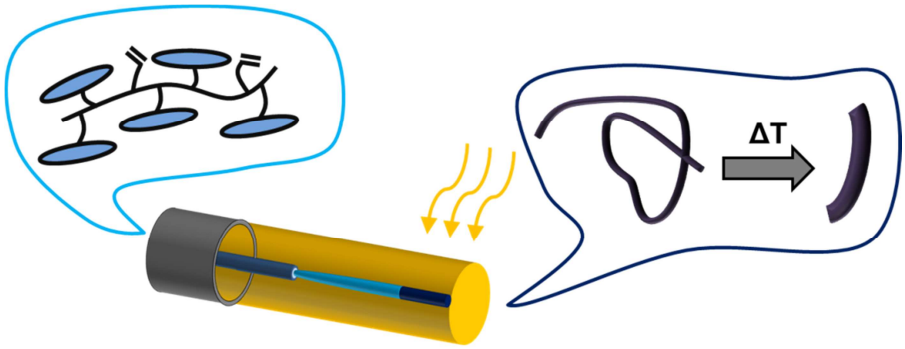

Figure 2.3: *Preparation of LCE fibers from a crosslinkable side-chain polymer. The liquid jet of the polymer solution is photo-crosslinked and the resulting elastomer fibers exhibit ultralarge length contractions of up to 3000%.*

So far, core-shell and bulk elastomer particles were prepared from droplets of liquid crystalline precursors in the microfluidic device. The droplets at the capillary tip predominantly form because of the high surface tension between the liquid crystalline dispersed phase and the ambient fluid silicone oil (PDMS). Alternatively to the formation of droplets, a jet of the dispersed phase can be extruded from the capillary nozzle and crosslinked to yield elastomer fibers. The deformation of droplets into a stable jet requires high shear rates, where viscous and inertial forces dominate over the surface tension of the liquid crystalline precursors and the ambient fluid.

With a suitable co-flowing continuous phase the LCE fibers can be prepared from the polymer precursor **CrP** described in Chapter 2.2. The ambient fluid, a polyether-modified hydrophilic silicone fluid lowers the interfacial tension, so that the formation of a liquid jet is favored above the formation of droplets even at low shear rates. Polymer

precursors **CrP** were used with different amounts of crosslinkable units. After crosslinking of the polymer jet by UV-light, LCE fibers with different mechanical properties were obtained, depending on the crosslinking density. The crosslinking density could be controlled by either the amount of crosslinkable units in the polymer or by the UV-irradiation times. Fibers with low crosslinking density contracted upon the nematic-isotropic phase transition of the elastomer with a length change of several hundred percent. Increasing the amount of crosslinkable units or the duration of UV-exposure yielded highly crosslinked fibers which did not contract, since the mesogens lack the flexibility to rearrange upon the transition to the disordered isotropic phase. Contractions of the fibers were, however, not reversible. Reversibility may be assisted by an additional weight attached to the fiber that acts as an external force, supporting the recovery of the nematic order.

Chapter 3.4:

E.-K. Fleischmann, F. R. Forst, R. Zentel **2013**, *in preparation.*

2.4 Microactuators from a main-chain liquid crystalline elastomer via thiol-ene "click" chemistry

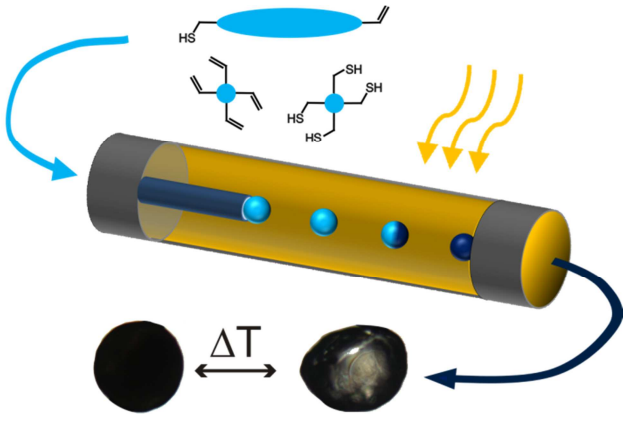

Figure 2.4: *Synthesis of liquid crystalline main-chain elastomers via thiol-ene polymerization in a microfluidic setup. The thermo-mechanical properties of the LCE particles demonstrate their feasibility as microactuators.*

The main body of this thesis focuses on side-chain elastomers, the mesogenic moieties of which are laterally attached to the polymer backbone via flexible spacers. In

case of main-chain elastomers, the mesogens are no longer attached to the polymer via spacers but are part of the polymer backbone. Compared to side-chain elastomers, main-chain elastomers usually exhibit stronger anisotropies of the polymer chains, resulting in considerably larger shape changes. These advantageous features illustrate the interest in main-chain elastomers for actuator applications. The preparation of main-chain elastomers in a microfluidic device comes, however, with a drawback. Most common synthetic procedures for the preparation of main-chain polymers and elastomers are poly-addition and poly-condensation reactions. Reaction times of these mechanisms are generally too slow to allow for sufficient conversions in a microfluidic device. In recent years, the advances made for the preparation of linear polymers by the thiol-ene "click" mechanism could be adapted to liquid crystalline main-chain polymers. Due to its fast kinetics, the thiol-ene polymerization reaction deems promising considering the short reaction times in microfluidic devices.

For the preparation of a main-chain elastomer in the microfluidic device, a nematic mesogen with terminal thiol and ene groups was chosen. It could successfully be converted with crosslinkers pentaerythritol tetrakis(3-mercaptopropionate) (PETMP) and glyoxal bis(diallyl acetal) (GBDA), both having a functionality of four, to form an elastomer network. While UV irradiation of the LC droplets in the microfluidic device lasted less than 2 seconds, analysis of the polymerization degree and sol content of the elastomer particles revealed, that this was sufficient for the formation of a crosslinked elastomer network. Polymerization and crosslinking primarily proceeded via "click" reactions between thiol and ene groups and only marginally by thiol-thiol bonding as verified by swelling experiments of the resulting particles in the reducing agent tributylphosphine.

The LCE particles are of spherical shape and demonstrate a temperature-driven shape change of up to 25%. The degree of actuation could be influenced by the polymerization temperature, with the largest shape change observed at 47°C. Close to the crystalline-nematic phase transition at lower temperatures, the viscosity increases, while at higher temperatures close to the isotropic phase the order of the mesogens decreases. Both effects lower the order parameter in the particles and, as a consequence,

lessen the shape change. The actuation properties could further be modified by varying the dimension of the polymerization tube. When decreasing the diameter of the tube, the increased confinement gives rise to a larger shear flow, which leads to a better orientation of the mesogens prior to crosslinking. Concerning the thermo-mechanical response of the LCE particles, contraction-recovery cycles were conducted and revealed full reversibility of the particles' shape change. While this work demonstrated the feasibility of the thiol-ene mechanism in a microfluidic "on the fly" process, it will need further optimization of the microfluidic parameters to reveal the full actuation potential of these main-chain elastomers.

Chapter 3.5:

E.-K. Fleischmann, F. R. Forst, K. Köder, R. Zentel *J. Mater. Chem. C* **2013**, *under revision.*

3 Publications

3.1 Towards micrometer sized core-shell actuators from liquid crystalline elastomers by a continuous flow synthesis

Eva-Kristina Fleischmann[#,a], Hsin-Ling Liang[#,a], Jan Lagerwall[b], Rudolf Zentel[*,a]

[a]*Institute of Organic Chemistry, Johannes Gutenberg-Universität Mainz, 55099 Mainz, Germany;*

[b]*Seoul National University, Graduate School of Convergence Science and Technology, Suwon-si, Gyeonggi-do, Korea 443-270*

# These authors contributed equally to this work.

*zentel@uni-mainz.de; phone +49 6131 3925873; fax +49 6131 3924778;

ak-zentel.chemie.uni-mainz.de

Keywords: Liquid crystalline elastomers, micro-actuators, microfluidics, core-shell particles, microelectromechanical systems (MEMS), stimuli-responsive materials.

Abstract

We present here the successful preparation of liquid crystalline core-shell elastomers via a microfluidic double-emulsion process. The customized set-up allows for a temperature-controlled fabrication of the core-shell particles from a thermoresponsive mesogenic monomer. The nematic liquid crystalline shell is filled with a non-mesogenic core of silicone oil. To verify the core-shell structure with optical microscopy, we prepared particles with a colored core using a red dye. We were also able to micro-manipulate the particles and penetrate them with a small glass capillary to extract the liquid core.

3.1.1 Introduction

While shape memory alloys (SMA) and piezoceramics have been the standard material for use as responsive devices, soft actuators derived from shape memory polymers have emerged in recent years as a low cost, environmentally friendly and mechanically flexible alternative [1]. The idea to exploit liquid crystalline elastomers (LCEs) as stimuli responsive polymers has already been proposed by de Gennes in 1975 [2]. LCEs combine the entropy-elasticity of elastomers with the self-organizing properties of liquid crystals [3; 4]. Due to the anisotropic form of the molecules, the mesogens orient in the liquid crystalline phase along a preferred axis, the so-called director. External stimuli like temperature, light or the application of an electric field trigger a phase transition from the ordered mesophase to the random isotropic state. The mesogens can be linked to a polymer, either as part of the polymer backbone (main-chain polymers) or attached via flexible spacers (side-chain polymers). With the mesogens aligned along the director, the polymer backbone adopts a stretched conformation. When losing the orientational order in the isotropic phase, the backbone returns to a random coil conformation. In case of a crosslinked elastomer, this microscopic conformational change during the phase transition causes a macroscopic contraction of the elastomer sample along the director (Figure 1). Without an external force, the director aligns randomly in the mesophase and the mesogens form oriented polydomains.

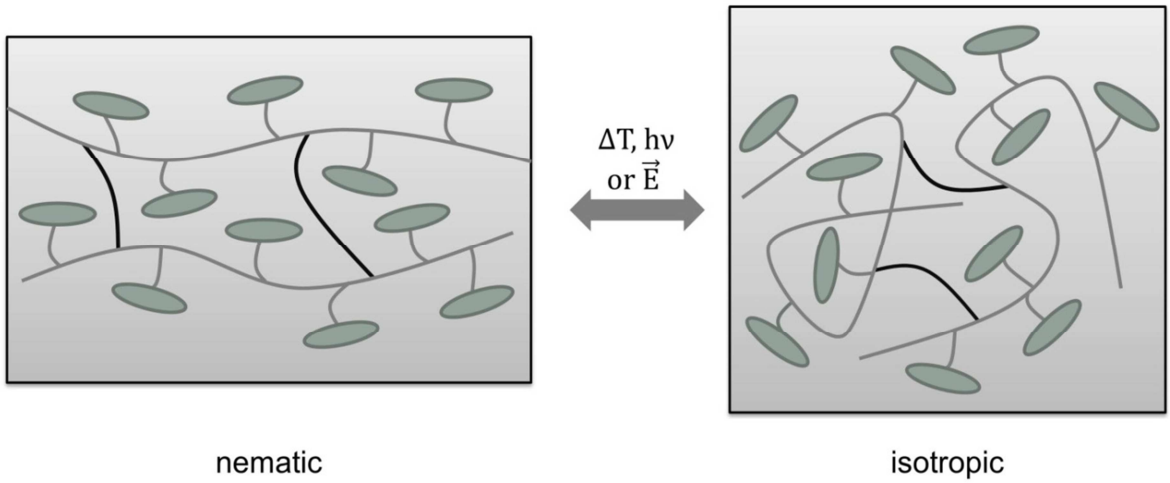

Figure 1. *The microscopic transition from the nematic to the isotropic state in a uniformly oriented sample is triggered by an external stimulus and results in a directed macroscopic change of shape.*

For a macroscopic elastomer the shape changes of the polydomains cancel out each other and no directed deformation is observed. To get a directed change of shape, the mesogens have to form a monodomain across the whole sample. This has been achieved by different fabrication methods such as a two-step crosslinking process of a mechanically stretched film [5], the use of magnetic [6] or electric fields [7] and surface alignment [8].

The actuation of a LCE is fully reversible and shape changes up to 400% have been reported [6]. This recommends them for the use in microelectronical systems (MEMS) as sensors and actuators [9; 10]. Owed to the need of micro- and nanometer sized LCEs, new methods of fabrication have been developed in recent years. This includes inkjet printing [11], micro- and nanotemplating [12; 13] as well as mini-emulsion polymerization [14] of liquid crystals. A particularly intriguing method for the fabrication of micrometer-sized LCEs is the processing of liquid crystals in microfluidic devices: The melt of a liquid crystalline monomer is extruded through a thin capillary in a co-flowing stream of silicone oil in a micrometer-sized tube. Droplets of the mesogen are constantly formed at the capillary tip and are ripped off by force exerted by the viscous drag of the continuous phase. A preferred director field of the mesogens inside the liquid crystalline droplets is induced by the flow conditions inside the microchannel. The orientational order is then permanently fixed by irradiation with UV light. This method allows the systematic control over particle size, geometry and director configuration of the micro-actuators [15; 16]. The possibility to manipulate the director field configuration makes microfluidics an important tool for the fabrication of liquid crystals. This unique control of the director field has been previously exploited in the microfluidic preparation of colloidal LC spheres, which were studied towards applications employing their electro-optical switching behavior [17]. Depending on the boundary conditions, for instance homeotropic or planar anchoring, a defined director field orientation can be imposed, where disclination lines and point defects cannot be entirely avoided due to the constraints of the topology (Figure 2). Amongst others, colloidal core-shell particles prepared via a microfluidic double-emulsion process attract considerable attention. Control over defect arrangement has been achieved by varying

the shell thickness [18]. Caused by the interplay of the liquid crystalline ordering and the topological confinement of the spherical surface, interesting textures have been engineered from nematic [19] as well as smectic [20] core-shell colloids. These engineered defects may then be functionalized with the objective to create colloids with directed particle interactions.

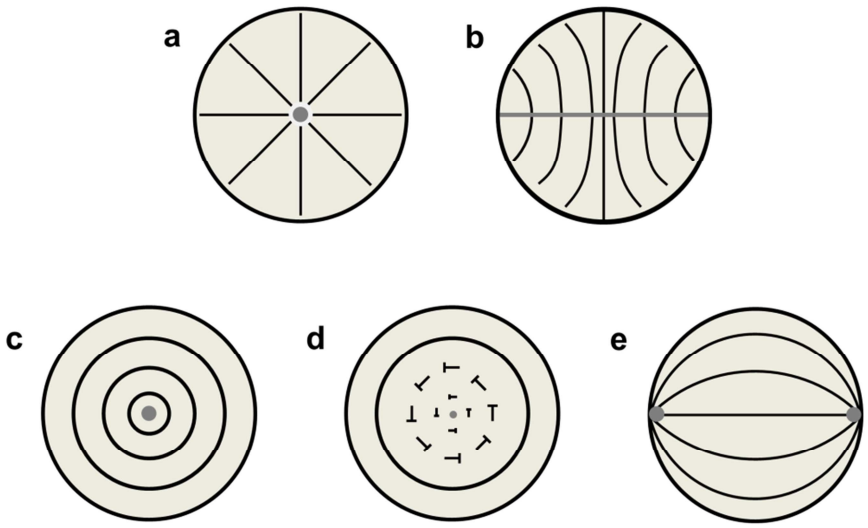

Figure 2. *Possible director configurations for nematic mesogens with homeotropic (**a**,**b**) and planar (**c**-**d**) anchoring along the surface of a spherical droplet: radial (**a**), axial (**b**), concentric (**c**), escaped concentric (**d**) and bipolar (**e**).*

So far the microfluidic fabrication of core-shell particles from liquid crystals has not been deployed for LC elastomers. Polymerizable mesogens exhibit phase transitions at elevated temperatures. Therefore, the fabrication of homogeneously oriented core-shell LCEs requires a customized microfluidic set-up, which allows a localized temperature control over the capillaries and tubing. With an induced bipolar orientation (Figure 2e) of the nematic mesogens inside the elastomer shell by the flow field, the core-shell particles should be able to actuate in response to an external stimulus. In analogy to a heart, a hollow muscle, the particles may be able to reversibly push out part of their liquid interior, making them suitable for MEMS applications.

3.1.2 Results and Discussion

We present here the fabrication of core-shell elastomers from a nematic mesogen. The mesogen has previously been processed in microfluidic and templating devices [21; 13; 12]. The rigid three-core mesogen has a flexible side chain with a polymerizable acrylate group attached to it and exhibits a nematic phase between 72°C and 98°C [8]. The monomer mixture consists of 10 mol% of crosslinker hexanedioldiacrylate and 3 wt% of photoinitiator Lucirin TPO (Figure 3). Due to the non-mesogenic admixtures, the crystalline-isotropic transition drops from 98°C to 80°C and a monotropic nematic phase forms below the melting point on cooling. With the phase transition occurring at elevated temperatures, the microfluidic set-up has to be temperature-controlled. Two hot stages are needed: the first hot stage is set to 90°C within the isotropic phase of the mixture for the shell formation. The second hot stage built at the downstream of the channel is set to 65°C within the nematic phase of the mixture. The droplets are cooled down to the nematic phase, and the orientation of the mesogens is permanently fixed upon UV-induced polymerization and crosslinking with a peak wavelength of 365 nm.

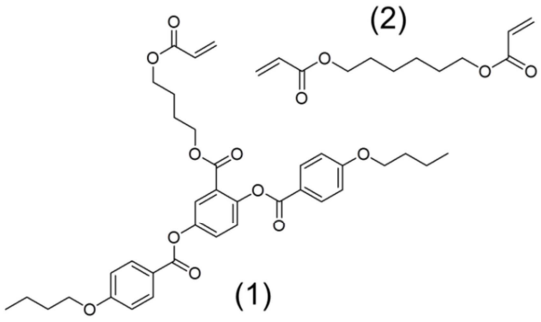

Figure 3. *Chemical structures of the nematic side-chain mesogen (1) and crosslinker (2).*

The core-shell particles are generated via a double-emulsion process (Figure 4). They consist of an elastomer shell filled with a core of silicone oil. Three co-flowing streams are needed: an inner phase of silicone oil (IP), the monomer mixture (MP) and an outer phase also consisting of silicone oil (OP). The silicone oil of the inner phase is injected through a round glass capillary. This capillary was inserted into a square glass capillary filled with the monomer mixture (MP). The outer diameter of the round capillary fits the inner dimension of the square capillary. Droplets of silicone oil form at the tip of the

round capillary and detach into the co-flowing stream of the monomer mixture (MP). With well-adjusted flow rates, the monomer droplets forming at the tip of the square capillary are filled with a single silicone oil droplet. After being ripped-off from the capillary tip, the core-shell droplets disperse in the outer silicone oil phase (OP). They are further stabilized by radical initiated polymerization using UV-light and can thus be easily collected in a container.

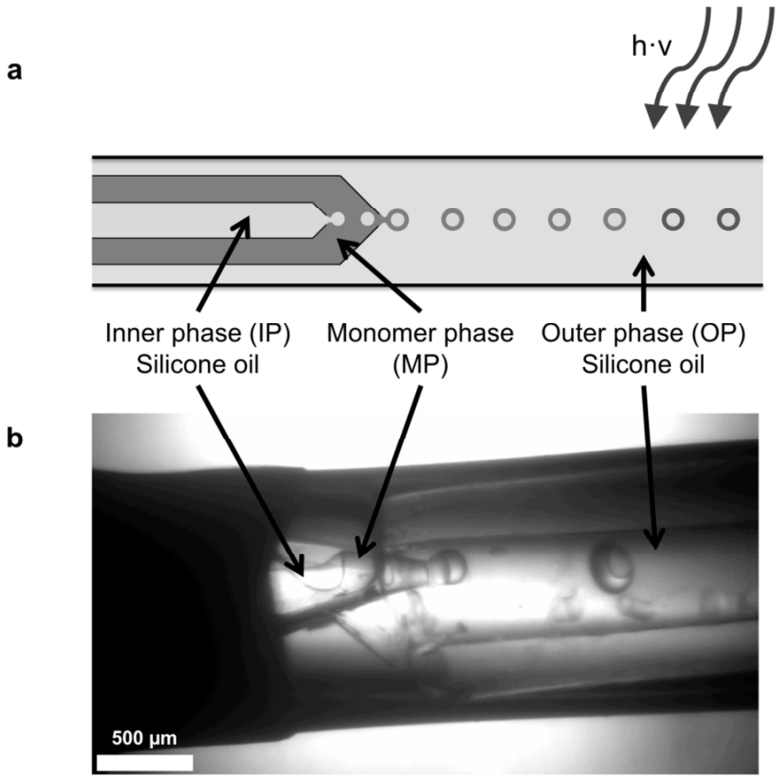

Figure 4. a *Schematic drawing of the microfluidic device for the fabrication of nematic core-shell elastomers.* ***b*** *Formation of core-shell droplets at the capillary tip.*

For a future application as a micropump, it is essential to produce core-shell particles, which only consist of one and not several core droplets. To check the number of core droplets inside the elastomer shell we colored the inner phase with a red dye. The resulting particles are shown in Figure 5. The dye is clearly visible in the center of the particle. Further, the inner phase forms a single spherical droplet inside the elastomer shell. Since the dye strongly absorbs light in the UV range, the particles are not fully polymerized and melt upon heating to the isotropic phase.

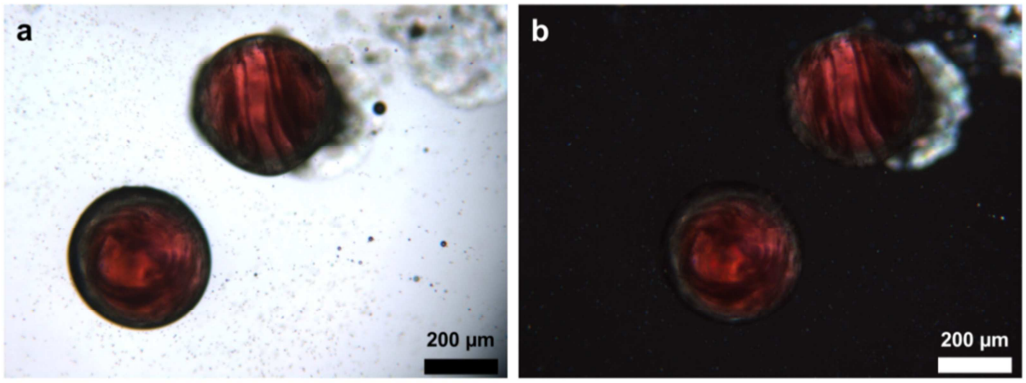

Figure 5. *Core-shell particles with a red colored core seen with an optical microscope:* ***a*** *bright field mode and* ***b*** *between crossed polarizers.*

The prepared core-shell particles have a diameter of several hundred micrometers. Due to their small size, the handling and manipulation of the particles is challenging. To be applicable as micropumps a method is needed to create an inlet and outlet. We demonstrate a penetration of the dense core-shell polymer particle by means of a thin glass capillary tip with an orifice smaller than 50 µm (Figure 6). The particle was carefully poked with the glass capillary and once the capillary penetrates the shell, the capillary is immediately filled with liquid. To make sure that the liquid stems from the core and not from residual silicone oil on the surface of the particle, a fluorescent dye is added to the inner phase during the preparation. The fluorescence image of the poked particle is shown in Figure 6b. A marked fluorescence of the liquid in the capillary unambiguously proves its origin from the core of the particle. This experiment validates that we have a core-shell system, which can be manipulated to extract and possibly refill the liquid core.

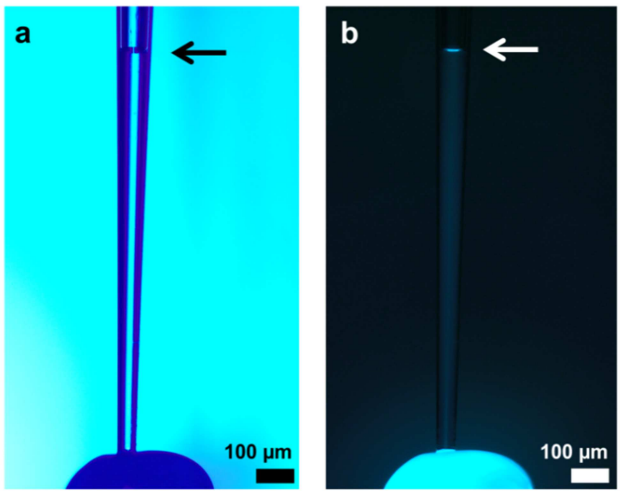

Figure 6. *Core-shell elastomer particle perforated with a glass capillary* ***a*** *optical micrograph and* ***b*** *fluorescence image.*

Heating experiments are conducted to test the actuation properties of the core-shell particles. The nematic-isotropic phase transition for the elastomer is slightly below 130 °C, hence, a macroscopic change of shape is expected at temperatures slightly below and above the phase transition. At 100 °C, the silicone oil core visibly contrasts the nematic shell (Figure 7). The shell clears optically at 130 °C indicating a loss of orientational order of the mesogens during the phase transition. However there is no observable deformation of the particle shape that is expected from an oriented LCE. While a non-uniform orientation of the director field in the core-shell elastomer may account for the absence of macroscopic actuation, previous work successfully demonstrated the macroscopic alignment of mesogenic units in a microfluidic channel through the influence of the flow field [21]. Since the flow field primarily acts on the particle surface, an impact of the flow field on a uniform director orientation is also expected for the core-shell particles. Further, the core-shell particles are polymerized and crosslinked at the appropriate temperature within the nematic phase of the monomer mixture, ensuring an ordering of mesogenic units along the director field. We therefore suspect that the inability of the core-shell particles to actuate may be due to the high viscosity of the silicone oil in the core. The influence of the liquid interior towards the actuation properties of the core shell particles will be further examined in future experiments using an inner phase with low viscosity.

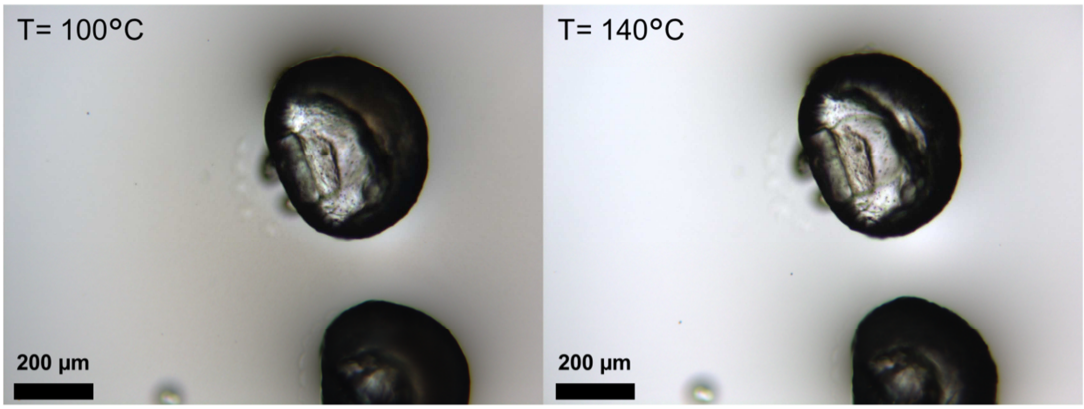

Figure 7. *Core-shell elastomer particle heated under a microscope to* ***a*** *100 °C and* ***b*** *140 °C.*

3.1.3 Conclusion

In this contribution we present the preliminary work towards the preparation of micro-pumps from liquid crystalline elastomers. We achieve the fabrication of core-shell elastomers from a nematic mesogen in a temperature controlled microfluidic set-up. By adjusting the flow rates of the monomer phase and the inner phase, the number of cores inside the elastomer shell can be controlled. Additionally, we demonstrate the feasibility of the particulate micro-manipulation. Specifically, we are able to extract the liquid interior of the core-shell particle with a thin capillary. The particles prepared so far have shown no actuation when being heated to the isotropic phase. We suspect that this is due to the high viscosity of the silicone oil-comprised inner core. To test this hypothesis, a less viscous liquid will be used as the inner phase in future experiments.

3.1.4 References

[1] Lendlein, A., Kelch, S., "Shape-memory polymers," Angew. Chem. Int. Edit. 41, 2034–2057 (2002).

[2] Gennes, P.-G. de, "One Type of Nematic Polymers," C. R. Acad. Sci. Ser. B 281 (5-8), 101–103 (1975).

[3] Terentjev, E. M., "Liquid-crystalline elastomers," Journal of Physics: Condensed Matter 24, R239 (1999).

[4] Demus, D. Boodby J. Gray G. W. Spiess H. W., "Handbook of Liquid Crystals, Wiley-VCH, Weinheim, Germany (1998).

[5] Kupfer, J., Finkelmann, H., "Nematic Liquid Single-Crystal Elastomers," Makromol. Chem. Rapid. Commun. 12, 717–726 (1991).

[6] Yang, H., Buguin, A., Taulemesse, J.-M., Kaneko, K., Méry, S., Bergeret, A., Keller, P., "Micron-Sized Main-Chain Liquid Crystalline Elastomer Actuators with Ultralarge Amplitude Contractions," J. Am. Chem. Soc 131 (41), 15000–15004 (2009).

[7] Brehmer, M., Zentel, R., Wagenblast, G., Siemensmeyer, K., "Ferroelectric liquid-crystalline elastomers," Macromol. Chem. Phys. 195 (6), 1891–1904 (1994).

[8] Thomsen, D. L., Keller, P., Naciri, J., Pink, R., Jeon, H., Shenoy, D., Ratna, B. R., "Liquid crystal elastomers with mechanical properties of a muscle," Macromolecules 34, 5868–5875 (2001).

[9] Yu, Y., Ikeda, T., "Soft actuators based on liquid-crystalline elastomers," Angew. Chem. Int. Edit. 45, 5416–5418 (2006).

[10] Ohm, C., Brehmer, M., Zentel, R., "Liquid Crystalline Elastomers as Actuators and Sensors," Adv. Mater. 22, 3366–3387 (2010).

[11] van Oosten, C. L., Bastiaansen, C. W. M., Broer, D. J., "Printed artificial cilia from liquid-crystal network actuators modularly driven by light," Nat. Mater. 8 (8), 677–682 (2009).

[12] Buguin, A., Li, M. H., Silberzan, P., Ladoux, B., Keller, P., "Micro-actuators: When artificial muscles made of nematic liquid crystal elastomers meet soft lithography," J. Am. Chem. Soc 128, 1088–1089 (2006).

[13] Ohm, C., Haberkorn, N., Theato, P., Zentel, R., "Template-Based Fabrication of Nanometer-Scaled Actuators from Liquid-Crystalline Elastomers," Small 7, 194–198 (2011).

[14] Haseloh, S., Ohm, C., Smallwood, F., Zentel, R., "Nanosized Shape-Changing Colloids from Liquid Crystalline Elastomers," Macromol. Rapid Comm. 32, 88–93 (2011).

[15] Ohm, C., Kapernaum, N., Nonnenmacher, D., Giesselmann, F., Serra, C., Zentel, R., "Microfluidic Synthesis of Highly Shape-Anisotropic Particles from Liquid Crystalline Elastomers with Defined Director Field Configurations," J. Am. Chem. Soc. 133, 5305–5311 (2011).

[16] Ohm, C., Fleischmann, E.-K., Kraus, I., Serra, C., Zentel, R., "Control of the Properties of Micrometer-Sized Actuators from Liquid Crystalline Elastomers Prepared in a Microfluidic Setup," Adv. Funct. Mater. 20, 4314–4322 (2010).

[17] Fernández-Nieves, A., Cristobal G., Garcés-Chávez, V., Spalding, G. C., Dholakia, K., Weitz D. A., "Optically Anisotropic Colloids of Controllable Shape," Adv. Mater. 17 (6), 680–684 (2005).

[18] Lopez-Leon, T., Koning, V., Devaiah, K. B. S., Vitelli, V., Fernandez-Nieves, A., "Frustrated nematic order in spherical geometries," Nat. Phys. (Nature Physics) 7 (5), 391–394 (2011).

[19] Lopez-Leon, T. and Fernandez-Nieves, A., "Topological transformations in bipolar shells of nematic liquid crystals," Phys. Rev. E, 79, 021707 (2009)

[20] Liang, H.-L., Schymura, S., Rudquist, P., Lagerwall, J., "Nematic-Smectic Transition under Confinement in Liquid Crystalline Colloidal Shells," Phys. Rev. Lett. 106, 247801-1 (2011).

[21] Ohm, C., Serra, C., Zentel, R., "A Continuous Flow Synthesis of Micrometer-Sized Actuators from Liquid Crystalline Elastomers," Adv. Mater. 21, 4859–4862 (2009).

3.2 One-piece micropumps from liquid crystalline core-shell particles

Eva-Kristina Fleischmann[#,a], Hsin-Ling Liang[#,a], Nadia Kapernaum[b], Frank Giesselmann[b], Jan Lagerwall*[,c], Rudolf Zentel*[,a]

[a]*Institute of Organic Chemistry, Johannes Gutenberg-Universität Mainz, 55099 Mainz, Germany*

[b]*Institute of Physical Chemistry, Universität Stuttgart, 70569 Stuttgart, Germany*

[c]*Seoul National University, Graduate School of Convergence Science and Technology, Suwon-si, Gyeonggi-do, Korea 443-270*

# These authors contributed equally to this work.

* e-mail: zentel@uni-mainz.de, janlagerwall@snu.ac.kr

Subject categories

Polymers and soft materials, materials chemistry.

Abstract

Responsive polymers are low-cost, light-weight, and flexible and thus an attractive class of materials for the integration into micromechanical and lab-on-chip systems. Triggered by external stimuli, liquid crystalline elastomers (LCEs) are able to perform mechanical motion and can be utilised as microactuators. We present the fabrication of one-piece micropumps from liquid crystalline core-shell elastomer particles via a microfluidic double-emulsion process, the continuous nature of which enables a low-cost and rapid production. The liquid crystalline elastomer shell contains a liquid core, which is reversibly pumped into and out of the particle by actuation of the liquid crystalline shell in a jellyfish-like motion. The LCE shells have the potential to be integrated into a microfluidic system as micropumps that do not require additional components except passive channel connectors and a trigger for actuation. This renders elaborate and high-cost micromachining techniques otherwise required for obtaining microstructures with pump function unnecessary.

3.2.1 Introduction

Microelectromechanical systems (MEMS) already form an integral part in our everyday lives, may it be as accelerometers for air bag deployment in cars, piezoelectrics in thermal drop-on-demand inkjet printers or biosensors in medical applications[1,2]. This demonstrates the need for miniature-sized mechanical actuators. From day one, it has however been a challenge to manufacture MEMS and other types of micromechanical actuator systems with a specific shape. Lithographic methods, etching processes and specially designed micromachines have been employed for their fabrication. Thereby silicones, shape memory alloys (SMA) and piezoceramics have been the most widely used materials[3,4]. In recent years, shape memory polymers have attracted considerable interest as active materials for responsive devices[5]. They are cheap, ecologically compatible and - due to their elasticity - fracture resistant, to name only a few key advantages for a potential use as actuators. Particularly, liquid crystalline elastomers (LCEs) uniquely combine the elasticity of elastomers with the anisotropic self-organization of liquid crystals as basis for mechanical actuation[6–12].

The microscopic transition from the ordered but soft mesophase to the isotropic state can be triggered by temperature, light or electric fields[13] and results in a directed macroscopic change of shape that can reach up to 400%, matching the performance of skeletal muscles[14,15]. Crucial to the preparation of LCEs is the uniform orientation of the anisotropic structural units, so-called mesogens, along a common axis, the director. Commonly done in a two-step crosslinking process accompanied by mechanical stretching of a film[16], novel approaches such as micro- and nano-templating[17,18] and inkjet printing techniques[19] recently opened up new possibilities to down-scale LCE actuators for micro-sized applications. Ohm *et al.* designed a microfluidic setup that allows a continuous production of micrometer-sized LCE fibres and particles by photopolymerization of an LC-monomer to obtain LCEs with customizable actuator geometry and control over the orientation of the director[20,21]. While the actuating properties of LCEs have mainly been exploited to simply trigger motion, more sophisticated applications such as peristaltic pumps and self-propelled robots have been proposed theoretically[22]. So far, a millimeter sized motor propelled by photo-induced

deformations of an LCE film and a microvalve for microfluidics with an actuating LCE film could be realised[23,24]. Besides microvalves, diaphragm and peristaltic micropumps are crucial for flow regulation in microchannels, which are commonly used in lab-on-chip systems.

Micromechanical systems are typically prepared by microfabricating procedures, with the drawback of having to be performed in a clean room at high cost. In that respect, soft lithographic methods have easier process parameters, but to achieve a three dimensional active device from 2D patterned elastomer layers, multi-layer structures have to be assembled. Based on this principle, a peristaltic micropump could be realised via a series of replica molding from multiple templates[25]. In this contribution, we present the successful continuous fabrication of one-piece micropumps from a thermoresponsive LCE which requires no elaborate micromachining techniques. They have the potential for further incorporation into three dimensional microfluidic systems, while present-day valveless lab-on-chip micropumps, commonly made of poly(dimethylsiloxane) (PDMS), are generally restricted to 2D flow.

3.2.2 Results

Preparation of core-shell elastomers in a microfluidic setup

Inspired by the contraction-pulsation movement of a jellyfish we aimed to create an analogous synthetic microsystem: one muscle-like shell, which reversibly contracts to push and pull a liquid core into and out of the shell. For this purpose shape changing liquid crystalline elastomer shells filled with a liquid core were produced for the first time in a specially designed microfluidic setup, depicted in Figure 1a. It allows for a facile and continuous fabrication of core-shell particles with controlled size. In our system no surfactants or shell stabilisers are introduced, as they may influence the LC orientation[26], which is the essential factor determining the actuation effect. The co-flow microfluidic geometry was specially chosen as it allows a good control of the preparation of core-shell particles[27,28] and as coalescence of the particles can be avoided until they are photo-polymerised further downstream. The microfluidic device is comprised of a triple co-flow channel: a cylindrical glass micropipette is nested into a tapered square

glass capillary, which is confined by teflon tubing. The combination of concentric cylindrical and square cross-section geometries allows one fluid (the middle phase: the LC monomer) to flow in the voids between the circular and square capillaries, and another fluid (the inner phase: glycerol) to flow through the innermost circular channel. In Figure 1 the inner and middle phases are drawn orange and blue respectively. Droplets of glycerol form at the inner capillary tip and detach into the co-flowing monomer phase delivered through the square capillary. The monomer phase is designed immiscible with the other fluids, including the outer phase (silicone oil; drawn yellow) which flows in the outer-most teflon tube. This results in glycerol droplets encapsulated by a monomer shell that are suspended in the continuous phase silicone oil.

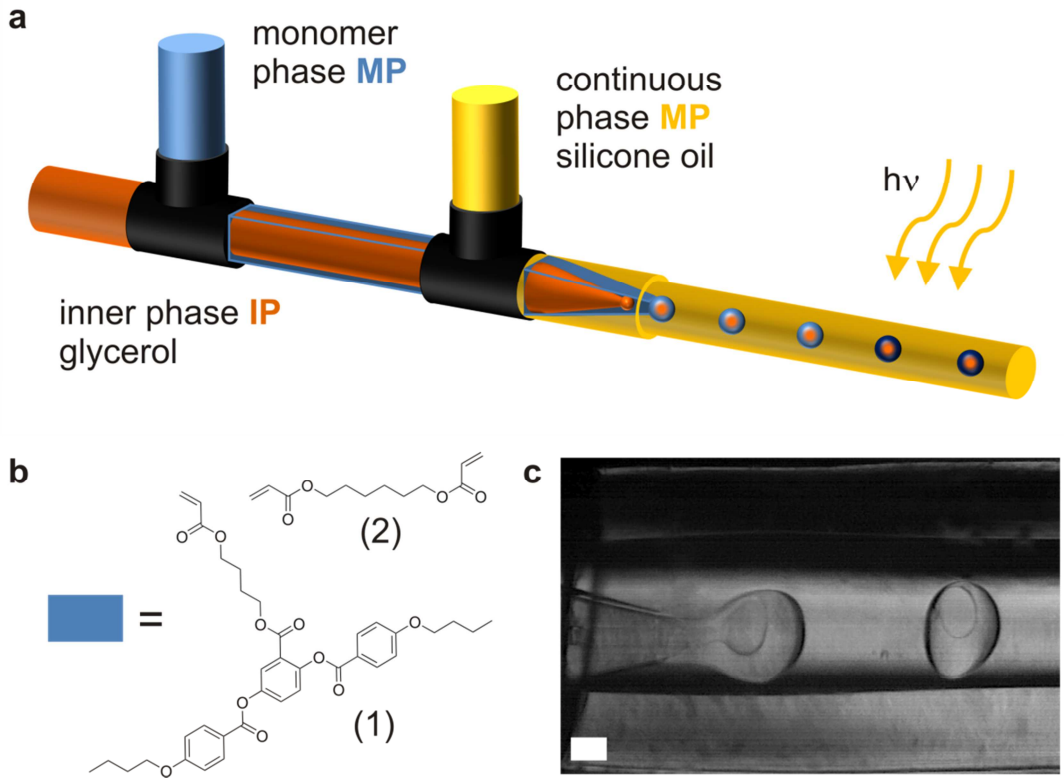

Figure 1: *Preparation of the core-shell elastomers.* ***a****, The triple co-flowing geometry of the microfluidic setup allows the fabrication of nematic shell particles filled with a glycerol core. Dispersed in the surrounding continuous phase silicone oil the monomer droplets are polymerized by UV-light.* ***b****, Chemical structures of the reactive mesogen (1) and crosslinker (2) in the monomer mixture.* ***c****, Core-shell droplet formation at the capillary tip (scale bar 100 μm).*

Following previously derived relations between the LCE droplet size, flow rates, and actuation properties[29], we chose glass capillary tips with an orifice diameter of 20

μm for the inner cylindrical capillary and 100 μm for the square capillary to provide for a well oriented LCE shell, which is the precondition for large actuation response. We decided on using glycerol for the inner phase and hence as the core of the core-shell particles. Glycerol is immiscible with the monomer phase and exhibits a sufficiently low viscosity at elevated temperatures (see Supplementary Table S1). It may be seen as a model fluid in the interior of the micropump, but it is interchangeable with other liquids after the fabrication of the latter. The LCE shell is composed of the three-core mesogen shown in Figure 1b, that has previously been processed in microfluidic and templating devices[17,18,30], but not for making core-shell particles. Attached to the rigid mesogenic unit are three flexible side chains, one of which comprises a polymerizable acrylate group. The monomer exhibits a nematic phase between 72 °C and 98 °C[15]. By addition of the non-mesogenic photoinitiator (3 wt% Lucirin TPO) and crosslinker (10 mol% 1,6-hexanedioldiacrylate), a crystalline-isotropic phase transition is observed on heating (80 °C) without any intermediate liquid-crystalline regime. However, a supercooled nematic phase forms below the melting point at 80 °C on cooling. This monotropic LC phase is of sufficient stability for our LCE shell production purposes. The low viscosity of the monomer in its high temperature isotropic phase makes it easily processable in a microfluidic device (formation of the core-shell particles), while the monotropic nematic state formed at lower temperatures within the polymerization tube allows flow induced orientation and photopolymerization to prepare oriented LCEs.

Previous work on LC shells was limited to low-molecular weight, non-polymerisable mesogens, which exhibit isotropisation temperatures slightly above room temperature. They could thus be manufactured at moderate temperatures in a surrounding aqueous medium[31–34]. With an isotropisation temperature of 80 °C, the reactive monomer mixture used in this study needs to be processed at elevated temperatures and requires a customised heat-resistant microfluidic device[30]. Thus temperature-tolerant silicone oil was chosen as the outer continuous phase. Precise control over temperature is enabled by mounting the microfluidic setup on two hot stages: the core-shell droplets are formed at the capillary tip in the isotropic phase at 90 °C while the polymerization tube is set to 65 °C well within the nematic phase of the monomer mixture. The flow-induced orientation of the mesogens is permanently fixed

through UV-initiated polymerisation and crosslinking. At flow rates of 1.7 mL/h for the continuous phase, 0.06 mL/h for the monomer phase, and 0.01 mL/h for the inner phase about 100 core-shell elastomers are obtained per minute, dispersed in silicone oil. This allows them to be easily collected in a vessel.

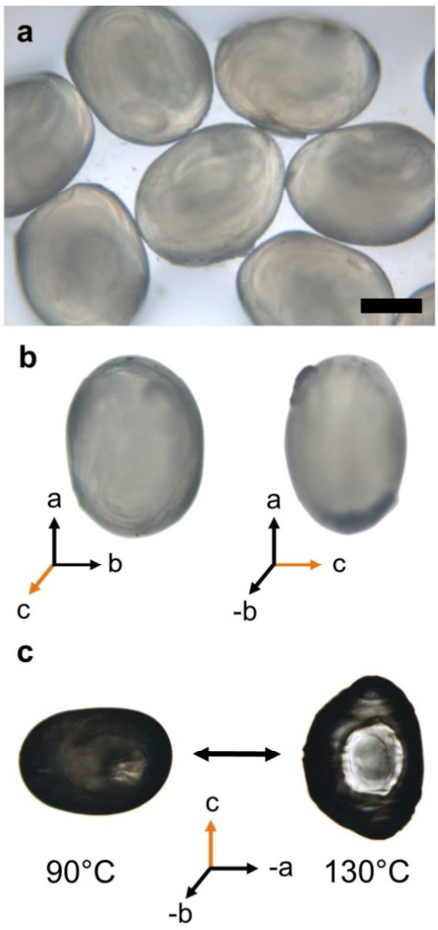

Figure 2: *Characterization of the core-shell elastomer particles by light microscopy.* ***a****, Examples of the ellipsoidal shaped core-shell particles at room temperature.* ***b****, Top view of a particle at room temperature (on the left) and the same particle flipped around its longest axis a, revealing a shorter axis c (on the right).* ***c****, Heating experiment demonstrating the actuation behaviour at the nematic-isotropic phase transition. The particle elongates along its short axis c. Note the glycerol core becoming visible above the clearing temperature (scale bar 200 µm.).*

Characterization of the core-shell elastomers

After UV-induced polymerisation the particles consist of a cross-linked LC elastomer shell formed after full conversion of the LC monomer and crosslinker.[29] For swelling ratios see ref. 29 and for the Young's modulus of a comparable film (0.4 MPa)

see ref. 15. They were characterised by light microscopy, some example images are shown in Figure 2a. At room temperature the ellipsoidal-shaped particles possess a minimum aspect ratio (length *a*/width *b*) of 1.3. The average length of the main axis *a* is 545 μm with a size dispersity below 2%. The particles can be flipped manually around their main axis to reveal a third axis *c*, which is slightly shorter than *b* (Figure 2b). The aspect ratio between *a* and *c* is 1.5. Figure 2c shows a core-shell elastomer particle with its main axis in the horizontal and its smallest axis in the vertical direction in the nematic phase at 90 °C. In this context it should be noted that the polymerization of the monomer to an LCE increases the phase transition temperature (nematic – isotropic) from 80 °C (monomer mixture) to 130 °C. Upon heating to the isotropic state at 130 °C, the particle shrinks along its original main axis *a* and expands along its initially shortest axis *c*. This is comparable to the behaviour of bulk particles from LCEs[20,29]. The aspect ratio changes from 1.5 at room temperature to 0.73 at 130 °C. The relative length change, defined as the ratio between the axis *c* in the actuated state and at room temperature, is 1.52. This reversible shape change leaves the total volume of the particle shell and core constant, since core and shell have low compressibilities and the density of the nematic and isotropic phase is rather similar. This does however not imply that there is no hydrostatic pressure build-up.

Core-shell elastomers as active micropumps

To verify the concept of a micropump for our core-shell elastomers we developed a setup where we could puncture the shell of the LCE to create an outlet for the glycerol core and also easily heat the particle to the isotropic phase. A schematic drawing of the micromanipulator is shown in Figure 3a. A glass capillary with an orifice of 40 μm in diameter and a cone angle of 3° for the capillary tip was clamped into an axially translatable holder. The core-shell particle was mounted on a glass slide between a hotplate and the capillary tip. Since glycerol is very polar and exhibits an affinity for glass, the surface of the glass capillary was hydrophobised with trichloro(3,3,3-trifluoropropyl)silane to suppress potential wetting. For a better handling, the particle was heated to 90 °C, which is well above its glass transition temperature, and pierced with the capillary tip in the rubbery state. As soon as the capillary penetrated the shell, a

fraction of the liquid glycerol core rose into the capillary, due to the pressure on the pinched particle (Figure 3b). Once the particle was lifted away from the hotplate, almost all liquid sank back into the particle core.

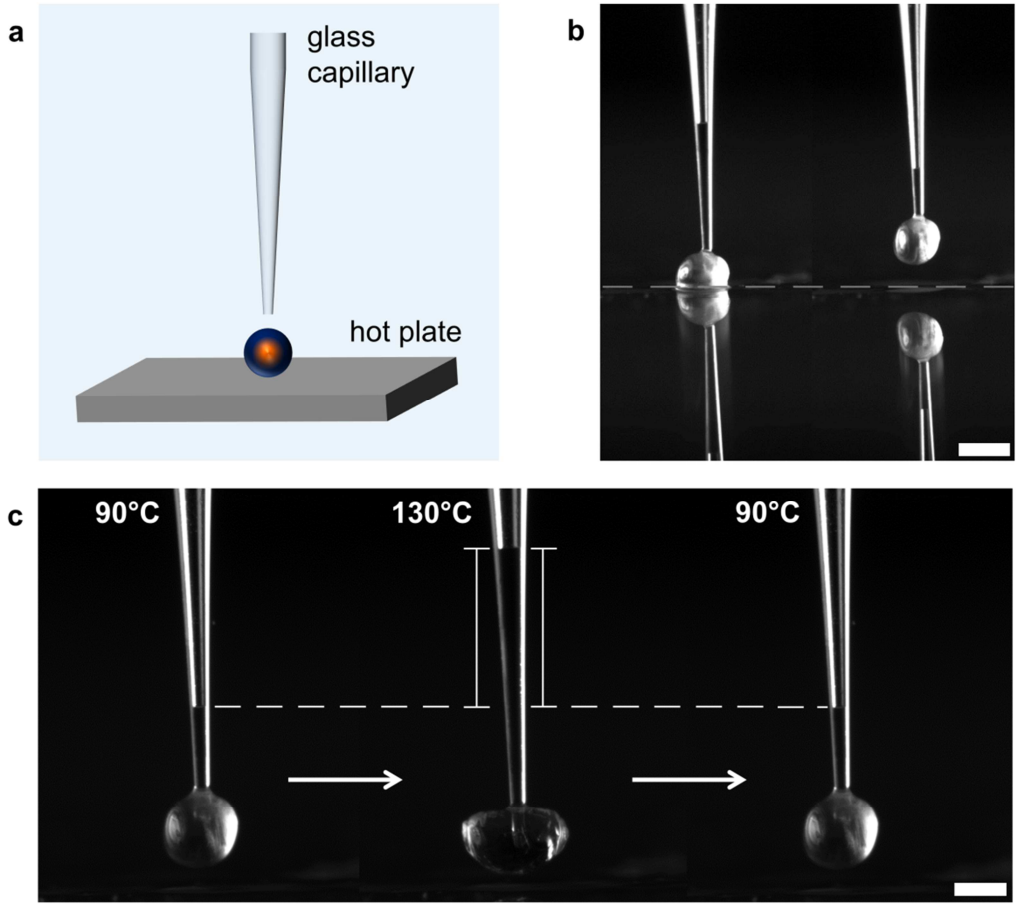

Figure 3: *Core-shell elastomer particles as micropumps.* ***a****, Schematic drawing of the micromanipulator to penetrate the particle shell with a thin glass capillary.* ***b****, Piercing the particle at 90 °C (above its glass transition temperature) squeezes the particle between hotplate and capillary and results in glycerol rising into the capillary. Most liquid sinks back into the core once it is lifted off the hotplate (scale bar 100 µm).* ***c****, When heated to the isotropic phase at 130 °C the phase transition results in a deformation of the LCE shell. The force exerted by the actuating shell pushes the liquid glycerol core into the capillary. Once the particle resumes its former shape in the nematic phase at 90 °C the glycerol sinks to its original level (scale bar 100 µm).*

The hotplate was then set to heat from 90 °C to 130 °C, which corresponds to the liquid crystalline-isotropic transition temperature of the elastomer, and the core-shell particle was slowly lowered towards the hotplate. The emitted heat induced the phase transition from nematic to isotropic within the shell, causing the particle to actuate a few

millimeters away from the surface of the hotplate. At 130 °C, the punctured LC core-shell elastomer reached the isotropic phase and consequently changed its shape, in analogy to the non-punctured particles (see Figure 2) but now at a constant hydrostatic pressure of the glycerol core. The shape deformation is then coupled to a corresponding reduction in core volume, leading to the expulsion of a considerable fraction of the glycerol through the shell hole and thus raising the liquid level in the capillary (Figure 3c).

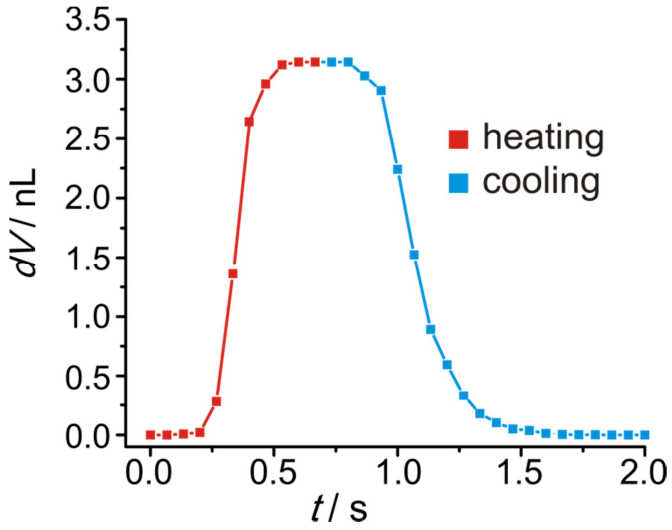

Figure 4: *Response speed of the micropumps upon fast heating and cooling. Heating the particle with a heat gun allows the temperature to be changed sufficiently fast to estimate the speed of actuation and relaxation (turning on and off the heat gun). The graph shows the ejected volume of glycerol as a function of time. The actuation response time is 0.1 s on heating and 0.35 s on cooling.*

Upon cooling, the particle reverts back to its original shape, causing the level of glycerol in the capillary to drop as the liquid is again sucked into the shell. Repeated heating and cooling cycles confirm a completely reversible actuation process through a constant increase and decrease of the glycerol level in the capillary, which is directly correlated with the shape change of the elastomer shell. Supplementary Movie 1 features several heating and cooling cycles of the punctured core-shell elastomer. The actuation response time (defined as the time from 10% to 90% of the final response) of the core-shell elastomer is about 0.1 s when using a heating gun as a fast heating device (see Figure 4). Upon cooling the corresponding relaxation time is about 0.35s, but the increase may here be due primarily to the lack of active cooling. Using simple geometric models we estimated the relative fraction of glycerol that is expelled from the core during

heating. Taking 220 μm as the average diameter of the core, as measured from the optical microscopy images in the isotropic state, and considering the amount of glycerol in the conical tip, the total volume of glycerol amounts to approximately 5.57 nL. Upon actuation of the LCE shell, the meniscus in the capillary rises 740 μm, corresponding to a volumetric change of 3.20 nL. Hence, 64% of the liquid interior is pumped out of and into the LCE shell during one actuation cycle. In comparison, the thermal expansion of glycerol only accounts for a volumetric increase of 0.35 nL. The volume pumped out as a result of the shell actuation is thus at least 2.85 nL.

Determination of the director configuration by WAXS

The actuation behaviour of the elastomer particles is related to the director alignment, which can adopt several possible configurations within the nematic shell[33]. Glycerol as well as silicone oil promote an LC alignment with the mesogens parallel to the interface, so-called planar alignment. Caused by the interplay of liquid crystalline ordering and topological confinement, the spherical topology does not allow for a defect-free planar director field[35], and the total defect sum has to fulfil the condition $s = +2$ on each shell surface (internal and external). We performed wide-angle X-ray scattering (WAXS) experiments on the core-shell particles in order to determine the director configuration within the elastomer shell. The small diameter of the X-ray beam of only 100 μm allowed measurements of different regions within the particle (~500 μm diameter). After a two-dimensional scan to localise the particles on the substrate, measurements were conducted at different points along the two axes *a* and *c* of the particle, as indicated in Figure 5a. The scattering pattern of position 3 is presented in Figure 5b. The scattering intensity profile along the scattering angle 2θ shows two broad reflections (Figure 5d), a commonly observed motif for nematic liquid crystals. The reflection at small angles corresponds to a repeat unit that reflects approximately the mesogen length while the second reflex in the wide-angle regime corresponds to the approximate lateral distance between the mesogens, typically 4.4 Å.

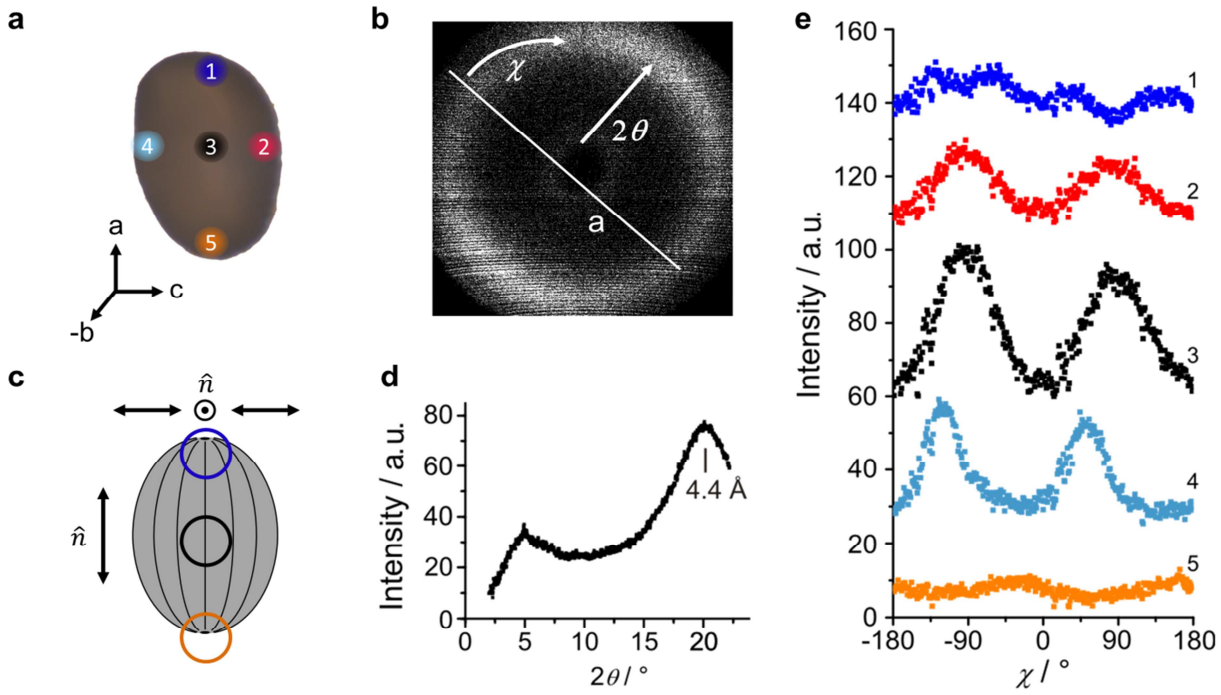

Figure 5: *Determination of the director configuration by WAXS.* ***a****, Positions on the core-shell elastomer particle where the X-ray measurements were performed.* ***b****, The scattering pattern obtained from the centre of the particle (black) as received by the detector exhibits two intensity maxima in the diffuse wide angle signal.* ***c****, Schematic drawing of the bipolar director alignment within the shell, depicted as seen from the outside. The approximate positions of the X-ray beam during the measurements of positions 1, 3 and 5 are highlighted.* ***d****, The diffraction pattern for position 3 shows two characteristic maxima at 5° and 20°, typical for aligned nematic liquid crystals.* ***e****, The intensities I(χ) obtained by radial integration over the wide-angle arc for positions 2, 3 and 4 exhibit two intensity maxima for nematic phases near χ = -90° and +90° and point to a uniform director orientation along the axis a. At the poles of the particle the director n̂ aligns normal to the axis a leading to a 90° shift of the two maxima (position 5). At position 1 the region with the director oriented parallel as well as perpendicular to the axis a is measured by the X-ray beam leading to an intensity distribution I(χ) with four maxima.*

Information about the director orientation is provided by the azimuthal intensity distribution I(χ) of the wide-angle halo (lateral packing). For measurements along the axis *c* (positions 2-4 in Figure 5e), radial integration over the wide-angle arc I(χ) from 2θ = 16.0° to 22.3° yields two intensity maxima near χ = -90° and +90°, which indicates the director $\hat{\mathbf{n}}$ to be aligned parallel to the main axis *a*[36]. In contrast, the radial intensity distributions for positions 1 and 5 near the poles of axis *a* (positions 1 and 5) exhibit intensity maxima at different angles χ. The scattering maxima of position 5 are near χ = 0° and 180° and indicate a local director field normal to the axis *a*. Four distinct

maxima near χ = -90°, 0°, 90°, and 180° observed at position 1 stem from the superposition of local preferential director orientations both normal and parallel to the axis *a*. The locally resolved azimuthal intensity distribution indicates that the director is indeed aligned in a bipolar configuration along the long axis *a*, with point defects situated at the top and bottom of this axis (Figure 5c).

This director field alignment can fully explain the deformation at the phase transition presented in Figure 2. In such a configuration, the director $\hat{\mathbf{n}}$ is preferentially oriented parallel to the axis *a* in most particle regions (positions 2-4), while around the poles the director aligns radial in all possible directions normal to the axis *a* (position 5). For position 1, the X-ray beam with a diameter of 100 μm samples both particle regions with director orientations perpendicular and parallel to axis *a* at the region vicinal to the pole.

X-ray data acquired along the axes *a* and *b* of a particle flipped on its oblate side support our conclusion of a bipolar orientation and are presented in the Supplementary Figures S1-S3. We note that the azimuthal intensity distribution I(χ) also reflects the quality of orientational ordering and can principally be used to determine the orientational order parameter[37,38]. We refrain, however, from such an evaluation procedure because the scattered X-ray intensity beam does not only monitor the oriented nematic shell but also the isotropic core, the admixture of which leads to a significant underestimation of the effective order parameter.

3.2.3 Discussion

Concerning the origin of the biaxial ellipsoidal shape of the elastomers, we identified two anisotropic aspects of the LCE shell production. First, there are two defects in the liquid crystal director fields on opposite sides of the shell, at the front and back as defined by the direction of flow and the repulsion between them can in principle induce an ellipsoidal shape distortion. It is however questionable if the forces involved are strong enough to impose any substantial distortion of the shell shape. Second, and probably more important, the absorption of optical energy during the photo-polymerisation is anisotropic in a fairly complex fashion. The central areas of the shell

can quickly be polymerised on both sides, since the director (and thus the transition moment of the dissolved dye) is in the same plane as the polarization of the UV light and as the thickness traversed at the top of the shell is minimal. Hence, almost the full light intensity also reaches the bottom part of the shell (here we consider the top being closest to the light source). In contrast, the peripheral regimes will be polymerised preferentially on the top side since the light now has a much greater path through the shell, such that much light may be absorbed close to the top, leaving less intensity to polymerise the bottom. Moreover, along the shell perimeter, a considerable difference in polymerisation speed can be expected between the front and back ends, on the one hand, and the intermediate region on the other. This is because the director field in the intermediate region is aligned along the flow; hence the dye transition moment is in the same plane as the light polarization. In contrast, at the front and back, close to the director field defects, the director field is largely vertical, moving the dye transition moment out of the light polarization plane and thus strongly reducing the absorption cross section. Thus, the front and back ends of the shell are expected to polymerise the latest in the process. Together with the change from viscoelastic to elastic behavior and consequent change in mechanical properties as the shell is polymerised, the time difference in polymerisation at different parts of the shell may plausibly be considered to play a major role for the resulting final LCE shell shape.

The director configuration within the LC shell is a direct result from the flow profile during polymerization inside the microfluidic setup. After detachment from the inner and middle fluid streams, the external flow of the surrounding silicone oil induces ~~a~~ shear flow parallel to the general flow direction at the shell exterior surface, whereas a corresponding antiparallel shear flow must occur at the internal interface with the glycerol droplet to conserve the LC phase material. The situation is sketched in Figure 6a for a core-shell droplet that for simplicity is drawn spherical. Singularities in the flow profile occur at the front and back of the shell, and these would be the natural loci of s = +1 director field defects located at each interface (internal and external). Along the shell beyond the two poles we expect the director field to be oriented along the flow profile, since the LC normally aligns in this way to minimize flow resistance (the minimum Miesovicz viscosity η_2 is for shear flow along the director), and thus we would obtain a

shell with bipolar director field. Since the integer defects are point and not line defects, the director field within the shell is expected to 'escape in the third dimension' (using the terminology coined by de Gennes) along the lines connecting the inner and outer s = +1 defects at each pole. The resulting director field is sketched in Figure 6b, as confirmed by our X-Ray measurements described above.

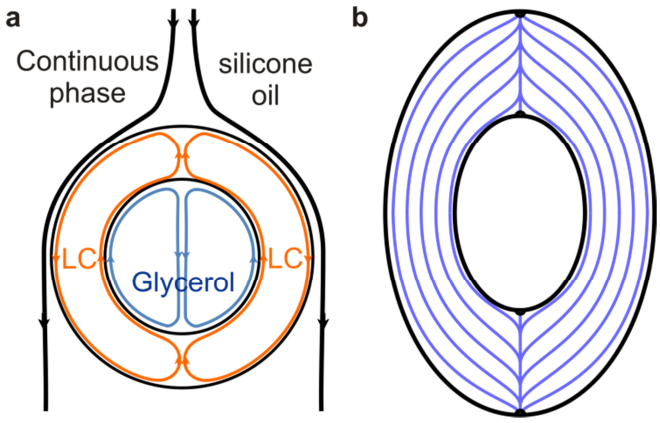

Figure 6: *Expected flow profile in the core-shell particles during polymerization and resulting director configuration.* ***a,*** *The continuous phase silicone oil induces a shear flow parallel to the general flow direction at the exterior surface of the shell. An antiparallel shear flow is created at the interior interface between monomer and glycerol.* ***b,*** *Schematic drawing of the bipolar director alignment within a cross section through the middle of the shell. Singularities in the flow profile create director field defects at the internal and external interfaces.*

The function of core-shell particles as micropumps is directly related to their heat-induced deformation. The change in shape happens because the nematic phase is aligned with the director along one preferred axis defined by the flow[20,29] and this forces the attached polymer backbone to adopt a stretched conformation along the director, a constraint that disappears in the isotropic phase. On heating, the loss of orientational order thus induces a conformational change of the stretched polymer backbone to a coiled conformation[9–13]. For a slightly cross-linked elastomer, this microscopic transition causes a macroscopic shrinkage parallel to the director and an expansion perpendicular to it. The observed shape change of the core-shell elastomers requires a director orientation along the main axis *a* of the shape anisotropic (here ellipsoidal) particles as confirmed by X-ray measurements.

Reciprocating micropumps rely on the periodic compression of tubes or the

movement of membranes for the transport of mass. This entails the use of surrounding machinery, such as a rotor for a peristaltic pump or a reservoir for a diaphragm pump. The here designed micropump from a core-shell elastomer particle already contains an integrated reservoir and thereby reduces problems occurring in hybrid integration, *e.g.* the gluing of components. A feasible approach to integrating our one-piece micropumps into micromechanical systems could be to employ the concept of a valveless micropump [39], in which two antiparallel conical diffuser/nozzle elements form the inlet and outlet of the pump. Due to their opposite geometries they act as flow-rectifying elements and provide a one-way fluid flow. This simple concept nicely illustrates the potential of the presented micropumps as active components on lab-on-chip devices.

3.2.4 Conclusion

In conclusion, we were able for the first time to fabricate actuating core-shell particles from liquid crystal elastomers. Our results illustrate their potential application as micropumps and the feasibility for their integration in microelectromechanical and lab-on-chip systems. Although the presented example is limited to temperature as the response-driving external stimulus, the method of fabrication is general and can easily be adapted to different LCEs or LCE composites. By incorporating azobenzene moieties in the LCE structure the nematic-isotropic transition can be induced by light irradiation instead of heating, thus actuating the micropump by light at constant temperature. Alternatively, by dispersing magnetic or gold nanoparticles within the LCE material, localized inductive or plasmonic heating triggered by electromagnetic irradiation offers an alternative path to trigger the phase transition, and thus the actuation, even when using a temperature-responsive LCE. Using mesogens with a lower clearing temperature a system suitable for pumping aqueous liquids would be achieved.

3.2.5 Methods

Materials and reagents

The liquid crystalline side-chain monomer (4''-Acryloyloxybutyl) 2,5-di(4'-butyloxybenzoyloxy)benzoate was synthesised according to literature[15]. Glycerol was obtained from Fluka. Silicone oil (1000 cSt), photoinitiator Lucirin TPO (2,4,6-trimethylbenzoyldiphenylphosphine oxide) and crosslinker 1,6-hexanedioldiacrylate were purchased from Sigma-Aldrich. The stabilising agent was removed from 1,6-hexanedioldiacrylate by distillation.

The monomer mixture used in the preparation of the core-shell particles was prepared by mixing 90 mol% monomer, 10 mol% crosslinker and 3 wt% photoinitiator in dichloromethane. Prior to use the solvent was evaporated, the mixture was melted at 90 °C and drawn into a PE tube (1.78 mm ID, 2.79 mm OD) connected to the microfluidic channel.

To obtain hydrophobic glass capillaries the silanizing agent trichloro(3,3,3-trifluoropropyl)silane (Aldrich) was used. A stirred solution of 95 vol% ethanol/5 vol% water was adjusted to pH 4 with acetic acid and 2 wt% of the silanizing agent were added. The glass capillaries were dipped into the solution for one minute and afterwards washed with ethanol. The coated capillaries were then cured in a vacuum oven for 1 h at 100 °C.

Microfluidic device

Square and round glass capillaries were purchased from Composite Metal Services (8100-100, inner dimension 1 mm) and Sutter Instrument (B100-50-10, outer diameter 1 mm), respectively. They were tapered by a micropipette puller (Sutter Instrument P97, USA) and cut to desired orifice sizes (100 μm diameter for the square and 20 μm diameter for the cylindrical capillary tip) using a microforge (Narishige MF830, Japan). The openings of the capillaries were connected to syringe pumps (Harvard 33 Double Syringe Pump) via plastic tubings. After shell formation, the droplets were polymerised by a UV-lamp from LOT Oriel LSH302 (500 W) equipped with a waveguide and a 323-358 nm gap filter.

Optical characterization of the core-shell particles

The formation of the core-shell droplets in the microfluidic reactor was observed with the Zeiss stereo microscope Stemi 2000-C equipped with an Olympus XM10 camera. The heating experiments (hot-stage Linkam TMS 94) were visualized with the optical microscope Olympus BX51 equipped with the camera ColorView II.

Measurement of particle size dispersity

The dimensions of the core-shell particles were evaluated under the optical microscope Olympus BX51 equipped with the camera ColorView II, using the imaging software Cell^D. The ellipsoidally shaped particles had to be manually flipped on a glass slide to allow measurements of all three different axes. By default, the core-shell particles tend to lie on their flattest side. This allows the longest axes *a* and *b* to be determined while axis *c* is oriented along the direction of view. The particle was then flipped 90° about axis *a*, such that axis *c* could be measured. Inevitably, when doing such a sensitive manipulation by hand, the tilting angle was not always precisely 90° and the particles were easily askew, leading to less accurate size determination and consequently slightly larger size dispersities for axes *b* and *c* than for axis a (see Supplementary Figure S4 for bar plots). A total of 20 particles were measured, giving the following results: axis *a*: 545 μm (±10 μm, 2%); axis *b*: 413 μm (±18 μm, 4%); axis *c*: 364 μm (±12 μm, 3%).

Wide-angle X-ray scattering (WAXS) experiments

The WAXS-experiments were performed with a Bruker NanoStar diffractometer, equipped with a HiStar area detector and crossed Goebel mirrors, using CuK_α (λ = 1.5418 Å) radiation.

Acknowledgements

We thank Dorothee Nonnenmacher for helpful discussions concerning the WAXS results. This work was financially supported by the DFG (Germany; grant nr. Ze 230/19-

1), IRTG Mainz – Seoul (= GRK 1404), the SNU-AICT (Korea; grant nr. 490-20100024), the NRF (Korea; grant nr. 490-20110016), as well as the DAAD (study and visiting stipends, respectively, for H.L.L. and J.L.).

Author contributions

E.K.F., H.L.L., J.L. and R.Z. conceived and designed the experiments. E.K.F. and H.L.L. carried out the experiments, analysed and interpreted the data, and co-wrote the article. N.K. and E.K.F. performed the WAXS measurements, analysed and interpreted the data. H.L.L., E.K.F., N.K., F.G., J.L. and R.Z. discussed the results and commented on the manuscript at all stages.

3.2.6 References

1. Amato, I. Micromachines: Fomenting a revolution, in miniature. *Science* **282,** 402–405 (1998).
2. Arlett, J., Myers, E. & Roukes, M. Comparative advantages of mechanical biosensors. *Nat. Nanotechnol.* **6,** 203–215 (2011).
3. Beeby, S., Ensell, G., Kraft, M. & White, N. *MEMS mechanical sensors* Ch. 2.2 Materials 7–11 (Artech House, Inc., Boston, 2004).
4. Mirfakhrai, T., Madden, J. D. W. & Baughman, R. H. Polymer artificial muscles. *Mater. Today* **10,** 30–38 (2007).
5. Behl, M., Razzaq, M. Y. & Lendlein, A. Multifunctional shape-memory polymers. *Adv. Mater.* **22,** 3388–3410 (2010).
6. Yu, Y. & Ikeda, T. Soft actuators based on liquid-crystalline elastomers. *Angew. Chem. Int. Edit.* **45,** 5416–5418 (2006).
7. Woltman, S. J., Jay, G. D. & Crawford, G. P. Liquid-crystal materials find a new order in biomedical applications. *Nat. Mater.* **6,** 929–938 (2007).
8. Camacho-Lopez, M., Finkelmann, H., Palffy-Muhoray, P. & Shelley, M. Fast liquid-crystal elastomer swims into the dark. *Nat. Mater.* **3,** 307–310 (2004).
9. Brand, H. R. & Finkelmann, H. *Handbook of Liquid Crystals* (eds Demus, D. Goodby, J. Gray, G.W. Spiess H.W. Wiley-VCH, Weinheim, Germany, 1998).
10. Terentjev, E. M. Liquid-crystalline elastomers, *J. Phys.-Condens. Mat.* **11,** R239 (1999).
11. de Gennes, P. G. One type of nematic polymers, *C. R. Hebd. Seances Acad. Sci. Ser. B* **281,** 101–103 (1975).
12. Warner, M. & Terentjev, E. M. *Liquid Crystal Elastomers (International Series of Monographs on Physics)*, (Oxford University Press, USA, 2007).
13. Ohm, C., Brehmer, M. & Zentel, R. Liquid crystalline elastomers as actuators and sensors. *Adv. Mater.* **22,** 3366–3387 (2010).
14. Yang, H. *et al.* Micron-sized main-chain liquid crystalline elastomer actuators with ultralarge amplitude contractions. *J. Am. Chem. Soc.* **131,** 15000–15004 (2009).
15. Thomsen, D. L. *et al.* Liquid crystal elastomers with mechanical properties of a muscle. *Macromolecules* **34,** 5868–5875 (2001).
16. Kupfer, J. & Finkelmann, H. Nematic liquid single-crystal elastomers. *Makromol. Chem.-Rapid* **12,** 717–726 (1991).

17. Buguin, A., Li, M. H., Silberzan, P., Ladoux, B. & Keller, P. Micro-actuators: When artificial muscles made of nematic liquid crystal elastomers meet soft lithography. *J. Am. Chem. Soc.* **128,** 1088–1089 (2006).

18. Ohm, C., Haberkorn, N., Theato, P. & Zentel, R. Template-based fabrication of nanometer-scaled actuators from liquid-crystalline elastomers. *Small* **7,** 194–198 (2011).

19. van Oosten, C. L., Bastiaansen, C. W. M. & Broer, D. J. Printed artificial cilia from liquid-crystal network actuators modularly driven by light. *Nat. Mater.* **8,** 677–682 (2009).

20. Ohm, C. *et al.* Microfluidic synthesis of highly shape-anisotropic particles from liquid crystalline elastomers with defined director field configurations. *J. Am. Chem. Soc.* **133,** 5305–5311 (2011).

21. Ohm, C. *et al.* Preparation of actuating fibres of oriented main-chain liquid crystalline elastomers by a wetspinning process. *Soft Matter* **7,** 3730–3734 (2011).

22. Selinger, R. L., Mbanga, B. L. & Selinger, J. V. Modeling liquid crystal elastomers: actuators, pumps, and robots. *Proc. SPIE,* 69110A (2008).

23. Yamada, M. *et al.* Photomobile polymer materials: Towards light-driven plastic motors. *Angew. Chem. Int. Edit.* **47,** 4986–4988 (2008).

24. Sánchez-Ferrer, A. *et al.* Liquid-crystalline elastomer microvalve for microfluidics. *Adv. Mater.* **23,** 4526-4530 (2011).

25. Unger, M. A., Chou, H. P., Thorsen, T., Scherer, A. & Quake, S. R. Monolithic microfabricated valves and pumps by multilayer soft lithography. *Science* **288,** 113–116 (2000).

26. Haseloh, S., van der Schoot, P. & Zentel, R. Control of mesogen configuration in colloids of liquid crystalline polymers. *Soft Matter* **6,** 4112 (2010).

27. Utada, A. S. *et al.* Dripping, jetting, drops, and wetting: The magic of microfluidics. *MRS Bull.* **32,** 702–708 (2007).

28. Chung, K.-Y., Mishra, N. C., Wang, C.-C., Lin, F.-H. & Lin, K.-H. Fabricating scaffolds by microfluidics. *Biomicrofluidics* **3,** 22403 (2009).

29. Ohm, C., Fleischmann, E.-K., Kraus, I., Serra, C. & Zentel, R. Control of the properties of micrometer-sized actuators from liquid crystalline elastomers prepared in a microfluidic setup. *Adv. Funct. Mater.* **20,** 4314–4322 (2010).

30. Ohm, C., Serra, C. & Zentel, R. A continuous flow synthesis of micrometer-sized actuators from liquid crystalline elastomers. *Adv. Mater.* **21,** 4859-4862 (2009).

31. Lopez-Leon, T., Koning, V., Devaiah, K. B. S., Vitelli, V. & Fernandez-Nieves, A. Frustrated nematic order in spherical geometries. *Nat. Phys.* **7,** 391–394 (2011).

32. Lopez-Leon, T., Fernandez-Nieves, A., Nobili, M. & Blanc, C. Nematic-smectic transition in spherical shells. *Phys. Rev. Lett.* **106,** 247802 (2011).

33. Fernández-Nieves, A., Link, D. R., Márquez, M. & Weitz, D. A. Topological changes in bipolar nematic droplets under flow. *Phys. Rev. Lett.* **98,** 87801 (2007).

34. Liang, H.-L., Schymura, S., Rudquist, P. & Lagerwall, J. Nematic-smectic transition under confinement in liquid crystalline colloidal shells. *Phys. Rev. Lett.* **106,** 247801 (2011).

35. Nelson, D. R. Toward a tetravalent chemistry of colloids. *Nano Lett.* **2,** 1125–1129 (2002).

36. Seddon, J. M. in *Handbook of Liquid Crystals* Vol. 1 (eds Demus, D. Goodby, J. Gray, G.W. Spiess H.W.) Ch. Fundamentals 633–678 (Wiley-VCH, Weinheim, Germany, 1998).

37. Giesselmann, F., Germer, R. & Saipa, A. Orientational order in smectic liquid-crystalline phases of amphiphilic diols. *J. Chem Phys.* **123,** 034906 (2005).

38. Davidson, P., Petermann, D. & Levelut, A. M. The measurement of the nematic order parameter by X-ray scattering reconsidered. *J. Phys. II (Paris)* **5**, 113-131 (1995).

39. Stemme, E. & Stemme, G. A valveless diffuser/nozzle-based fluid pump. *Sensor. Actuat. A-Phys.* **39,** 159–167 (1993).

3.2.7 Supplementary Information

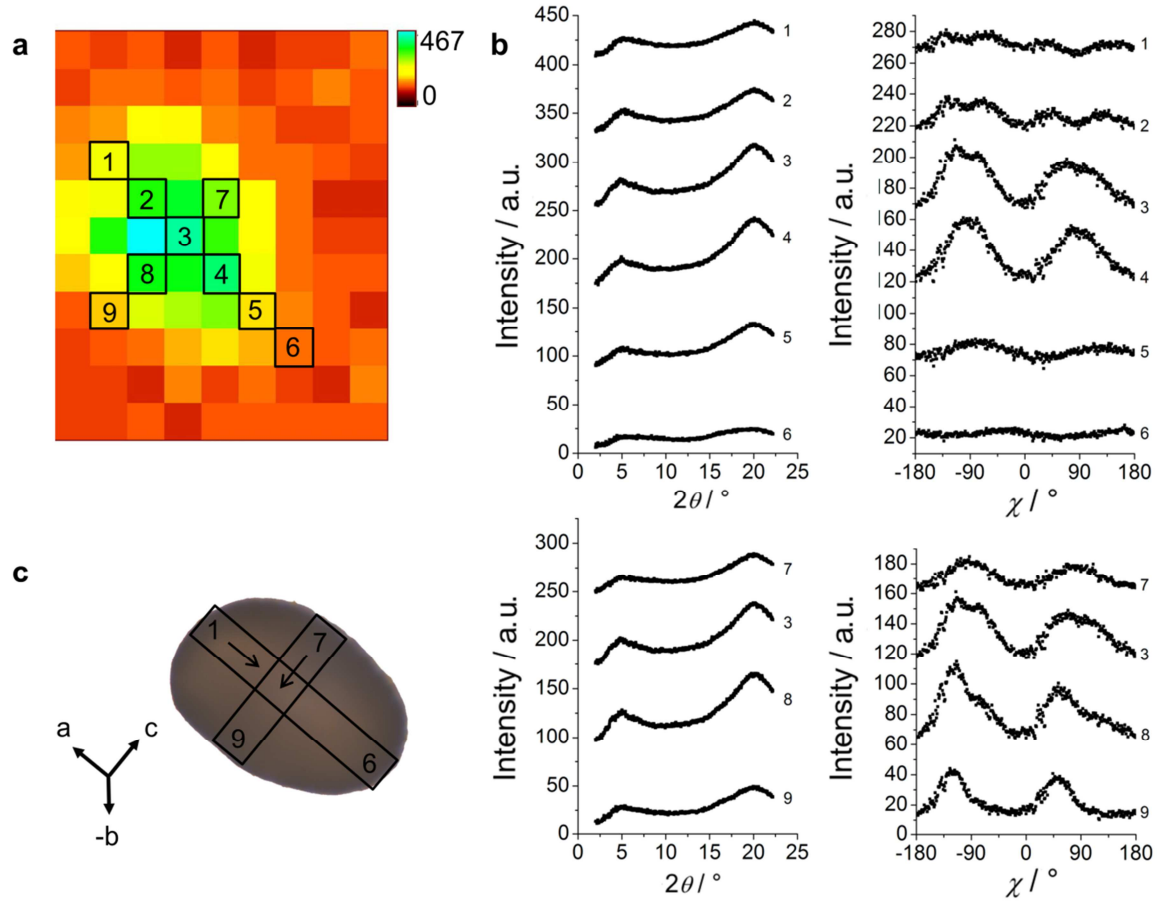

Supplementary Figure S1 | Detailed representation of the WAXS data of the LCE core-shell particle in Figure 4. a, X-ray absorption scan to localize the core-shell particle on the substrate. The particle was placed on a low-scattering adhesive stripe attached to the sample holder. Measurements were conducted along the axis *a* and *c* of the particle. **b**, Diffraction patterns I(2θ) and their corresponding azimuthal intensity distribution I(χ) for all measured positions: $\chi = 0°$ was shifted to compensate the tilted position of 60° of the core-shell particle with respect to the X-ray beam as seen in the nanography. The diffraction patterns I(2θ) show two broad halos as expected for nematics. A detailed explanation for the observed azimuthal intensity distributions I(χ) is given in the main text. **c**, Light microscope photo of the particle with a graphical representation of the particle regions sampled by the X-ray beam.

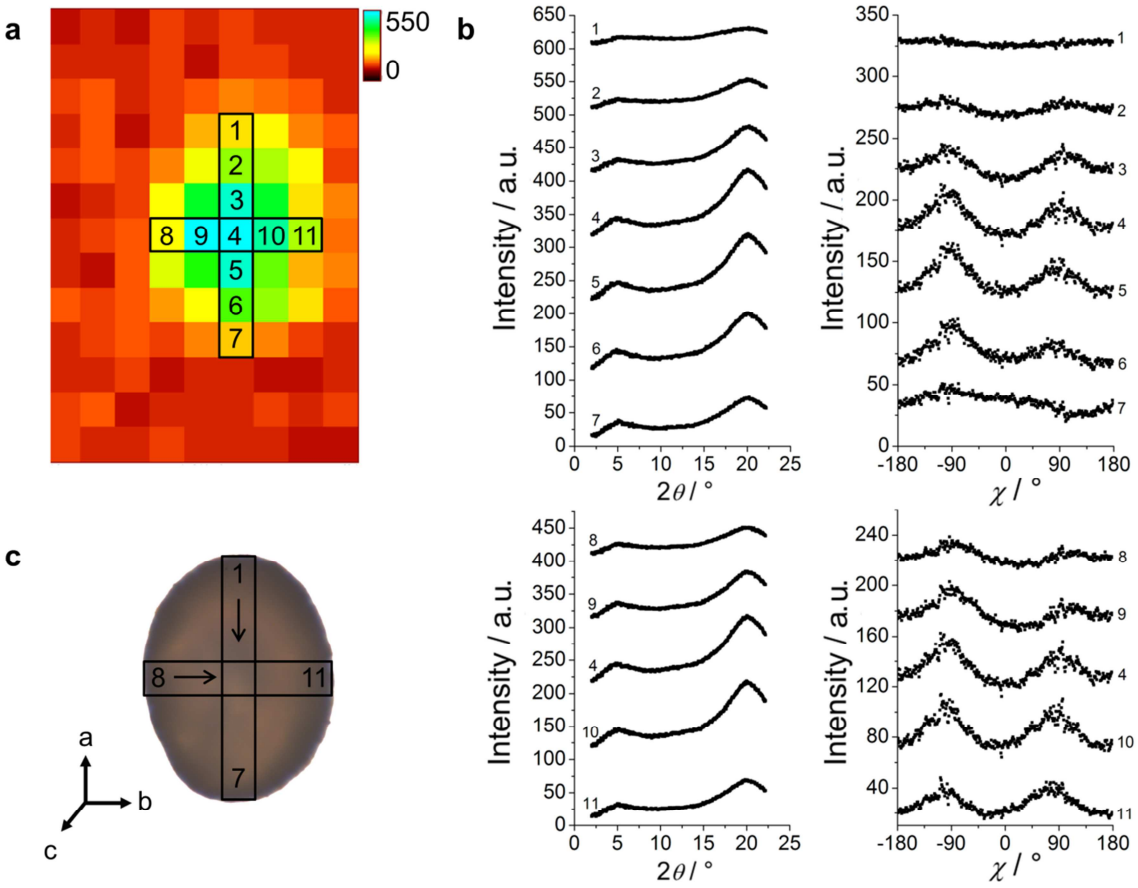

Supplementary Figure S2 | WAXS data of a second LCE core-shell particle flipped on its oblate side. a, X-ray absorption scan. Measurements were conducted along the axis *a* and *b* of the particle. **b,** Diffraction patterns I(2θ) and azimuthal intensity distributions I(χ). With two maxima at χ = -90° and +90° the radial intensity distributions I(χ) of the wide-angle halo indicate a director orientation along the long axis *a* of the particle. At positions 1 and 7, the top and bottom of axis *a*, the maxima deviate caused by the locally changing director field n̂ at the poles of the particle. **c**, Position of the particle on the substrate with respect to the X-ray beam, as observed with light microscopy.

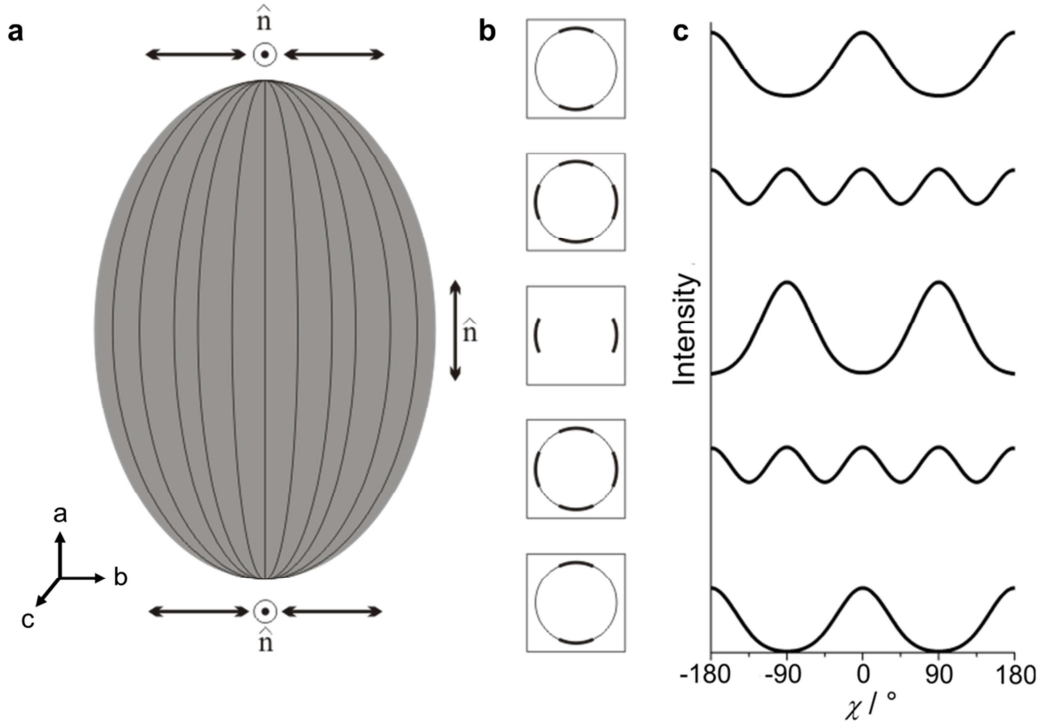

Supplementary Figure S3 | Influence of the director configuration on the azimuthal intensity distribution I(χ). **a**, Schematic drawing of the bipolar director alignment within the shell. **b**, Two-dimensional X-ray patterns measured at different positions along the axis *a* in the particle. **c**, Integration of the X-ray pattern in dependence of the azimuthal angle χ. At the top and the bottom of the particle the director is aligned perpendicular to the axis *a* which leads to two maxima in the integrated X-ray intensity I(χ) at χ = 0° and 180°. In the middle of the particle the director n̂ aligns parallel to the axis *a*. The intensity profile shows here also two maxima which are now located at the angles χ = 90 and -90°. If the X-ray measurements are performed close to the top or the bottom of the particle both orientations of the director can be observed. In this case, the intensity profile I(χ) shows four distinct maxima.

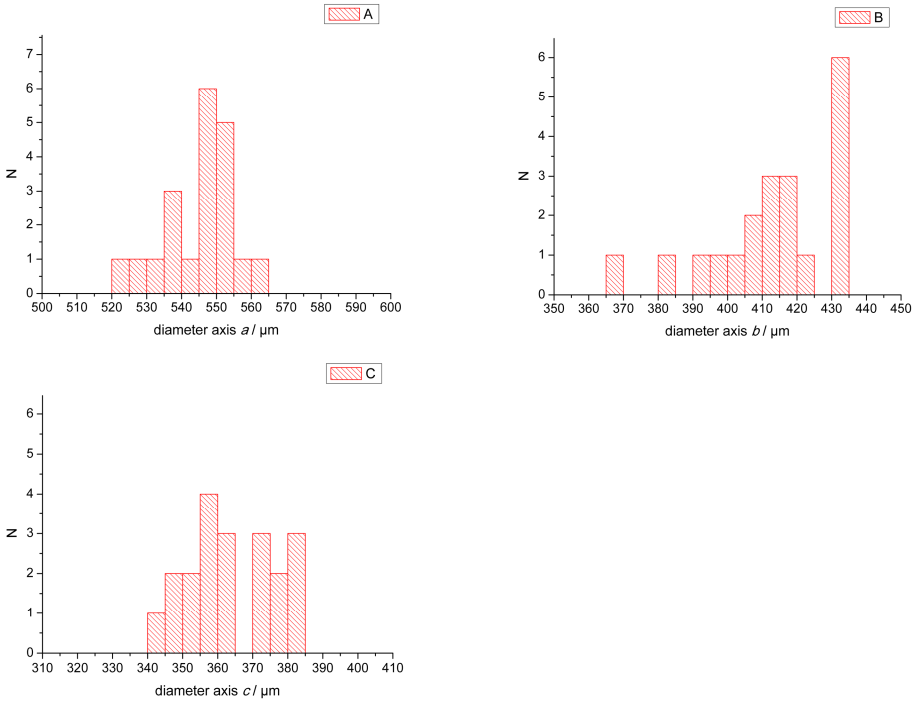

Supplementary Figure S4 | Bar plots of the particle size dispersity. 20 Particles were measured in total, giving the following results: axis A: 545 µm (±10 µm, 2%); axis B: 413 µm (±18 µm, 4%); axis C: 364 µm (±12 µm, 3%).

Supplementary Table S1 | Temperature dependence of glycerol viscosity. The viscosity values of glycerol in the temperature range relevant for this study decrease as follows.

T (°C)	viscosity (P)
37.0	3.8
42.0	2.7
48.0	1.8
60.0	0.9
65.0	0.7
73.0	0.5
83.0	0.4
90.0	0.3
130.0	0.3

3.3 Preparation of soft microactuators in a continuous flow synthesis using a liquid crystalline polymer crosslinker

Eva-Kristina Fleischmann[1], Christian Ohm[1,3], Christophe Serra[2], Rudolf Zentel[1,*]

[1]*Institute of Organic Chemistry, Johannes Gutenberg-Universität Mainz, D-55099 Mainz, Germany*

[2]*Groupe d'Intensification et l'Intrapolation des Procédés Polymères (G2IP) - Laboratoire d'Ingénierie des Polymères pour les Hautes Technologies (LIPHT) – EAc(CNRS) 4379, Ecole de Chimie Polymères et Matériaux (ECPM), Université de Strasbourg (UdS), F-67087 Strasbourg Cedex 2, France*

[3]*Current address: Material Science & Engineering, Cornell University, Ithaca, NY 14853-1501, USA*

*Corresponding author: zentel@uni-mainz.de

Keywords:

crosslinking; liquid crystalline elastomers (LCE); microfluidics; reversible addition–fragmentation chain transfer (RAFT); stimuli-sensitive polymers

Abstract

We present the synthesis of a polymeric liquid crystalline (LC) crosslinker and its usage in the preparation of soft microactuators. The microactuators, comprised of thermoresponsive liquid crystalline elastomers (LCE), are fabricated in a microfluidic device in a continuous "on the fly" process. The LC polymer crosslinker is miscible with the LC monomer and provides for a rapid polymerization and crosslinking. Most importantly it promotes an enantiotropic mesophase of the mobile monomer phase, which is not provided by conventional non-mesogenic crosslinkers. This allows an isothermal handling inside the microfluidic setup. Temperature-driven shape changes up to 65% could be achieved by judiciously optimizing the crosslinking density of the LCE particles.

3.3.1 Introduction

Liquid crystals are an attractive class of self-organizing materials with a wide field of applications. Due to their form anisotropic structure, liquid crystals form so-called mesophases, in which they adopt a certain degree of positional order.[1] If covalently linked to a polymer, the spontaneous self-organization of liquid crystals contrasts the entropy-driven behavior of the polymer backbone. In their liquid crystalline state, the mesogens force the polymer backbone into a partially stretched conformation, while in their isotropic state the mesogens arrange randomly and allow the polymer backbone to adopt a random coil conformation. If the mesogens are aligned along a common director, the liquid crystalline-isotropic phase transition results in a macroscopic shape change of a slightly crosslinked polymer network, making such liquid crystalline elastomers (LCEs) suitable as soft actuators.[2–4] The phase transition can be triggered by external stimuli, the most common being temperature and light.

Traditionally, a uniform orientation of the director is achieved by a two-step crosslinking process of a previously stretched macroscopic film[5] or the application of electric[6] or magnetic fields.[7] Recently, microfluidic flow profiles have been exploited for the fabrication of oriented, microscopic LCEs with morphologies different from those of typical LCE films.[8] Microfluidic devices have become an important tool for the handling and transport of liquids and gasses in a controlled environment, with micropumps and valves enabling an accurate preparation and dosage of mixtures and emulsions.[9] In materials science and engineering technology, microfluidics allows for the fabrication of numerous materials with precise control over the particles' size and shape as well as composition and morphology.[10–12] For example, a continuous "on-the-fly" preparation of monodisperse polymer beads was achieved by dispersing monomer droplets in a co-flowing continuous phase and subsequent UV-initiated photopolymerization.[13,14] We adapted this process for the fabrication of LCE microactuators.[15] LCE particles with a defined size and narrow size dispersity were produced from a mixture of the nematic thermoresponsive mesogen **M1**, the commercial low-molecular weight crosslinker hexanedioldiacrylate and the photoinitiator Lucirin TPO. The microscopic LCE particles exhibited excellent actuation properties with shape

changes up to 80% and are suitable for the integration into lab-on-chip and microelectromechanical systems.[2,8,16]

A challenge in the fabrication process of oriented LCEs is the necessity of a temperature-controlled environment. The liquid crystalline order of the material needs to be permanently fixed by crosslinking within the LC phase. However due to the addition of the non-mesogenic crosslinking agent hexanedioldiacrylate, only a monotropic nematic mesophase forms upon cooling of the melt of the monomer mixture. This imposes certain temperature limitations to the microfluidic device. The monomer droplets have to be formed in the liquid isotropic state (non-oriented), while the UV-induced polymerization has to be performed at lower temperatures within the nematic mesophase of the monomer mixture (oriented). To simplify this complicated fabrication process, we aimed at modifying the components and composition of the monomer mixture such that macroscopically oriented LCE particles can be produced at a single temperature within the nematic mesophase of the mixture. This can be achieved by replacing the non-LC crosslinker hexanedioldiacrylate by a mesogenic crosslinker. The stabilizing effect of the latter converts the metastable monotropic mesophase of the reaction mixture into a stable enantiotropic mesophase, which can also be accessed by heating of the mixture. Since the microfluidic processing also requires a rapid "on-the-fly" photo-polymerization and crosslinking of the formed monomer droplet, we decided on designing a poly-functional crosslinker, which promotes a rapid conversion of the mixture. The two above-mentioned requirements can conveniently be met by a polymeric crosslinker containing both mesogenic and reactive acrylate units. In the following, the synthesis of such a crosslinker system and its successful application in the fabrication of actuating LCE particles is presented. Additional amenities of the novel crosslinker including reduced leakage properties and promotion of laminar flow conditions are discussed in light of the corresponding characterization techniques.

3.3.2 Experimental Section

Materials

The radical initiator 2,2′-azobisisobutyronitrile (AIBN, from Fluka) was recrystallized from diethyl ether prior to use. Silicone oil (100 cSt and 1000 cSt), the photoinitiator Lucirin TPO (2,4,6-trimethylbenzoyldiphenylphosphine oxide), acryloylchloride, 4-hydroxybutylacrylate and the crosslinker hexanedioldiacrylate were purchased from Sigma-Aldrich. The stabilizing agents were removed from 4-hydroxybutylacrylate using an inhibitor remover column and from hexanedioldiacrylate by distillation. The liquid crystalline side-chain monomer **M1** (4″-acryloyloxybutyl) 2,5-di(4′-butyloxybenzoyloxy)benzoate[17] and the chain transfer agent (CTA) benzyldithiobenzoate[18] were synthesized according to the literature. The solvents dioxane and THF were dried over sodium and distilled before use.

Synthesis

The crosslinker polymers **CrP** were prepared by a two-step synthetic scheme as depicted in Figure 1. Detailed information on the copolymer compositions and the corresponding amounts of reagents can be found in the Supplementary Information. In the first step, AIBN and the RAFT agent benzyldithiobenzoate were added to a solution of the mesogen (**M1**) and 4-hydroxybutylacrylate (**M2**) in dioxane. The reaction mixture was degassed with three freeze-pump-thaw cycles and the polymerization was carried out in a Schlenk tube under nitrogen atmosphere at 80°C for 3 days. The resulting copolymer **CoP** was precipitated two times in cold methanol. The homopolymer **HoP** of **M1** was synthesized analogously for reference purposes. The percentage of the co-monomer 4-hydroxybutylacrylate was varied and the amount incorporated in the polymer was determined by ^{1}H NMR spectroscopy. ^{1}H NMR data for the synthesized polymers is given in Table S3. Exemplary ^{1}H NMR data for **CoP4**: ^{1}H NMR (400 MHz, $CDCl_3$) δ = 0.97 (br, 6H; CH_3), 1.48 – 1.85 (br, 12H; CH_2, 3.5H; CH_2), 3.51 (br, 1.7H; CH_2OH), 3.80-4.19 (br, 6H, CH_2O, 2H; CH_2OCO, 1.7H; CH_2OCO), 6.96 (br, 4H; Ar H), 7.24 (br, 1H; Ar H), 7.43 (br, 1H; Ar H), 7.86 (br, 1H; Ar H), 8.12 (br, 4H; Ar H).

In the second step, the crosslinking unit was attached by esterification of the hydroxyl groups within the copolymer. *Tert*-butylparacresol was added as an inhibitor to prevent crosslinking during the synthesis. The amounts of base and acryloylchloride were chosen according to the number of hydroxyl groups in the copolymer. 6 eq. acryloylchloride were added dropwise to an ice-cooled solution of copolymer and 4 eq. triethylamine in chloroform. After warming to room temperature the reaction mixture was stirred for 48 hours. The resulting crosslinker polymer **CrP** was purified by twofold precipitation in cold methanol with quantitative yields. Exemplary ^{1}H NMR data for **CrP4**: ^{1}H NMR (400 MHz, $CDCl_3$) δ = 0.96 (br, 6H; CH_3), 1.48 – 1.85 (br, 12H; CH_2, 3.5H; CH_2), 3.47 (br, 0.8H; CH_2OH), 3.80-4.11 (br, 6H; CH2O, 2H; CH_2OCO, 1.7H; CH_2OCO), 5.74-6.31 (br, 1.2H; $CH=CH_2$), 6.93 (br, 4H; Ar H), 7.21 (br, 1H; Ar H), 7.41 (br, 1H; Ar H), 7.83 (br, 1H; Ar H), 8.09 (br, 4H; Ar H).

Microfluidic Processing

The microactuators were produced in a microfluidic setup in a co-flowing ambient fluid. The monomer mixture used as the dispersed phase in the microfluidic setup contained the mesogen **M1**, the polymer crosslinker **CrP** and 3 wt% photoinitiator Lucirin TPO in dichloromethane. After evaporation of the solvent, the mixture was heated to the isotropic state and filled into a PTFE tube (ID 1.59 mm). The tube was mounted between two PTFE tubes (OD 1.59 mm), one of which was filled with silicone oil (100 cSt) and connected to the syringe pump (Harvard 33). The second PTFE tube was connected to the T-junction. The second inflow into the T-junction is the continuous phase silicone oil (1000 cSt). The dispersed phase was pushed through a fused silica capillary (ID: 100 μm, OD: 165 μm) leading into a PTFE tube (ID: 750 μm). The resulting particles were irradiated with a LOT Oriel LSH302 500 W UV lamp equipped with a 365 nm line filter and a waveguide. The setup was immersed into a water bath and heated to a temperature within the nematic phase of the monomer mixture.

Characterization

^{1}H NMR spectra were acquired in $CDCl_3$ at room temperature on a Bruker Avance II spectrometer at a ^{1}H Larmor frequency of 400 MHz. The molecular weight of the synthesized polymers (given in the Supplementary Information) was determined by gel permeation chromatography (GPC) in 2 mg/mL THF with polystyrene as external standard. Differential scanning calorimetry (DSC) measurement was carried out on a Perkin-Elmer DSC 7 calibrated with lead and indium standards (Figure S7). Typical heating/cooling rates were 10 °C min^{-1}. The temperature-triggered actuation of the LCE particles (placed on the hot-stage Linkam TMS 94) was recorded by the optical microscope Olympus BX51 equipped with the camera ColorView II and the micrographs were further evaluated using the imaging software Cell^D. Viscosity measurements were conducted with a cone-plate viscometer (Advanced Rheometer AR 1000, TA Instruments) with a shear rate of 100 s^{-1} between 50 °C and 100 °C with a constant heating rate of 1 °C min^{-1}. The interfacial tension was measured with a pendant drop apparatus and the resulting data were evaluated with the program Pendant Drop Analysis PDA 3.1.[19,20]

3.3.3 Results and Discussion

To design a poly-functional crosslinker we decided on using a polymer with several crosslinkable units. To promote miscibility and prevent phase separation between the mesogenic monomer **M1** and the polymer crosslinker we incorporated **M1** units into the crosslinker. These **M1** units also provide for the mesogenic properties of the crosslinker. The synthesis of the crosslinker polymers **CrP**$_n$ is schematically depicted in Figure 1A. The mesogen **M1** was copolymerized with monomer **M2**, 4-hydroxybutylacrylate. Similar side-on mesogen/hydroxyl-functionalized copolymer systems have been synthesized by using ATRP.[21,22] We added the chain transfer agent benzyldithiobenzoate providing for a controlled radical polymerization of the monomers **M1** and **M2**. This so-called RAFT polymerization allows the synthesis of polymers with a defined structure and molecular weight.[23,24] We were aiming at low molecular weight

polymers, since a high molecular weight polymer substantially increases the viscosity of the material. This is problematic for its processing in the microfluidic setup since it may clog the thin capillary used in the device.

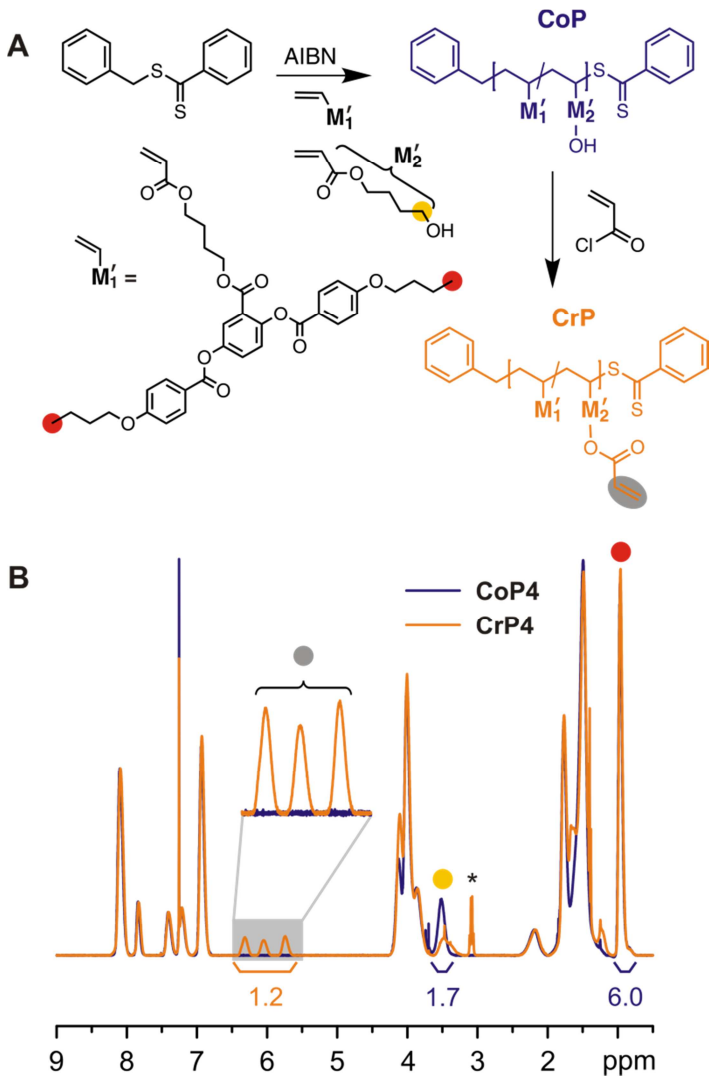

Figure 1. A *Reaction scheme for the synthesis of the crosslinker polymer* ***CrP****. A copolymer* ***CoP*** *is synthesized from the reactive mesogen* ***M1*** *and 4-hydroxybutylacrylate* ***M2*** *using the RAFT agent benzyldithiobenzoate for a controlled polymerization. The crosslinking double bond is introduced into the polymer* ***CrP*** *through esterification with acryloyl chloride.* ***B*** *^{1}H NMR spectra of* ***CoP4*** *(blue) and* ***CrP4*** *(orange) acquired in $CDCl_3$. Colored circles assign certain ^{1}H moieties of the copolymer to their respective signals in the NMR spectrum. Signals from residual solvent impurities are marked with an asterisk.*

After copolymerization of the monomers **M1** and **M2**, the crosslinkable unit was introduced to the polymer through a polymer functionalization of **CoP**. In this reaction, the hydroxyl group of **M2** is converted into a crosslinkable unit by esterification with

acryloyl chloride.[7] An exemplary ^{1}H NMR spectrum of the polymers **CoP4** (blue) and **CrP4** (orange) is shown in Figure 1B. The amount of **M2** incorporated into **CoP** can easily be determined by relating the integrals of the NMR signals for the CH_3 groups of **M1** (0.9 ppm, marked yellow) and the C**H**$_2$OH group of **M2** (3.5 ppm, marked red). After the polymer functionalization, the intensity of the C**H**$_2$OH signal decreases, since the chemical shift of the CH_2 group in vicinity to the converted esterified hydroxyl group is displaced to higher frequencies (4.2 ppm). Since the conversion is not complete the original C**H**$_2$OH signal does not fully disappear. The success of the polymer functionalization is further demonstrated by the appearance of three signals (marked gray) at 6 ppm corresponding to the protons of the acrylate double bond. A list of the synthesized crosslinker polymers and their specific composition derived from the NMR spectra as well as data for the homopolymer **HoP** of **M1** are given in Table 1.

Table 1: *Summary of the synthesized polymer crosslinkers* ***CrP$_n$*** *by polymer functionalization of* ***CoP$_n$*** *(see Figure 1).* ***CoP6*** *exhibits no mesophase due to the high amount of incorporated* ***M2*** *and was not converted to* ***CrP6****. The amounts of* ***M2*** *and crosslinkable units were determined by ^{1}H-NMR spectroscopy.*

Polymer	Amount M2 / mol%	M_n / g/mol	PDI	T(Cr,N) / °C	T(N,Iso) / °C	Amount of crosslinkable units / mol%
HoP	0	3580	1.2	46.7	101.7	0
CrP1	9.1	2822	1.1	90	141	1
CrP2	24.0	3198	1.4	80	113	4
CrP3	44.3	6636	1.6	60	78	15
CrP4	46.5	7365	1.9	50	74	29
CrP5	50.4	9361	2.3	40	62	21
CoP6	85.7	2842	1.5	no mesophase		--

All copolymers exhibit a stable nematic mesophase on repeated heating and cooling cycles as revealed by optical microscopy with crossed polarizers (Figure 2A). The occurrence and temperature range of the nematic phase strongly depends on the ratio between the mesogenic monomer **M1** and the isotropic monomer **M2** in the copolymer. An increasing amount of **M2** causes the phase transition temperatures and the temperature range of the nematic phase to decrease. For **CoP6** containing 85.7 mol% **M2**,

there are too few mesogenic units in the polymer to provide for a liquid crystalline phase which is in accordance with previous works on thermotropic liquid crystalline polymers.[25,26] Compared to the homopolymer **HoP**, the polymer **CoP1** exhibits a higher clearing temperature even though it contains a non-mesogenic component. This might be due the fact that a minimum amount of non-mesogenic comonomer acts as relieve for the sterically demanding mesogenic units **M1**. Such, the flexibility of the polymer backbone is increased and the mesophase is stabilized.[27]

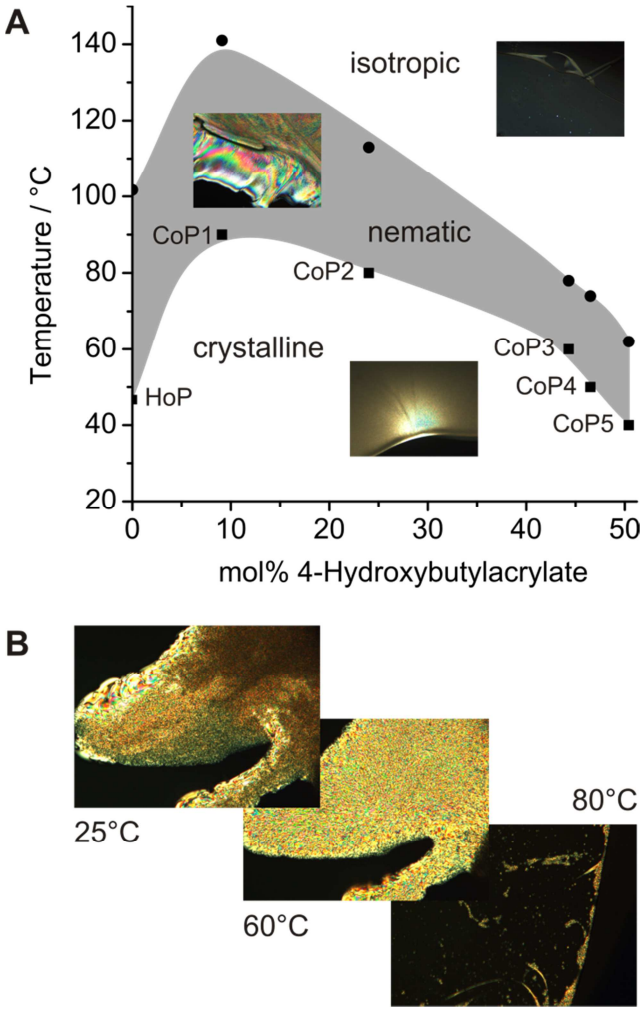

Figure 2. ***A*** *Phase diagram of the polymers* ***HoP*** *and* ***CoP****, all of which exhibit a nematic mesophase. The insets shows representative micrographs of polymer* ***CoP4*** *at 40°C, 55°C, and 74°C in its semicrystalline, nematic, and isotropic phase, respectively.* ***B*** *Micrographs of a mixture containing 77 wt% monomer* ***M1****, 20 wt%* ***CrP4****, and 3 wt% photoinitiator Lucirin TPO, which is used for the microfluidic fabrication of LCE particles. The mixture exhibits a stable enantiotropic mesophase between 60°C and 75°C on heating, despite the high relative ratio of polymeric crosslinker containing 46.5 mol% non-mesogenic units.*

To demonstrate miscibility of the crosslinker polymers with monomer **M1** and their ability to promote a stable enantiotropic nematic mesophase, a mixture of monomer **M1** with 20 wt.% **CrP4** and 3 wt.% photoinitator Lucirin TPO was prepared (**MM6**). **MM6** contains the highest amount of converted and non-converted 4-hydroxybutylacrylate units of all monomer mixtures in this study. It is thus well-suited to act as reference point for the phase behavior of other mixtures containing less non-mesogenic units. Despite its high amount of non-mesogenic units (47 mol%), **CrP4** promotes a stable nematic phase of the mixture on heating, with a (semi)crystalline-nematic phase transition at 60 °C and a nematic-isotropic phase transition at 75 °C (Figure 2B). Table 2 lists all mixtures **MM**$_x$, their corresponding crosslinker polymers **CrP**$_n$, and the final amount of crosslinkable groups in the mixtures.

Table 2: *Monomer mixtures* ***MM***$_x$ *and their corresponding polymer crosslinkers* ***CrP***$_n$ *used for the preparation of the LCE microactuators. The shape change of the microactuators is related to the amount of crosslinking units in the mixtures. Instead of a polymer crosslinker, mixture* ***MM0*** *(not listed) contains 10 mol% non-mesogenic crosslinker hexanedioldiacrylate.*

Monomer mixture	Crosslinker	Amount of crosslinker / wt.%	Amount of crosslinkable groups / mol%	T(Cr,N) / °C	T(N,Iso) / °C	Processing temperature / °C	Relative length change
MM1	**CrP1**	9.6	0.1	64	84	80	melting
MM2	**CrP2**	9.7	0.5	66	87	80	--
MM3	**CrP5**	4.9	1.4	72	88	80	1.65
MM4	**CrP3**	10.1	2.2	68	89	75	1.55
MM5	**CrP5**	17.0	5.0	60	80	70	1.25
MM6	**CrP4**	20.1	8.2	60	75	70	1.15

Next we characterized the viscosity of nematic mixtures to ensure laminar flow within the microfluidic device. This is important to ensure a preferred orientation of the mesogens in the LC particles which is then permanently fixed by UV-induced polymerization.[8] The hydrodynamic conditions inside the microfluidic device are typically described by the dimensionless Reynolds number *Re* and the capillary number *Ca*. The capillary number $Ca = \eta Q/\sigma$ corresponds to the ratio between the viscosity η and

interfacial tension σ. *Re* is inversely proportional to the viscosity of the reaction mixture and is given as the ratio between inertial force and viscous forces: $Re = \rho Qd/\eta$ with the density of the fluid ρ, the mean flow rate Q, the diameter of the tubing d, and the viscosity η. Typically for microfluidics the transition from laminar to turbulent flow occurs at $Re > 10$.[3 28,29]

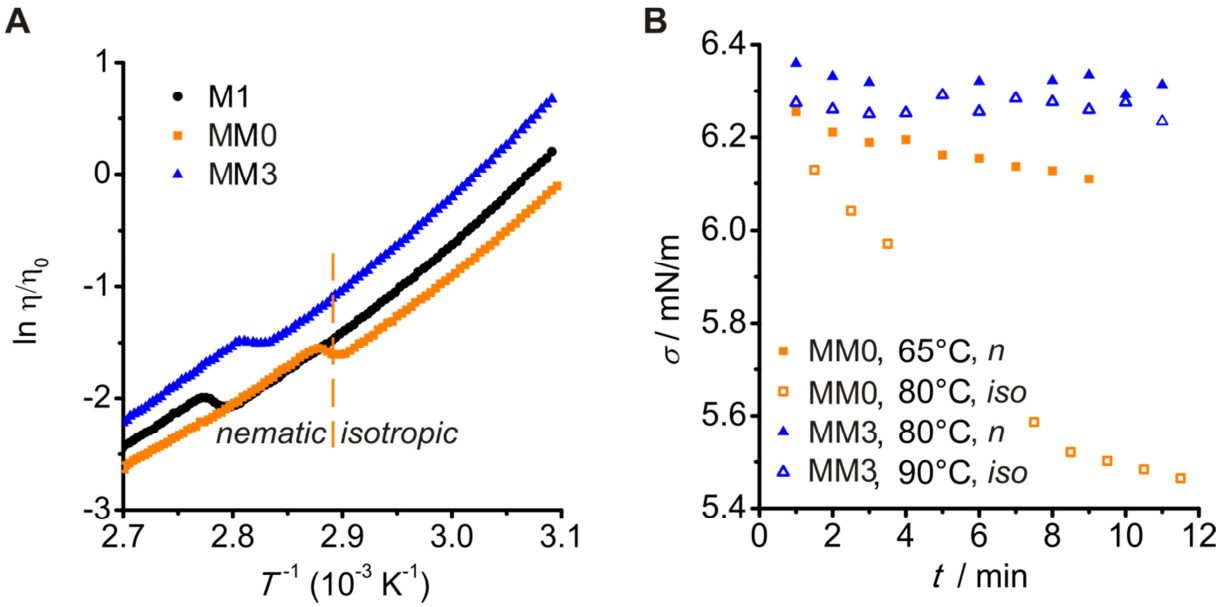

Figure 3. *Viscosity and interfacial tension of monomer **M1** and mixtures of monomer **M1** with 10 mol% crosslinker hexandioldiacrylate and 3 wt% photoinitator Lucirin TPO (**MM0**) and monomer **M1** with 1,4 mol% **CrP5** and 3 wt% photoinitator Lucirin TPO (**MM3**). **A** The addition of the polymer crosslinker increases the viscosity compared to the pure monomer **M1** and **MM0**. The pronounced drop of the viscosity is due to the isotropic-nematic phase transition. **B** The interfacial tension of the mixture containing crosslinker polymer **CrP5** remains constant over time, while the interfacial tension of the mixture **MM0** containing hexanedioldiacrylate (HDD) decreases steadily. This behavior is more distinct at higher temperatures and is due to the diffusion of HDD into the silicone oil phase.*

The viscosity for nematics depends on the director alignment with respect to the velocity gradient and the flow velocity. For simple shear three viscosity coefficients η_i can be distinguished by the alignment of the director towards the shear gradient.[30] Under shear the director usually aligns along the direction of lowest viscosity, typically along the flowing direction and normal to the shear gradient. Thus the viscosity of LC-polymers decreases on cooling to the nematic phase. This is called "nematic flow alignment".[31] Figure 3A shows the temperature dependent viscosity of monomer **M1** and two selected reaction mixtures **MM0** and **MM3**, which were processed in the

microfluidic reactor. **MM0** corresponds to the "conventional" formulation, consisting of 90 mol% monomer **M1** and 10 mol% of the isotropic crosslinker hexandioldiacrylate. **MM3** contains 92 wt.% monomer **M1** and 5 wt.% of the novel crosslinker polymer **CrP5**, which provides for 1.4 mol% crosslinkable groups. 3 wt.% photoinitator Lucirin TPO was added to each mixture. The phase transition isotropic-nematic is marked by a decline of the viscosity due to the alignment of the mesogens along the flowing direction. Compared to the pure mesogen **M1** the addition of the liquid low molecular weight crosslinker hexanedioldiacrylate reduces the viscosity, while the addition of the polymer crosslinker expectedly leads to an increase of the viscosity. Flow curves measured in dependence of the shear rate show newtonian behavior and are presented in the Supplementary Information.

With a density of 1.133 g/cm^3, a flow velocity of 0.097 cm/s, and an inner diameter of the microfluidic tubing of 0.750 cm, Reynolds numbers of $3.70 \cdot 10^{-3}$ and $5.14 \cdot 10^{-3}$ were determined for **MM0** and **MM3** at their processing temperatures of 80°C. Accordingly, even though the incorporation of the polymeric crosslinking agent slightly increases the mixture's viscosity compared to the conventional crosslinker, the flow parameters are still far within the laminar flow regime. Hence, addition of a polymeric crosslinker sustains the laminar flow regime, which is crucial for a preferred orientation of the mesogens inside the monomer droplets.

The interfacial tension between the outer phase silicone oil and the mixtures **MM0** and **MM3** are important for the particle formation and were measured by the pendant drop method. This technique is well-suited for the characterization of liquid crystals.[19,20] The measurements were conducted in the nematic and isotropic phase, with the corresponding temperatures being 65°C and 80°C for **MM0** (hexanedioldiacrylate) and 80°C and 90°C for **MM3** (**CrP5**), respectively. Generally, the adsorption of additives to the surface results in a decrease of the interfacial tension.[32,33] The interfacial tensions for the pure mesogen **M1** are 9.12 mN/m at 80°C (nematic phase) and 9.27 mN/m at 90°C (isotropic phase). These values are lowered by approximately 3 mN/m by addition of the photoinitator Lucirin TPO and the conventional and polymeric crosslinkers, respectively.

A steady decrease of the interfacial tension from 6.26 nN/m to 6.11 nN/m (65°C) and from 6.13 nN/m to 5.47 nN/m (80°C) could be observed for the mixture **MM0** for the measured time period (10 min). This is attributed to the diffusion of the low molecular weight crosslinker hexandioldiacrylate into the silicone oil. The effect is more distinct in the isotropic phase due to increased diffusivity at higher temperatures. On the contrary, the polymeric crosslinker **CrP5** exhibits no such tendency and the interfacial tension for mixture **MM3** remains constant. This provides for long-term stable process conditions and a constant composition of the mixture.

To demonstrate the effectiveness of the new polymeric crosslinkers, soft microactuators were prepared within a microfluidic setup. The microactuators were prepared from monomer mixtures incorporating different crosslinker polymers **CrP*n*** (Table 2). A scheme of the microfluidic setup is depicted in Figure 4A. The monomer mixture (dispersed phase, blue) containing the mesogen **M1**, a polymer crosslinker **CrP*n*** and 3 wt.% photoinitiator Lucirin TPO was ejected through a thin fused silica capillary. Drops of the monomer mixture formed at the tip of the capillary and detached into the co-flowing mobile phase of silicone oil (yellow). These droplets were irradiated with UV-light (365 nm) "on the fly", resulting in solid elastomer particles. The whole setup was heated to accommodate the liquid crystalline phase of the monomer mixture. For particles made from the monotropic mixture **MM0** containing the crosslinker hexanedioldiacrylate, the droplet formation had to be performed at higher temperatures than the subsequent UV-polymerization.[15] For mixtures containing polymeric crosslinkers the fabrication of the microactuators could be performed isothermally, rendering the need for two individual temperature controls unnecessary. The phase transition temperatures of these mixtures depended on the crosslinker polymers used; hence the microactuators were fabricated at different temperatures within the nematic phase of the mixtures. The flow rate for the dispersed monomer phase was set between 1.0 mL/h and 1.5 mL/h. The mobile phase (silicone oil) was delivered at flow rates between 4.6 mL/h and 20 mL/h, resulting in particle diameters between 200 and 500 μm.

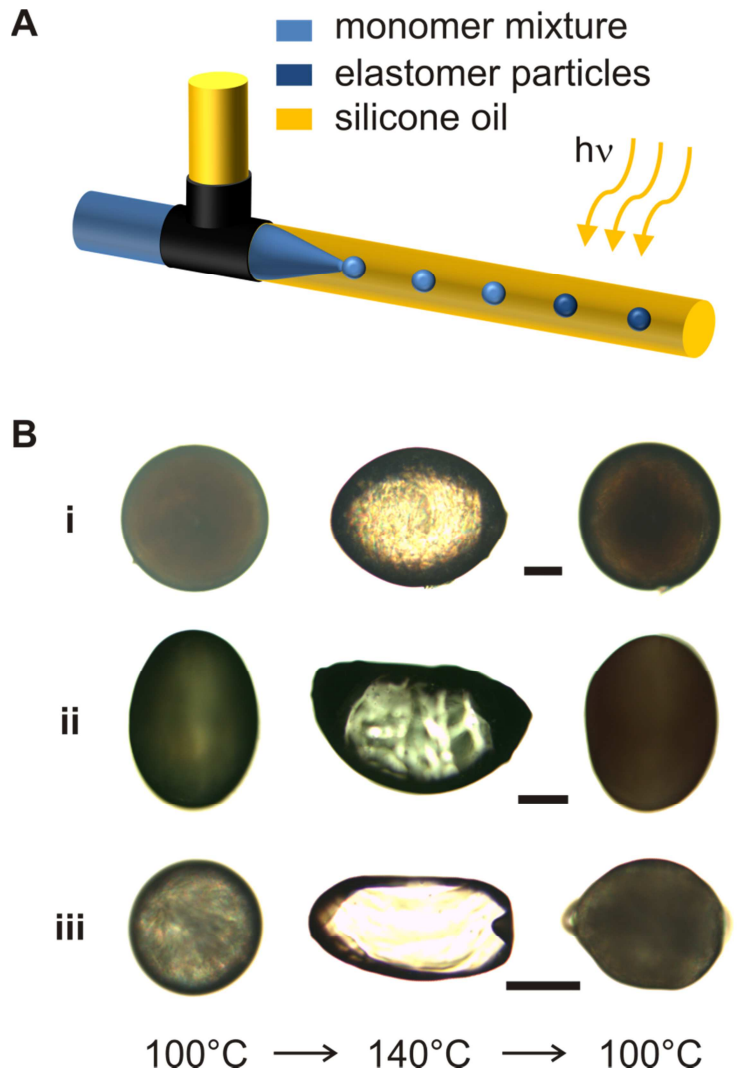

Figure 4. A *Schematic drawing of the microfluidic setup. Droplets of the monomer mixture disperse in the continuous phase silicone oil and are polymerized by UV-light "on the fly".* ***B*** *Soft LCE actuators prepared in the microfluidic device. The quality of the particles' actuation upon the nematic-isotropic phase transition depends on the relative amount of crosslinkable units in the monomer mixture, with a decreasing amount of crosslinks resulting in a higher degree of deformation:* ***i*** *With 5 mol% crosslinkable units in* ***MM5*** *(****CrP5****) the shape change is 25%,* ***ii*** *With 2.2 mol% crosslinkable units in* ***MM4*** *(****CrP3****) the actuation increases to 55%,* ***iii*** *Further decreasing the amount of crosslinkable units to 1.4 mol% in* ***MM3*** *(****CrP5****) increases the deformation up to 65%, but the shape change is no longer fully reversible. The scale bar corresponds to 100 μm.*

We examined the amount of crosslinkable units needed for obtaining dimensionally stable, reversibly actuating microactuators. Particles made from **MM1** (0.1 mol% crosslinkable units) were stable only at room temperature and melted upon heating to the isotropic phase at 130°C. Increasing the amount of crosslinker to 0.5 mol% (**MM2**) provided a sufficient degree of crosslinking to prevent the particles from melting.

However the resulting crosslinking density is still so low that the particles are very soft and sticky, leading to fusion with one another on the glass substrate. Thus a reversible shape change of those particles is not possible (Figure S6). Particles containing 1.4 mol% and more crosslinking groups were found to be sufficiently crosslinked. They were dimensionally stabile at high temperatures and showed no stickiness. Figure 4 exemplary shows microactuators made from **MM3**, **MM4** and **MM5** and their behavior when heated to the isotropic phase (140°C) and cooled back to the nematic phase (100°C). Particles made from **MM3** exhibit the strongest shape change (65%), but the effect is not fully reversible. Particles with an even higher crosslinking density (**MM4**, **MM5**, **MM6**) showed fully reversible actuation. A further increase in crosslinking density decreased the actuation properties of the particles to a shape change of 15%. This effect is well known and is due to the increasing stiffness of the material.[34] Concluding, we were able to show that by using our new polymeric crosslinker we could prepare particles with a crosslinking density sufficient to promote reversible actuation with rather small amounts (about 2 mol%) of crosslinkable groups. In comparison, the conventional system required 10 mol% of hexanedioldiacrylate.[16]

3.3.4 Conclusion

We successfully designed a polymeric crosslinking agent that exhibits a nematic phase. Its crosslinking characteristics can be customized by varying the ratio of mesogenic and non-mesogenic sub-units. These LC crosslinker systems promote a stable enantiotropic mesophase of the monomer mixture used in the preparation of soft LCE actuators. Hence, macroscopically oriented LCE particles could be fabricated isothermally in a microfluidic device, eliminating the necessity for multiple temperature-controlled regions. Tuning the crosslinking density of the LCE particles allows them to be designed accordingly, with the focus on either a strong actuation behavior or highly crosslinked, mechanically robust particles. Measurements of the interfacial tension support the amenities of the new polymeric crosslinkers with respect to a common low-molecular weight crosslinker like hexanedioldiacrylate. No diffusion of the polymer

crosslinker into the surrounding mobile phase silicone oil was observed. Further, the polymer crosslinker reduces the Reynolds number *Re* and benefits the laminar flow conditions by slightly increasing the viscosity of the reaction mixture.

Acknowledgements

We thank Professor B. A. Wolf and WEE Solve for the measurements of viscosity and interfacial tension. Dr. Nadine Metz kindly provided the RAFT agent benzyldithiobenzoate. This work was financially supported by the Deutsche Forschungsgemeinschaft (Ze 230/19-1).

3.3.5 References

[1] D. Demus, J. Goodby, G. W. Gray, H. W. Spiess, Eds., *Handbook of Liquid Crystals,* Wiley-VCH, Weinheim, **1998**.

[2] R. Zentel, *Angew. Chem. Adv. Mater.* **1989,** *101*, 1437.

[3] C. Ohm, M. Brehmer, R. Zentel, *Adv. Mater.* **2010,** *22*, 3366.

[4] Y. Yu, T. Ikeda, *Angew. Chem. Int. Edit.* **2006,** *45*, 5416.

[5] J. Küpfer, H. Finkelmann, *Makromol. Chem., Rapid Commun.* **1991,** *12*, 717.

[6] H. Ringsdorf, R. Zentel, *Makromol. Chem.* **1982,** *183*, 1245.

[7] M.-H. Li, P. Keller, J. Yang, P.-A. Albouy, *Adv. Mater.* **2004,** *16*, 1922.

[8] C. Ohm, N. Kapernaum, D. Nonnenmacher, F. Giesselmann, C. Serra, R. Zentel, *J. Am. Chem. Soc.* **2011,** *133*, 5305.

[9] V. Hessel, A. Renken, J. C. Schouten, J.-I. Yoshida, Eds. *Micro Process Engineering*. *A comprehensive handbook,* Wiley-VCH, Weinheim, **2009**.

[10] A. Fernández-Nieves, G. Cristobal, V. Garcés-Chávez, G. C. Spalding, K. Dholakia, D. A. Weitz, *Adv. Mater.* **2005,** *17*, 680.

[11] P. B. Umbanhowar, V. Prasad, D. A. Weitz, *Langmuir* **1999,** *16*, 347.

[12] J. I. Park, A. Saffari, S. Kumar, A. Günther, E. Kumacheva, *Annu. Rev. Mater. Res.* **2010,** *40*, 415.

[13] M. Bouquey, C. Serra, N. Berton, L. Prat, G. Hadziioannou, *Chem. Eng. J.* **2008,** *135*, S93.

[14] C. A. Serra, Z. Chang, *Chem. Eng. Technol.* **2008,** *31*, 1099.

[15] C. Ohm, C. Serra, R. Zentel, *Adv. Mater.* **2009,** *21*, 4859.

[16] C. Ohm, E.-K. Fleischmann, I. Kraus, C. Serra, R. Zentel, *Adv. Funct. Mater.* **2010,** *20*, 4314.

[17] D. L. Thomsen, P. Keller, J. Naciri, R. Pink, H. Jeon, D. Shenoy, B. R. Ratna, *Macromolecules* **2001,** *34*, 5868.

[18] Y. K. Chong, J. Krstina, T. P. T. Le, G. Moad, A. Postma, E. Rizzardo, S. H. Thang, *Macromolecules* **2003,** *36*, 2256.

[19] B. Song, B. J. Springer, *J. Colloid. Interf. Sci.* **1996,** *184*, 64.

[20] B. Song, B. J. Springer, *J. Colloid Interf. Sci.* **1996,** *184*, 77.

[21] W. Deng, M.-H. Li, X. Wang, P. Keller, *Liquid Crystals* **2009,** *36*, 1023.

[22] M.-H. Li, P. Keller, P.-A. Albouy, *Macromolecules* **2003,** *36*, 2284.

[23] J. Chiefari, J. Y. K. Chong, F. Ercole, F. J. Krstina, J. Jeffery, T. P. T. Le, R. T. A. Mayadunne, G. F. Meijs, C. L. Moad, G. Moad, E. Rizzardo, S. H. Thang, *Macromolecules* **1998,** *31*, 5559.

[24] G. Moad, E. Rizzardo, S. H. Thang, *Austr. J. Chem.* **2005,** *58*, 379.

[25] N. A. Platé, R. V. Talroze, V. P. Shibaev, *Makromol. Chem.* **1984,** *8*, 47.

[26] T. Yamaguchi, M. Okada, T. Hayashi, N. Nakamura, *Mol. Cryst. Liq. Crys.* **1988,** *155*, 501.
[27] C. T. Imrie, F. E. Karasz, G. S. Attard, *Macromolecules* **2002,** *26*, 3803.
[28] K. V. Sharp, R. J. Adrian, *Exp. Fluids* **2005,** *38*, 132.
[29] V. K. Natrajan, K. T. Christensen, *Phys. Fluids* **2009,** *21*, 34104.
[30] M. Miesowicz, *Nature* **1946,** *158*, 27.
[31] P. G. de Gennes, J. Prost, *The physics of liquid crystals,* Oxford, Clarendon, **1993**.
[32] J.-W. Kim, H. Kim, M. Lee, J. J. Magda, *Langmuir* **2004,** *20*, 8110.
[33] P. K. Rai, M. M. Denn, C. I. Maldarelli, *Langmuir* **2003,** *19*, 7370.
[34] J. Küpfer, E. Nishikawa, H. Finkelmann, *Polym. Adv. Technol.* **1994,** *5*, 110.

3.3.6 Supplementary Information

Table S1. Reaction mixtures of the polymer synthesis.

Polymer	M1	M2	RAFT agent	AIBN	M_n / g/mol	PDI	Con-version
HoP	410 mg 0.65 mmol	--	5.4 mg 0.022 mmol	1.1 mg 0.007 mmol	3580	1.2	80%
CoP1	308 mg 0.49 mmol	3.6 mg 0.025 mmol	12.0 mg 0.048 mmol	4.0 mg 0.024 mmol	2822	1.1	38%
CoP2	300 mg 0.47 mmol	7.6 mg 0.053 mmol	7.0 mg 0.027 mmol	2.0 mg 0.097 mmol	3198	1.4	36%
CoP3	690 mg 1.09mmol	41.0 mg 0.28 mmol	10.0 mg 0.041 mmol	2.0 mg 0.012 mmol	6636	1.6	43%
CoP4	508 mg 0.80 mmol	51.0 mg 0.35 mmol	12.0 mg 0.049 mmol	4.0 mg 0.024 mmol	7365	1.9	54%
CoP5	497 mg 0.79 mmol	28.0 mg 0.19 mmol	8.0 mg 0.033 mmol	3.0 mg 0.018 mmol	9361	2.3	27%
CoP6	148 mg 0.23 mmol	153.0 mg 1.06 mmol	9.0 mg 0.037 mmol	2.5 mg 0.015 mmol	2842	1.5	86%

Table S2. Polymer analogous reaction of **CoP** to yield the polymer crosslinkers **CrP**.

Polymer crosslinker		Polymer CoP	Acryloylchloride	Triethylamine
CrP1	CoP1	38 mg	38 mg 0.42 mmol	23 mg 0.23 mmol
CrP2	CoP2	110 mg	95 mg 1.05 mmol	76 mg 0.75 mmol
CrP3	CoP3	215 mg	341 mg 3.77 mmo	254 mg 2.51 mmo
CrP4	CoP4	104 mg	75 mg 0.82 mmol	56 mg 0.55 mmol
CrP5	CoP5	107 mg	137 mg 1.51 mmol	99 mg 0.98 mmol

Table S3. ^{1}H-NMR data for polymers **HoP**, **CoP*n*** and **CrP*n***.

Polymer	^{1}H NMR (400 MHz, $CDCl_3$, δ):
HoP	0.95 (br, 6H; CH3), 1.47 (br, 8H; CH2), 1.75 (br, 4H; CH2), 4.00 (br, 6H; CH2O, 2H; CH2OCO), 6.91 (br, 4H, ArH), 7.23 (br, 1H; ArH), 7.39 (br, 1H; ArH), 7.82 (br, 1H; ArH), 8.08 (br, 4H; ArH).
CoP1	0.97 (br, 6H; CH3), 1.41-1.77 (br, 12H; CH2, 0.4H; CH2), 3.48 (br, 0.2H; CH2OH), 3.75-4.11 (br, 6H; CH2O, 2H; CH2OCO, 0.2H; OCOCH2), 6.94 (br, 4H; ArH), 7.21 (br, 1H; ArH), 7.40 (br, 1H; ArH), 7.83 (br, 1H; ArH), 8.09 (br, 4H; ArH).
CrP1	0.97 (br, 6H; CH3), 1.43-1.85 (br, 12H; CH2, 0.4H; CH2), 3.48 (br, 0.2H; CH2OH), 3.76-4.11 (br, 6H; CH2O, 2H; OCOCH2, 0.2H, OCOCH2), 5.75 (br, 0.03H, CH2=C), 6.04 (br, 0.03H, C=CH), 6.30 (br, 0.03H; CH2=C), 6.93 (br, 4H; ArH), 7.22 (br, 1H; ArH), 7.41 (br, 1H; ArH), 7.83 (br, 1H; ArH), 8.09 (br, 4H; ArH).
CoP2	0.98 (br, 6H; CH3), 1.42-1.84 (br, 12H; CH2, 1.3H; CH2), 3.54 (br, 0.6H; CH2OH), 3.75-4.13 (br, 6H; CH2O, 2H; OCOCH2, 0.6H; OCOCH2), 6.94 (br, 4H; ArH), 7.22 (br, 1H; ArH), 7.42 (br, 1H; ArH), 7.85 (br, 1H; ArH), 8.11 (br, 4H; ArH).
CrP2	0.97 (br, 6H; CH3), 1.44-1.85 (br, 12H; CH2, 1.3H; CH2), 3.48 (br, 0.6H; CH2OH), 3.76-4.11 (br, 6H; CH2O, 2H; OCOCH2, 0.6H; OCOCH2), 5.75 (br, 0.05H; CH2=C), 6.04 (br, 0.05H; C=CH), 6.30 (br, 0.05H; CH2=C), 6.94 (br, 4H; ArH), 7.22 (br, 1H; ArH), 7.41 (br, 1H; ArH), 7.84 (br, 1H; ArH), 8.10 (br, 4H; ArH).
CoP3	0.97 (br, 6H; CH3), 1.50-1.77 (br, 12H; CH2, 3.2H; CH2), 3.52 (br, 1.6H; CH2OH), 3.87-4.20 (br, 6H; CH2O, 2H; OCOCH2, 1.6H; OCOCH2), 6.94 (br, 4H; ArH), 7.24 (br, 1H; ArH), 7.42 (br, 1H; ArH), 7.85 (br, 1H; ArH), 8.12 (br, 4H; ArH).
CrP3	0.97 (br, 6H; CH3), 1.48-1.85 (br, 12H; CH2, 3.2H; CH2), 3.47 (br, 1.6H, CH2OH), 3.78-4.11 (br, 6H; CH2O, 2H; OCOCH2, 1.6H; OCOCH2), 5.75 (br, 0.2H; CH2=C), 6.04 (br, 0.2H; C=CH), 6.30 (br, 0:2H; CH2=C), 6.93 (br, 4H; ArH), 7.22 (br, 1H; ArH), 7.41 (br, 1H; ArH), 7.83 (br, 1H; ArH), 8:09 (br, 4H; ArH).
CoP4	0.97 (br, 6H; CH3), 1.48-1.85 (br, 12H; CH2, 3.5H; CH2), 3.51 (br, 1.7H; CH2OH), 3.80-4.19 (br, 6H, CH2O, 2H; CH2OCO, 1.7H; CH2OCO), 6.96 (br, 4H; Ar H), 7.24 (br, 1H; Ar H), 7.43 (br, 1H; Ar H), 7.86 (br, 1H; Ar H), 8.12 (br, 4H; Ar H).
CrP4	0.96 (br, 6H; CH3), 1.48-1.85 (br, 12H; CH2, 3.5H; CH2), 3.47 (br, 0.8H; CH2OH), 3.80-4.11 (br, 6H; CH2O, 2H; CH2OCO, 1.7H; CH2OCO), 5.74-6.31 (br, 1.2H; CH=CH2), 6.93 (br, 4H; Ar H), 7.21 (br, 1H; Ar H), 7.41 (br, 1H; Ar H), 7.83 (br, 1H; Ar H), 8.09 (br, 4H; Ar H).
CoP5	0.98 (br, 6H; CH3), 1.42-1.84 (br, 12H; CH2, 4H; CH2), 3.54 (br, 2H, CH2OH), 3.75-4.13 (br, 6H, CH2O, 2H; OCOCH2, 2H; OCOCH2), 6.94 (br, 4H; ArH), 7.22 (br, 1H; ArH), 7.42 (br, 1H; ArH), 7.85 (br, 1H; ArH), 8.11 (br, 4H; ArH).

CrP5	0.97 (br, 6H; CH3), 1.44-1.85 (br, 12H; CH2, 4H; CH2), 3.48 (br, 2H; CH2OH), 3.76-4.11 (br, 6H; CH2O, 2H; OCOCH2, 2H; OCOCH2), 5.75 (br, 0.2H; CH2=C), 6.04 (br, 0.2H; C=CH), 6.30 (br, 0.2H; CH2=C), 6.94 (br, 4H; ArH), 7.22 (br, 1H; ArH), 7.41 (br, 1H; ArH), 7.84 (br, 1H; ArH), 8.10 (br, 4H; ArH).
CoP6	0.99 (br, 6H; CH3), 1.48-1.80 (br, 12H; CH2, 24H; CH2), 3.60 (br, 12H; CH2OH), 3.80-4.19 (br, 6H; CH2O, 2H; OCOCH2, 12H; OCOCH2), 6.96 (br, 4H; ArH), 7.24 (br, 1H; ArH), 7.43 (br, 1H; ArH), 7.86 (br, 1H; ArH), 8.12 (br, 4H; ArH).

Table S4. Monomer mixtures used for the preparation of the LCE particles.

Monomer Mixture		Crosslinker Polymer	M1	Lucirin TPO
MM1	CrP1	22 mg	199 mg	6.6 mg
MM2	CrP2	33 mg	296 mg	9.9 mg
MM3	CrP5	16 mg	300 mg	9.4 mg
MM4	CrP3	26 mg	223 mg	7.5 mg
MM5	CrP5	36 mg	169 mg	6.2 mg
MM6	CrP4	77 mg	295 mg	10.5 mg

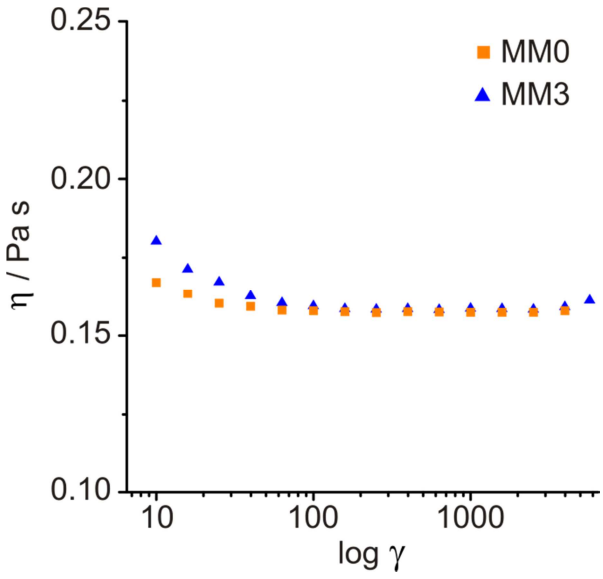

Figure S5. Flow curves of **MM0** (monomer **M1** with 10 mol% crosslinker hexandioldiacrylate and 3 wt% photoinitator Lucirin TPO)and **MM3** (monomer **M1** with 1,4 mol% **CrP5** and 3 wt% photoinitator Lucirin TPO) measured in dependence of changing shear rates show newtonian behaviour.

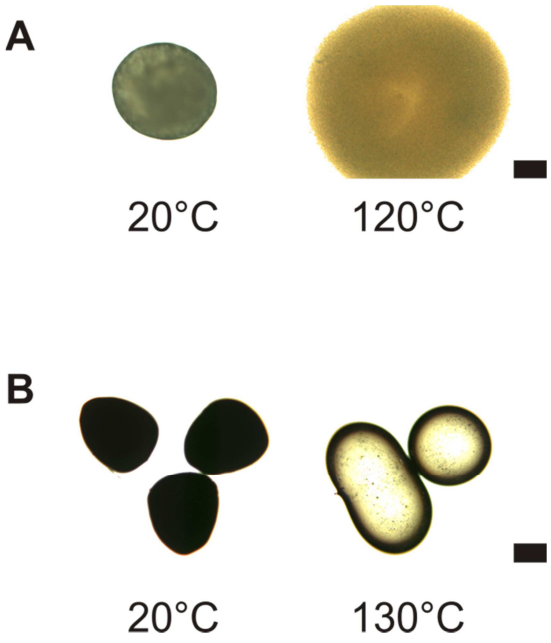

Figure S6. **A** Microactuators made of **MM1** (**CrP1**) melt upon heating to the isotropic phase due to an insufficient crosslinking density of 0.1 mol%. Scale bar corresponds to 100 µm. **B** Increasing the amount of crosslinkable units to 0.5 mol% with the mixture **MM2** (**CrP2**) prevents the particles from melting above the phase transition temperature, however no reversible shape change of the particles is observed. Scale bar corresponds to 200 µm.

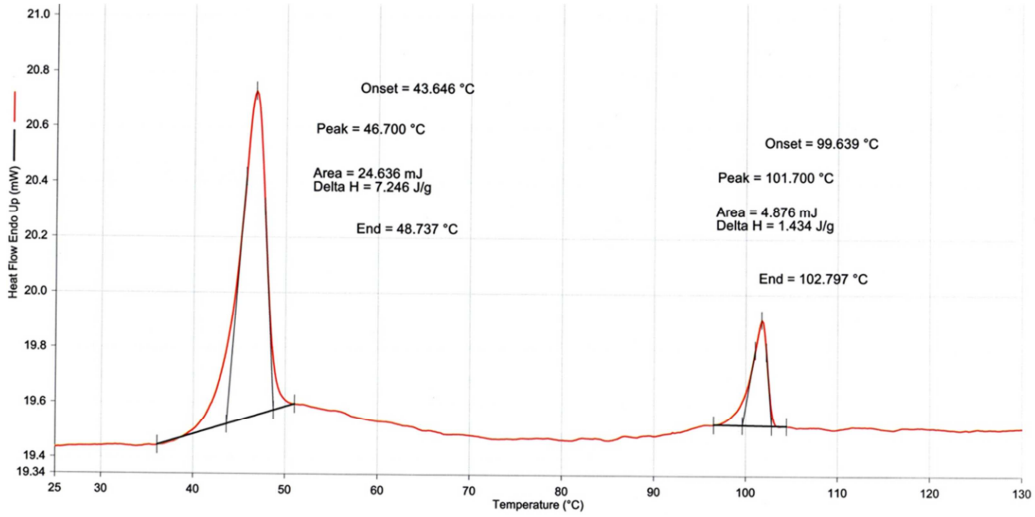

Figure S7. DSC thermogram of **HoP**.

3.4 Liquid crystalline elastomer fibers exhibiting ultralarge length contractions

Eva-Kristina Fleischmann, F. Romina Forst, Rudolf Zentel*

Institute of Organic Chemistry, Johannes Gutenberg-Universität Mainz, D-55099 Mainz, Germany

*Corresponding author: zentel@uni-mainz,de

Abstract

We present the preparation of thermo-responsive fibers made from a liquid crystalline side-chain polymer. Liquid crystalline polymers with crosslinkable units were synthesized and processed in solution in a microfluidic co-flowing device. Due to the high viscosity of the polymer and the low interfacial tension between the dispersed polymer solution and the immiscible ambient fluid, the formation of a liquid jet was favored above the formation of droplets, even at low shear rates. The polymer jet was stabilized by UV-initiated photo-polymerization and the resulting elastomer fibers exhibited contractions of up to 2900% upon the nematic-isotropic phase transition.

3.4.1 Introduction

Due to their anisotropy in molecular shape, liquid crystals (LC) are known to exhibit long-range orientational order in soft amorphous materials, where they align along one common axis, the so-called director.[1] This behavior is not limited to low molecular weight molecules but can easily be transferred to polymer systems containing liquid crystalline moieties (mesogens).[2] In the case of calamitic liquid crystals, the rod-like mesogens can covalently be linked to the polymer backbone in a side-on fashion via laterally attached alkyl chains. The anisotropy of the mesogens forces the polymer into a spheroidal chain conformation, where the radius of gyration changes with respect to the director orientation.[3] Like their low molecular weight counterparts, these polymers exhibit a temperature-dependent phase transition from the semi-ordered mesophase to the disordered isotropic state at higher temperatures, where the polymer chains assume their unperturbed spherical shape.

In slightly crosslinked polymer networks, the nematic-isotropic phase transition causes a macroscopic contraction parallel to the director, a unique behavior observed for liquid crystalline elastomers (LCEs).[4] The reversibility of the shape change established LCEs as an attractive material for actuator and sensor applications.[5] Actuating LCEs require a uniform macroscopic alignment of the mesogens before their positional order is fixed via crosslinking. Several procedures have been developed so far to orient LC polymers, including mechanical stretching[6] and the utilization of magnetic[7] or electric fields[8]. Alternatively, microfluidic procedures have proven to be a versatile tool for the preparation of LCEs. The shear flow present in the microfluidic tubing induces a preferred orientation of the director, while the microfluidic setup allows the design of different actuator-geometries, ranging from bulk[9] to core-shell particles.[10] The microfluidic technique is especially intriguing since it allows the preparation of micrometer-sized LCE actuators, which are otherwise only obtainable by lithographic or templating procedures[7,11] Micro- and nanosized LCEs are of considerable interest due to their potential applications in microelectromechanical systems, biosensors and active surfaces.[12]

Aligned LCE fibers can, for example, be prepared by drawing from a polymer melt with a pair of tweezers.[13] The average diameter of these fibers was of several hundred micrometers and shape changes between 20% and 35% were observed. Thinner fibers with diameters ranging between several hundred nanometers to some micrometers are accessible by electrospinning.[14] While it could be demonstrated that electrospinning is a useful tool for orienting liquid crystals within the fiber structure[15], no shape changes was reported for fibers consisting of LCE material.[16] This is most likely due to the electrospinning process itself, which produces a fleece-like assembly of the fibers: This renders the extraction of single fibers impossible and prohibits both their analysis and application. With the use of a microfluidic device, the preparation of fibers with diameters between 20 and 50 μm becomes possible. This wet-spinning process yields single fibers, which are not interwoven in a fleece-like net. Made from a main-chain LC polymer, these fibers contracted irreversibly during the liquid crystalline phase transition. Put under a constant load, the contraction of the fiber became reversible, since the additional weight operated as an external force and stretched the fiber back to its original length.[17,18]

In this paper, we utilize a microfluidic device for the preparation of LCE fibers made from a solution of crosslinkable side-chain polymers. During the microfluidic processing, a hydrophilic silicone fluid is used as continuous phase. The low interfacial tension of between this ambient fluid and the polymer solution facilitates the formation of a liquid jet even at low shear rates, which is then photo-crosslinked “on the fly”. Polymers with varying amount of crosslinker units were used, yielding elastomer fibers with different mechanical and actuation properties.

3.4.2 Results and Discussion

We aimed at preparing fibers from so-called side-chain LCEs in which the mesogens are laterally attached to the polymer backbone via flexible spacers. We decided on using an LC polymer as starting material instead of more commonly used LC monomers, since polymers possess higher viscosities. The LC material, processed in a microfluidic device,

was extruded through a thin glass capillary into a co-flowing liquid. To obtain fibers, the LC material has to leave the glass capillary as a liquid jet which can then be crosslinked by UV-initiated photo-polymerization before the jet breaks off into single droplets. The increased viscosity of the polymer is beneficial for the creation of a jet. LC polymers exhibiting smectic phases are known to have slower dynamics of the polymer chains, since the formation of additional smectic layers requires a high activation energy.[19] Therefore a LC polymer was used, which exhibits only a nematic mesophase.

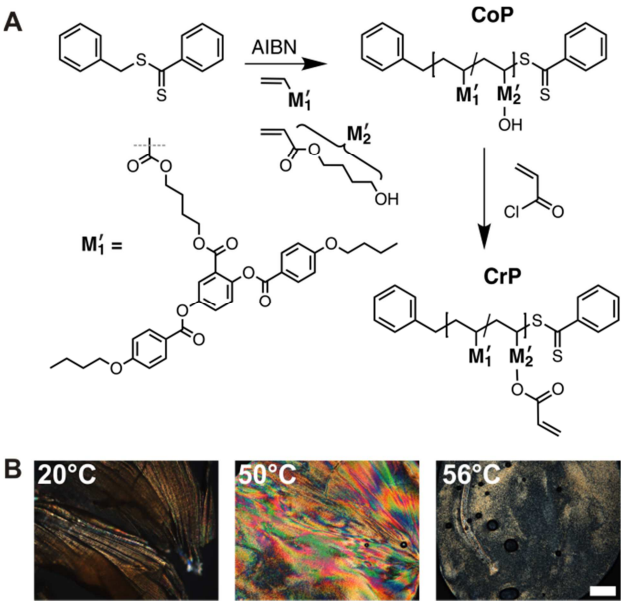

Figure 1: A *Synthesis of the crosslinkable polymers* ***CrP****: Monomers* ***M1*** *and* ***M2*** *are copolymerized via a RAFT mechanism to yield polymers* ***CoP*** *and the crosslinkable vinyl groups are introduced in a post-polymerization reaction.* ***B*** *Liquid crystalline behavior of polymer* ***CrP3*** *as observed with an optical microscope under crossed polarizers. The nematic phase of the polymer extends from 40°C to 56°C. At the latter temperature the polymer loses its birefringence. The scale bar corresponds to 100 µm.*

The synthesized nematic LC polymer **CoP** is comprised of the side-chain mesogen **M1** and the non-mesogenic monomer 4-hydroxybutylacrylate **M2**. The mesogen **M1** exhibits a nematic phase between 72°C and 98°C.[20] Monomers **M1** and **M2** were co-polymerized in a controlled fashion via RAFT (radical addition-fragmentation chain-transfer) polymerization. The polymer has to contain crosslinkable reactive groups to allow the formation of an elastomer network. In a post-polymerization modification, the hydroxyl group (attached to the monomer unit 4-hydroxybutylacrylate) was esterified with acryloyl chloride to yield the crosslinkable polymer **CrP**. For a detailed description

of the polymer synthesis see Reference [21]. The quantity of crosslinkable acrylate units attached to the copolymer can easily be controlled by adjusting the amount of 4-hydroxybutylacrylate during the polymerization. Polymers were synthesized containing between 6 and 45 mol% crosslinkable units. The amount of non-mesogenic 4-hydroxybutylacrylate units also influences the temperature range of the polymer's liquid crystalline phase. An increasing amount of incorporated 4-hydroxybutylacrylate decreases the phase transition temperatures and narrows the nematic phase of the polymer. This has to be considered when handling the LC polymers in the temperature-controlled microfluidic device since the liquid crystalline order in the fibers has to be frozen in the nematic state of the material. The temperature ranges of the liquid crystalline phase of the polymers were analyzed with polarized optical microscopy (POM). Table 1 lists the synthesized polymers **CrP** including their key characteristics.

Table 1: *Key characteristics of the crosslinkable polymers **CrP** processed in the microfluidic device, including the amount of crosslinkable units and phase transition temperatures.*

Polymer	M_n (g/mol)	Amount of crosslinkable units (mol%)	T_g (°C)	T_{NI} (°C)
CrP1	8.800	45	38	54
CrP2	5.300	31	35	60
CrP3	4.100	24	40	56
CrP4	4.700	9	60	79
CrP5	4.500	6	57	85

The challenge of producing fibers in a microfluidic device is the creation of a stable liquid jet of the dispersed phase. The microchannel walls strongly affects the formation of perturbations and influences the stability of the jet.[22] We determined low Reynolds numbers for comparable experimental setups and therefore expect laminar flow conditions to prevail in the microfluidic tubing.[21] Further parameters determine if a jet is favored above the formation of droplets. Generally, high velocities v_c of the continuous phase, a high viscosity η_d of the dispersed phase and a low interfacial tension σ between

dispersed and continuous phase promote the stability of a jet.[23,24] A thinning jet, which breaks of into droplets after a certain distance, is observed for high flow velocities of the continuous phase. On the other hand, an increased flow velocity of the dispersed phase at a constant flow velocity of the continuous phase generates a widening straight jet.[23] Both types of jets depend on the ability of inertial and viscous forces to overcome the surface tension of the dispersed phase and deform droplets into a jet. This process is quantified by the capillary number *Ca* and Weber number *We*. Large values for capillary number Ca_c and Weber number We_d indicate that the shear stress of the continuous phase *c* and the inertial force of the dispersed phase *d* dominate over the surface tension, leading to jetting.[23]

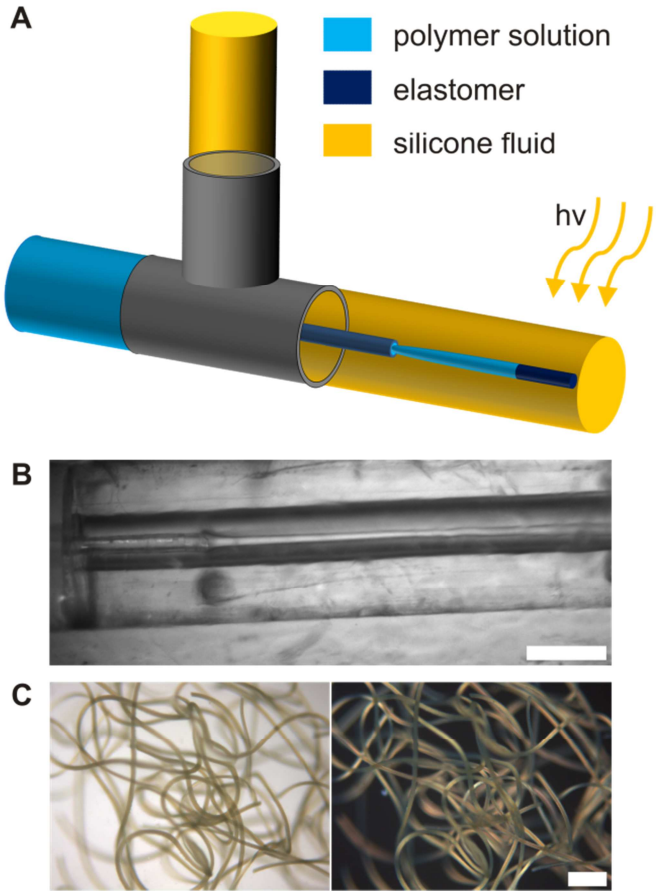

Figure 2: ***A*** *Schematic illustration of the preparation of LCE fibers in a microfluidic device. The polymer solution is extruded through a thin capillary into the silicone fluid and subsequently crosslinked by UV irradiation.* ***B*** *Snapshot of the liquid jet of the polymer solution within the microfluidic capillary. The scale bar corresponds to 500 µm.* ***C*** *Optical micrograph of the LCE fibers under crossed polarizers. The scale bar corresponds to 200 µm.*

In our approach to prepare LCE fibers, we used the dispersed phase of the liquid crystalline side-chain polymers **CrP** mixed with 5 wt.% photoinitator Lucirin TPO. While the high viscosity of the polymer enhances the tendency for a jet formation, it prohibits the polymer to be directly injected into the co-flowing continuous phase through a thin glass capillary. To process the polymer in the microfluidic device, its viscosity has to be decreased by dilution with a solvent. The best results were achieved for polymer solutions in chlorobenzene with a weight ratio of polymer to solvent of 0.4. To achieve the formation of a liquid jet, we attempted to reduce the interfacial tension between the dispersed and the continuous phase. In previous works dealing with the preparation of LCE particles in a microfluidic device, silicone oil (polydimethylsiloxane, PDMS) was used as a continuous phase and droplets were predominantly formed in the ambient hydrophobic phase.[9,21] We observed similar behavior in our experiments with PDMS as continuous phase, namely that the tendency of drop formation is high and can only be overcome at high shear rates. Even then, due to high surface tension, the liquid jet of the polymer solution is only stable for several millimeters. This distance between the tip of the glass capillary and the break-off of the polymer jet does not suffice to accomplish crosslinking with UV-irradiation. Thus we switched to the polyether modified silicone fluid L053 (viscosity: 800 cSt), which is hydrophilic and miscible with water. When used as continuous phase in the microfluidic device, this change of polarity promotes the formation of a jet above the formation of droplets. We observed the polymer solution to be extruded from the glass capillary as a jet into the hydrophilic continuous phase L053. As displayed in Figure 2b, the liquid jet of the polymer solution is already present at a flow velocity of 0.03 cm s^{-1} of the continuous phase (this equals a flow rate of 0.4 mL/h). For a comparable system with a similar microfluidic setup and PDMS as continuous phase, higher shear rates were necessary to allow the formation of a jet from a polymer solution and minimal flow velocities of the continuous phase of 0.10 cm s^{-1} were reported for the polymer jet to first appear.[17] The here produced jet is stable and, after diffusion of the solvent chlorobenzene into the surrounding silicone fluid, the pure polymer jet can be crosslinked by irradiation with UV light at 365 nm. This allows LCE fibers to be continuously produced in a wet-spinning type process as shown in Figure 2c.

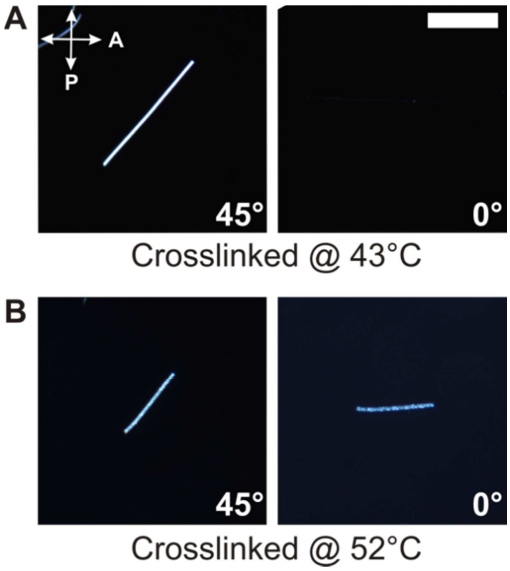

Figure 3: *Microscopy images of the fibers from polymer **CrP1** prepared at the same flow rates, but photo-crosslinked at either (**A**) 43°C or (**B**) 52°C. Between crossed polarizers, the LCE samples appear brightest at an angle of 45° with respect to the transmission axis of either polarizer or analyzer. Rotated to an angle of 0°, fiber **A** exhibits uniaxial orientation of the director, turning completely dark. Fiber **B** only darkens slightly, indicating inferior alignment of the director. The scale bar corresponds to 200 µm.*

Liquid crystalline elastomers demonstrate a macroscopic shape change on the nematic-isotropic phase transition if the mesogens are uniformly oriented throughout the sample during the crosslinking step. This requires the crosslinking reaction to be carried out within the semi-ordered nematic phase of the LC polymer precursors. The LC polymers **CrP** exhibit different phase transition temperatures, depending on the amount of incorporated 4-hydroxybutylacrylate. The quality of the director orientation within the LCE fiber can be studied with an optical microscope under crossed polarizers. Figure 3 shows pieces of LCE fibers made from polymer **CrP1**, which were processed in the nematic phase of the polymer (between 38 and 54°C) and crosslinked at T = 43°C (fiber A) and T = 52°C (fiber B), respectively. While both temperatures are well within the nematic phase of the polymer, fiber B is crosslinked at a temperature close to the liquid crystalline-isotropic phase transition of the polymer. Both fiber pieces are highly birefringent at an angle of 45° with respect to the transmission axis of the polarizers. Rotated by 45°, fiber A turns completely dark, indicating a uniaxial orientation of the director. Fiber B only darkens slightly, indicating that the director orientation is macroscopically not as homogeneous as in sample A. Since both fibers were prepared at the same flow rates (0.06 mL/h for the polymer solution and 1 mL/h for the silicone

fluid), the different quality of director orientation is caused by the change in the crosslinking temperature. Crosslinking at 48°C near the phase transition to the chaotic isotropic state leads to an inferior orientation of the director.

Assuming that the director is aligned along the long fiber axis, one expects a contraction of the fibers when they are heated above the clearing temperature, i.e. to the isotropic phase of the LC elastomer. However, both fibers did not contract upon heating to 140°C, independent of the quality of the director alignment. Studying the fiber in more detail, we learned that with 45 mol% of crosslinkable units in polymer **CrP1**, a highly crosslinked elastomer forms, whose properties are that of a highly crosslinked thermoset. Here the mesogens lack the flexibility to rearrange upon the transition to the disordered isotropic phase and the LC order is preserved even above T_{NI} (Figure 4a). It is essential to increase the flexibility of the mesogens to enable efficient actuation and prepare slightly crosslinked LCE samples with elastic moduli of several megapascals (MPa).[25] With regard to this results, the amount of acrylate groups in the crosslinker polymers was lowered.

Table 2: *Processing parameters for polymers* ***CrP*** *and dimensions and degree of contractions of the resulting LCE fibers.*

Polymer	Processing temperature (°C)	UV exposure time	Diameter (μm)	Contraction (%) = (A_{RT}/$A_{140°C}$)-1
CrP1	43	13 s	3	0
CrP1	52	13 s	9	0
CrP2	45	13 s	22	440
CrP2	45	16.7 min	6	0
CrP3	45	13 s	28	330
CrP3	50	13 s	27	280
CrP3	45	2.7 min	75	5
CrP4	65	13 s	8	2900
CrP5	65	2.7 min	24	590
CrP5	65	16.7 min	22	0

The polymer precursors **CrP2** to **CrP5** contain between 6 and 31 mol% crosslinkable acrylate groups. The temperature ranges of their liquid crystalline phases are listed in Table 1, and the processing temperatures are listed in Table 2. The processing temperature and the resulting quality of the director orientation influence the contraction behavior of the fibers. For example, fibers were prepared from polymer **CrP3** (24 mol%) and crosslinked at 45°C and 50°C, respectively. The actuation behavior of the fibers was analyzed with a hot stage connected to an optical microscope. Heating pieces of the fiber samples to the isotropic state at 140°C results in a contraction along the long axis of the fiber for both fiber samples. By measuring the aspect ratios of the fiber at room temperature (A_{RT}) and at 140°C ($A_{140°C}$), the amount of contraction is expressed by the ratio ($A_{RT}/A_{140°C}$)-1. The fibers crosslinked close to the nematic-isotropic phase transition (T_{NI} = 56°C) exhibited large contractions of 280%. Those fibers crosslinked at a lower temperature contracted even to a larger extent (330%), indicating a more uniform orientation of the director (compare Figure 4c).

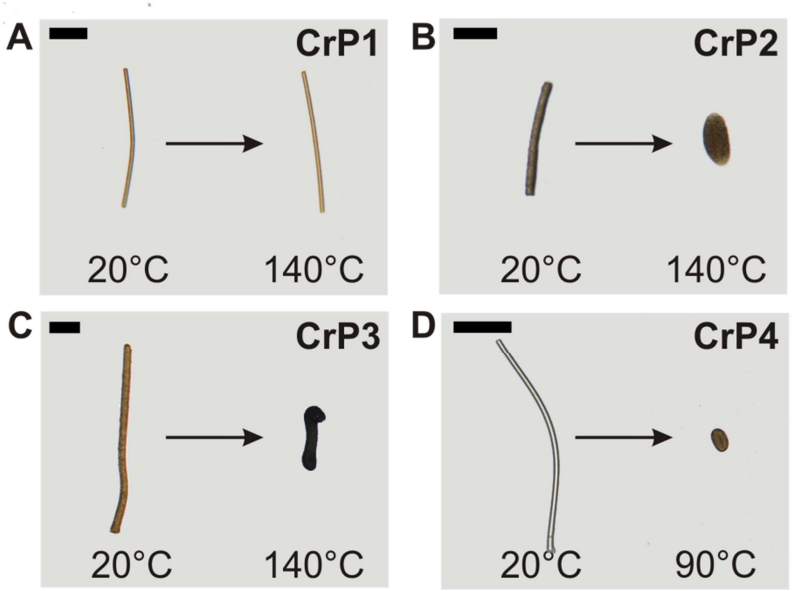

Figure 4: *Overview of the contraction behavior of LCE fibers crosslinked for 13 s.* ***A*** *Fibers made from polymer* ***CrP1*** *(45 mol%) do not contract due to the high amount of crosslinking.* ***B-D*** *Fibers made from polymers* ***CrP2-CrP4*** *with decreased amounts of crosslinkable units (31 mol% to 9 mol%) contract when heated to the isotropic phase at 140°C. Scale bars correspond to 100 µm.*

Figure 4 depicts the actuation behavior of the LCE fibers made from polymers **CrP1** to **CrP4** that were irradiated with UV-light for 13 s. As mentioned above, fibers from **CrP1** did not exhibit any contraction upon heating above the nematic-isotropic phase transition, due to the high amount of crosslinking. Decreasing the amount of crosslinkable units to 31 mol% (**CrP2**), yields LCE fibers that contract upon heating. The degree of contraction depends on the crosslinking density of the elastomer, with larger contractions being observed for fibers with smaller crosslinking densities (see Figure 4). While fibers made from **CrP3** with 24 mol% crosslinkable units contract by 330%, fibers made from **CrP4** (9 mol% crosslinking units) exhibit a maximum contraction of 2900%. The contraction of fibers made from polymer **CrP4** is already completed at 90°C. The low molecular weight of polymer **CrP4** (4.700 g/mol) and the incorporated non-mesogenic units **M2** increase the nematic-isotropic phase transition by only ten degrees compared to the clearing temperature of the corresponding polymer (79°C).

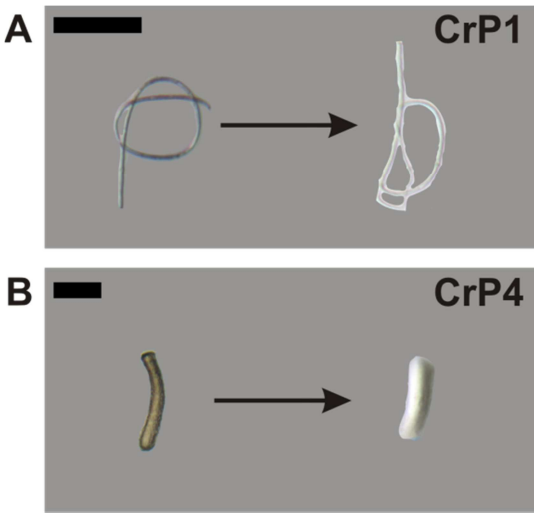

Figure 5: *Exemplary microscopy images of fibers swollen in the solvent diglyme.* ***A*** *Highly crosslinked fibers made from polymer* ***CrP1*** *(45 mol%) and irradiated for 13 s do not swell in the solvent.* ***B*** *Fibers made from* ***CrP4*** *with less amount of crosslinkable units (9 mol%) experience anisotropic swelling. Scale bars correspond to 100 µm.*

To exclude that the fibers are not properly crosslinked and that no LCE network was formed by UV-irradiation, we processed polymer **CrP1** without photoinitiator and subsequent UV-irradiation. When heating this non-crosslinked LC polymer to 140°C, a simple melting of the fibers without any noticeable contraction was observed. We also

performed swelling experiments of crosslinked fibers in diglyme (diethylene glycol dimethyl ether). Exemplary results are presented in Figure 5. No swelling of the fibers was observed in case of polymer **CrP1**, as expected for a sample with high crosslinking density. Fibers from **CrP4**, the polymer with the lowest crosslinker amount, did not dissolve in diglyme, but experienced anisotropic swelling. A contraction in length and increase in diameter could be observed, confirming that the fibers are sufficiently crosslinked even at low crosslinking densities and that the mesogens are anisotropically aligned along the long axis of the fiber.

Even with sufficient crosslinks for an elastomer network, the crosslinking density affects the quality of actuation. Low crosslinking densities increase the capacity of actuation at the expense of reversibility, while higher crosslinking densities promote the reversibility but decrease the amount of actuation.[21] While the amount of crosslinking units of polymers **CrP** should be sufficient for the formation of a stable elastomer network that performs reversible actuation, the processing in the microfluidic setup may interfere with the full conversion of the crosslinkable acrylate groups. The jet of the polymer melt is irradiated with UV light for 13 s. For bulk particles made of monomer **M1** this time frame is sufficient for a full conversion of monomer droplets to elastomer particles.[26] The small monomer molecules can easily diffuse to the growing polymer chain, allowing for rapid polymerization of the acrylate group to full conversion. In the case of our crosslinkable polymers, the acrylate groups are already attached to polymer chains. This limits the diffusion of the reactive groups and increases the minimum irradiation time necessary to form an elastomer network.

To facilitate the conversion from polymer jet to elastomer fibers with bulk polymerization characteristics, monomer **M1** was added to the polymer solution. A mixture of polymer **CrP2** with 20 wt.% monomer **M1** was diluted in chlorobenzene at a weight ratio of 0.3. The mixture was processed at 50°C and the resulting jet was polymerized for 13 s. The mixture yielded fibers that contracted by 150%. This is only less than half the amount of contraction observed for fibers prepared from the neat polymer **CrP2**, which contracted by 440%. The total amount of crosslinking groups (31 mol%) remains the same for polymer and the polymer/monomer mixture. However, the

addition of the monomer provides for a faster conversion of the crosslinker groups due to increased diffusion. Hence, the crosslinking density of the fiber increases, yielding fibers with a less pronounced contraction.

Additionally, longer UV exposure times were tested as an alternative route to increase the crosslinking densities of the LCE fibers. To achieve an exposure time of 16.7 min, the microfluidic tube was rolled up beneath the light cone of the UV lamp. Since crosslinked fibers from polymer **CrP1** did not exhibit any contraction even at a low exposure time of 13 s, fibers of polymers **CrP2** (containing 31 mol% crosslinkable units) and **CrP5** (6 mol%) were crosslinked at this irradiation time. None of these fibers contracted upon heating above the clearing temperature. This behavior is similar to the fibers obtained from polymer **CrP1** at an irradiation time of 13 s, the crosslinking density of which was too high to allow for the contraction of the sample. This observation is in accordance with our assumption, that an exposure time of 13 s is too short for a full conversion of the reactive acrylate groups. With longer exposure times, even fibers from polymer **CrP5** containing only 6 mol% of crosslinking units are too densely crosslinked to permit any change of shape on the nematic-isotropic phase transition (see Figure 6).

Fibers were prepared from polymers **CrP5** (6 mol%) and **CrP3** (24 mol%) with an intermediate exposure time of 2.7 min. The fibers obtained from polymer **CrP5** contracted by 590% on the liquid crystal's phase transition. Despite the decreased amount of crosslinkable units in polymer **CrP5** compared to polymer **CrP4** (9 mol%), the resulting shape change of 590% is less pronounced compared to fibers obtained from polymer **CrP4** at an irradiation time of 13 s (2900%). Despite the lesser amount of crosslinkable units, the longer exposure time resulted in a higher conversion of the acrylate groups and hence a higher crosslinking density. This hypothesis is supported by the contraction observed for fibers made from polymer **CrP3** (24 mol%) with exposure times of 13 s and 2.7 min, respectively. While the shorter exposure time yielded fibers exhibiting a contraction of 330%, an increase of UV exposure resulted in fibers that only contracted slightly by 5%.

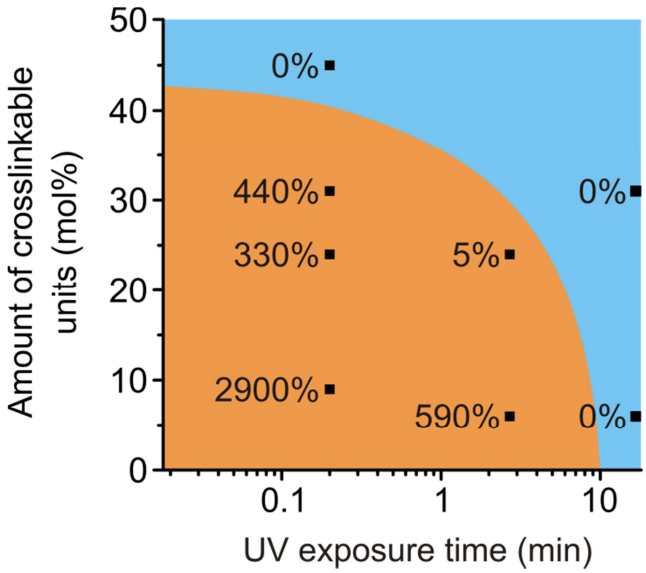

Figure 6: *Influence of irradiation time and crosslinker amount on the contraction behavior of the LCE fibers. Polymers with only few crosslinkable units and short irradiation times yield contracting fibers with the amplitude of the contraction depending on their crosslinking density (orange domain). Above a certain threshold, the LCE fibers do not undergo any change of shape due to the high amount of crosslinks (blue domain).*

Figure 6 visualizes the relationship of UV exposure time and the amount of acrylate groups of the crosslinkable polymers on the mechanical contraction of the obtained LCE fibers. Fibers obtained from either polymers with a low crosslinker amount or short UV exposure times exhibit large contractions (Figure 6, area marked orange). Both effects are equivalent to low crosslinking densities in the elastomer fibers. Higher crosslinking densities can be obtained by increasing the crosslinker amount or the exposure time, which both result in a decrease of the fiber's contraction. At a certain threshold the elastomer is too densely crosslinked and the mesogens lack the flexibility to rearrange upon the nematic-isotropic phase transition. As a result, the fibers are no longer able to contract (area marked blue in Figure 6).

The preparation of LCE fibers from a smectic main-chain polymer has previously been reported, where the shape-change of the fibers was not reversible on cooling to the liquid crystalline phase. The formation of the ordered liquid crystalline phase on cooling was inhibited, since the formation of additional smectic layers needed a high amount of activation energy. The latter could be provided by an external force, for instance a weight, which was put on the actuated fiber and stretched it back to its original length.[17]

Similar results are expected for the here described nematic side-chain LCE fibers: A reversible contraction should be obtainable when a small weight is used as an external force to support the reset force of the elastomer network. This hypothesis will be tested in a future study.

3.4.3 Experimental Section

Materials and reagents

The silicone oil Wacker L053 was kindly provided by IMCD Deutschland. The photoinitiator Lucirin TPO (2,4,6-trimethylbenzoyldiphenylphosphine oxide), acryloylchloride and 4-hydroxybutylacrylate were purchased from Sigma-Aldrich. Chlorobenzene (99%) was purchased from Acros Organics. The liquid crystalline monomer **M1** (4''-acryloyloxybutyl) 2,5-di(4'-butyloxybenzoyloxy)benzoate[20] and the chain transfer agent (CTA) benzyldithiobenzoate[27] were synthesized according to the literature. The radical initiator 2,2'-azobisisobutyronitrile (AIBN, Fluka) was recrystallized from diethyl ether prior to use. Components for the microfluidic device were obtained from Postnova Analytics GmbH (fused silica capillary, T-junction, nuts and ferrules) and WICOM (PTFE tubings). The crosslinkable polymers were synthesized according to the literature.[21]

Processing in the microfluidic device

To allow processing in the microfluidic device, the viscosity of the polymers **CrP** was adjusted through dilution with chlorobenzene at a weight ratio of 0.4. 5 wt.% photoiniator Lucirin TPO were added to the mixture and the solution was filled into a microliter syringe (Hamilton). The polymer solution (dispersed phase) and the silicone fluid L053 (continuous phase) were pumped with a syringe pump (Harvard 33) through PTFE tubings connected to a T-junction. The polymer phase was ejected through a fused silica capillary (ID: 100 μm, OD: 165 μm) into the polymerization tube (PTFE, inner diameter 750 μm) filled with the co-flowing silicone fluid. The setup was immersed into a water bath and the formation of the liquid jet and subsequent crosslinking were

conducted at a temperature within the nematic phase of the respective polymer. Flow rates were set between 0.4 - 1 mL/h for the continuous phase and 0.04 - 0.06 mL/h for the dispersed phase. Crosslinking was initiated by irradiation with a LOT Oriel LSH302 500 W UV lamp with a 365 nm line filter.

Characterization

^{1}H NMR spectra of the crosslinkable polymers **CrP** and their precursors **CoP** were acquired in $CDCl_3$ at room temperature on a Bruker Avance II spectrometer at a ^{1}H Larmor frequency of 400 MHz. The relative amount of crosslinking units in polymers **CrP** was determined by relating the integrals of the NMR signals for the CH_3 groups of **M1** (0.9 ppm) and the signals corresponding to the protons of the acrylate double bond (6 ppm).[21] The molecular weight of the polymers was determined by gel permeation chromatography (GPC) in 2 mg/mL THF with polystyrene as external standard. The microfluidic processes were observed with a Zeiss stereo microscope Stemi 2000-C equipped with an Olympus XM10 camera. For optical characterization of the fibers, the light microscope Olympus BX51 equipped with a hot-stage (Linkam TMS 94) and a camera (Olympus ColorView II) was used. The optical data were evaluated with the imaging software Cell^D.

3.4.4 Conclusion

Nematic side-chain polymers with integrated crosslinkable acrylate groups were synthesized and processed in a microfluidic device. The high viscosity of the polymer and the use of a hydrophilic silicone fluid as a continuous phase promoted the fabrication of LC elastomer fibers from the solution of the crosslinker polymers in chlorobenzene. The polymer solution was extruded as a liquid jet through a thin capillary into the ambient silicone oil, even at low shear rates. The polymer jet was highly stable and could be crosslinked by irradiation with UV-light. The obtained LCE fibers performed contractions upon the nematic-isotropic phase transition of several hundred percent in magnitude. Relative length changes of up to 500% were reported for

LCE fibers made from a main-chain triblock copolymer[28], a value that is easily matched by our LCE fibers. The amplitude of the contraction could be controlled by the amount of crosslinker groups in the precursor polymers, where lower amounts produced larger contractions. Polymers with high crosslinker percentage yielded non-contracting fibers, since the mesogens lack the flexibility to rearrange upon the transition to the disordered isotropic phase. Additionally, the influence of the UV exposure time on the polymer jet was tested in regard to the contraction behavior of the corresponding fibers. Longer exposure times benefited the full conversion of the acrylate groups and fibers with higher crosslinking density were produced. The shape changes of the fibers were, however, not reversible at any crosslinking density since the elastic reset force parallel to the director does not suffice to elongate the fiber back to its original length. The reversibility of the shape change, i.e. the extension of the fibers in the nematic phase, may be assisted by an additional weight that acts as an external force and supports the recovery of the nematic order.

3.4.5 References

1 D. Demus, J. Goodby, G. W. Gray, H.-W. Spiess, V. Vill, *Handbook of Liquid Crystals Set*, Wiley-VCH Verlag GmbH, Weinheim, 1998.

2 H. Finkelmann, *Angew. Chem. Int. Ed.*, 1987, **26**, 816.

3 a) R. G. Kirste and H. G. Ohm, *Makromol. Chem., Rapid Commun.*, 1985, **6**, 179. b) H. Mattoussi, R. Ober, M. Veyssie and H. Finkelmann, *Europhys. Lett.*, 1986, **2**, 233. c) N. Leroux, P. Keller, M. F. Achard, L. Noirez and F. Hardouin, *J. Phys. II France*, 1993, **3**, 1289. d) H. Finkelmann, W. Kaufhold, L. Noirez, A. ten Bosch and P. Sixou, *J. Phys. II France*, 1994, **4**, 1363.

4 a) R. Zentel, *Angew. Chem. Int. Ed.*, 1989, **101**, 1437. b) J. Küpfer and H. Finkelmann, *Macromol. Chem. Phys.*, 1994, **195**, 1353. c) E. M. Terentjev, *J. Phys.: Condens. Matter*, 1999, R239. d) M. Warner and E. M. Terentjev, *Liquid crystal elastomers*, Clarendon Press, Oxford, 2007, Vol. 120.

5 a) Y. Yu and T. Ikeda, *Angew. Chem. Int. Edit.*, 2006, **45**, 5416. b) C. Ohm, M. Brehmer and R. Zentel, *Adv. Mater.*, 2010, **22**, 3366.

6 J. Küpfer and H. Finkelmann, *Makromol. Chem., Rapid Commun.*, 1991, **12**, 717.

7 A. Buguin, M.-H. Li, P. Silberzan, B. Ladoux and P. Keller, *J. Am. Chem. Soc.*, 2006, **128**, 1088.

8 H. Ringsdorf and R. Zentel, *Makromol. Chem.*, 1982, **183**, 1245.

9 C. Ohm, C. Serra and R. Zentel, *Adv. Mater.*, 2009, **21**, 4859.

10 E.-K. Fleischmann, H.-L. Liang, N. Kapernaum, F. Giesselmann, J. Lagerwall and R. Zentel, *Nat Commun.*, 2012, **3**, 1178.

11 C. Ohm, N. Haberkorn, P. Theato and R. Zentel, *Small*, 2011, **7**, 194.

12 H. Yang, G. Ye, X. Wang and P. Keller, *Soft Matter*, 2011, **7**, 815.

13 a) J. Naciri, A. Srinivasan, H. Jeon, N. Nikolov, P. Keller and B. R. Ratna, *Macromolecules*, 2003, **36**, 8499. b) P. Beyer, L. Braun and R. Zentel, *Macromol. Chem. Phys.*, 2007, **208**, 2439.

14 A. Greiner and J. H. Wendorff, *Angew. Chem. Int. Ed.*, 2007, **46**, 5670.

15 a) J. P. Canejo, J. P. Borges, M. H. Godinho, P. Brogueira, P. I. C. Teixeira and E. M. Terentjev, *Adv. Mater.*, 2008, **20**, 4821. b) K. Nakashima, K. Tsuboi, H. Matsumoto, R. Ishige, M. Tokita, J. Watanabe and A. Tanioka, *Macromol. Rapid Commun.*, 2010, **31**, 1641.

16 S. Krause, R. Dersch, J. H. Wendorff and H. Finkelmann, *Macromol. Rapid Commun.*, 2007, **28**, 2062.

17 C. Ohm, M. Morys, F. R. Forst, L. Braun, A. Eremin, C. Serra, R. Stannarius and R. Zentel, *Soft Matter*, 2011, **7**, 3730.

18 R. Stannarius, A. Eremin, K. Harth, M. Morys, A. DeMiglio, C. Ohm and R. Zentel, *Soft Matter*, 2012, **8**, 1858.

19 E. Nishikawa, H. Finkelmann and H. R. Brand, *Macromol. Rapid Commun.*, 1997, **18**, 65.
20 D. L. Thomsen, P. Keller, J. Naciri, R. Pink, H. Jeon, D. Shenoy and B. R. Ratna, *Macromolecules*, 2001, **34**, 5868.
21 E.-K. Fleischmann, C. Ohm, C. Serra and R. Zentel, *Macromol. Chem. Phys.*, 2012, **213**, 1871.
22 P. Guillot, A. Colin, A. Utada and A. Ajdari, *Phys. Rev. Lett.*, 2007, **99,** 104502.
23 A. S. Utada, A. Fernandez-Nieves, H. A. Stone and D. A. Weitz, *Phys. Rev. Lett.*, 2007, **99**, 94502.
24 C. Cramer, P. Fischer and E. J. Windhab, *Chem. Eng. Sci.*, 2004, **59**, 3045.
25 a) P. Martinoty, P. Stein, H. Finkelmann, H. Pleiner and H. R. Brand, *Eur. Phys. J. E*, 2004, **14**, 311. b) T. Pakula and R. Zentel, *Makromol. Chem.*, 1991, **192**, 2401. c) R. Zentel and J. Wu, *Makromol. Chem.*, 1986, **187**, 1727.
26 C. Ohm, E.-K. Fleischmann, I. Kraus, C. Serra and R. Zentel, *Adv. Funct. Mater.*, 2010, **20**, 4314.
27 Y. K. Chong, J. Krstina, T. P. T. Le, G. Moad, A. Postma, E. Rizzardo and S. H. Thang, *Macromolecules*, 2003, **36**, 2256.
28 S. V. Ahir, A. R. Tajbakhsh and E. M. Terentjev, *Adv. Funct. Mater.*, 2006, **16**, 556.

3.5 Microactuators from a main-chain liquid crystalline elastomer via thiol-ene "click" chemistry

Eva-Kristina Fleischmann, F. Romina Forst, Katrin Köder, Rudolf Zentel*

Institute of Organic Chemistry, Johannes Gutenberg-Universität Mainz, D-55099 Mainz, Germany

*Corresponding author: zentel@uni-mainz.de

Abstract

We present the preparation of micrometer-sized liquid crystalline elastomer (LCE) particles of the liquid crystalline main-chain type. The LCE particles are UV-crosslinked via thiol-ene click chemistry of the nematic monomer, carrying a terminal thiol and a terminal ene group, and isotropic tetrathiol and tetraene crosslinkers. The preparation of the LCE particles with a microfluidic device in a continuous "on the fly" technique allows their fast processing with irradiation times of less than 2 seconds. The resulting particles perform a temperature-driven shape change up to 25% upon the nematic-isotropic phase transition and the extent of the shape change can be controlled by adjustment of the microfluidic parameters. The reversibility of the shape change and the chemical durability of the thiol-ene network towards reducing agents demonstrate the usability of the LCE particles as soft microactuators.

3.5.1 Introduction

Liquid crystalline elastomers (LCEs) are known to exhibit reversible motion of much larger amplitude than classical quartz piezo-elements[1] which recommends them as soft actuators and sensors.[2] Their unique behavior is based on the anisotropic properties of the liquid crystalline components (mesogens) and the entropy elasticity of the elastomer network.[3] The directed macroscopic shape change of an LC elastomer is driven by the phase transition between the ordered LC phase and the random isotropic phase of the mesogens. Conceived by de Gennes[4], the concept of LCEs as actuators was realized by grafting vinyl-substituted mesogenic units to a siloxane polymer backbone via platinum-catalyzed addition.[5,6] The synthetic routes of forming LCEs have been extended since then and include polymerization of mesogenic acrylate[7] and methacrylate[8] monomers, hydroxyl group-containing LC polymer chains converted with bis-isocyanates[9], and click-chemistry between azide-terminated LC polymers and triacetylenes.[10] These methods allow different architectures of LCEs to be realized, with the mesogens being either part of the polymer backbone (main-chain elastomer) or laterally attached to it via flexible spacers. Due to the strong coupling between the mesogens and the polymer backbone, main-chain elastomers are very attractive as actuators. They are known to give the largest shape changes and contractions of up to 500% upon the phase transition have been reported.[11] Main-chain elastomers are commonly synthesized by poly-addition[12] and poly-condensation[13] reactions. The reaction times are relatively long and therefore unsuitable for our purposes, namely the fast processing of main-chain elastomers in a microfluidic device.

In recent years, however, thiol-ene click chemistry emerged as a convenient method to prepare linear polymers by sequential addition of a thiol group to a double bond.[14] Thiol-ene mediated polymerization could be adapted for LC chemistry by designing mesogens with terminal thiol and ene groups on the same molecule. These mesogens can be successfully polymerized to yield linear polymers exhibiting liquid crystalline phases.[15,16] To obtain an actuating LC elastomer the elastic modulus of the polymer network has to be on the order of several megapascals.[17] This was achieved by further converting the above described mesogenic monomers with a mesogenic dithiol-diene

crosslinker. The resulting main-chain elastomer actuators, prepared by replica molding, showed contractions of 400%.[18]

A crucial processing step for the preparation of actuating LCEs is the orientation of the mesogens along one common axis, termed the director. Only under the condition of uniform alignment do LCEs show a directed shape change. This orienttaion can be achieved by mechanical force[6], suitable surface alignments[19] or use of electric[20] or magnetic fields[21]. The increasing demand of active micromechanical devices promoted the development of new adaption techniques for micro- and nano-scaled LCE samples[22], which includes different templating methods[23], inkjet printing[24] and microfluidics[25]. Microfluidic techniques allow the production of monodisperse droplets by emulsification in a surrounding continuous phase.[26] and the shear flow inside the microtube induces the orientation of the mesogens inside the monomer droplets.[27] Polymer beads are then obtained by UV-initiated "on the fly" polymerization of monomer droplets.[28] The microfluidic technique allows the preparation of different LCE shapes, ranging from bulk particles[29] to fibers[30] and core-shell particles.[31].

We present the preparation of LCE microactuators from a thiol-ene main-chain-type monomer in a microfluidic device. The use of the thiol-ene reaction in microfluidics has to our knowledge only been used for the preparation of functionalized macroporous polymer beads with potential use in solid phase synthesis[32] and for the preparation of cell-laden microgels made from thiol-ene modified polyethyleneglycol (PEG) and hyperbranched polyglycerol (hPG) derivatives.[33] The macropourous polymer beads are formed via UV-initiated click chemistry with irradiation times lasting up to one hour, while the PEG/hPG microgel is formed in a thiol-Michael addition reaction requiring several minutes until reaching sufficient conversion. In this work we demonstrate that for the thiol-ene monomer and crosslinkers presented, a few seconds of UV irradiation are sufficient to polymerize and crosslink the monomer droplets. The orientation of the mesogens inside the monomer droplets, induced by the shear flow of the microfluidic tube, is locked during polymerization and the resulting LCE particles show a reversible shape change upon heating.

3.5.2 Results and Discussion

For a successful preparation of LCE microactuators with the microfluidic setup, the thiol-ene monomer should possess moderate transition temperatures and be suitable for UV-initiated radical polymerization. For our purposes we chose the thiol-ene monomer **LC1**, which has already been used for the fabrication of soft actuators.[18] The broad nematic phase between 59°C and 80°C facilitates its processing within the microfluidic device, which is temperature-controlled in a water bath. The liquid crystalline phase is relatively stable towards non-mesogenic impurities, which allows isotropic crosslinkers without an LC phase to be used.[7,34] We chose the commercially available crosslinkers pentaerythritol tetrakis(3-mercaptopropionate) (PETMP) and glyoxal bis(diallyl acetal) (GBDA). Both have a functionality of four and are expected to rapidly promote the formation of the elastomer, considering the short UV irradiation times of only a few seconds within the microfluidic device. The structural formulas of monomer and crosslinkers are depicted in Figure 1a.

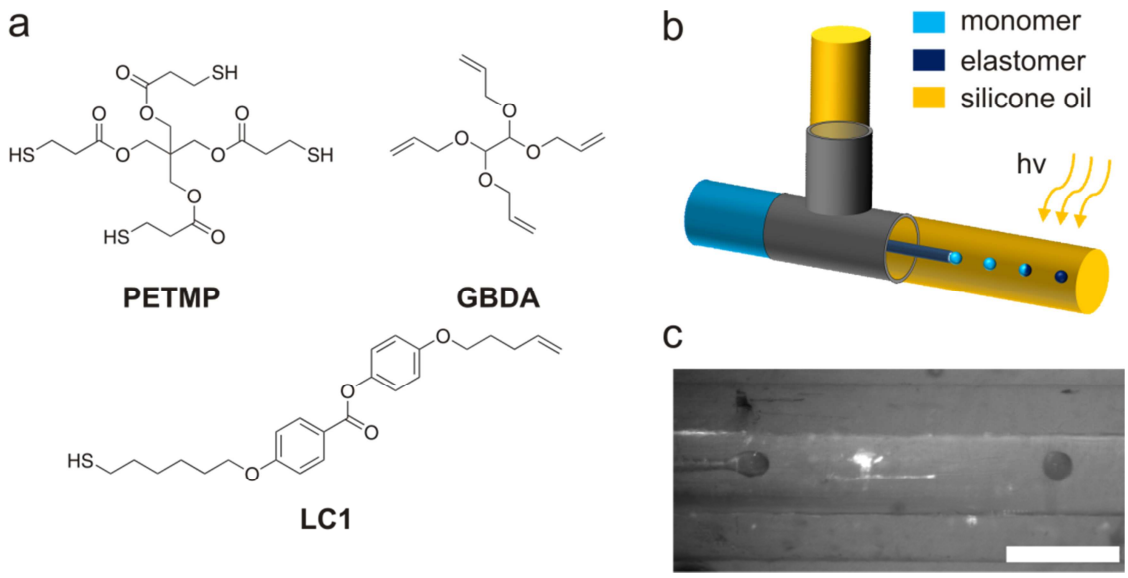

Figure 1. a *Chemical structure of the thiol-ene crosslinkers pentaerythritol tetrakis(3-mercaptopropionate) (PETMP), glyoxal bis(diallyl acetal) (GBDA) and the liquid crystalline monomer* ***LC1****. **b** Scheme and **c** live image of the droplet formation inside the microfluidic device (scale bar 1000 µm).*

A mixture of monomer **LC1**, crosslinkers PETMP and GBDA and photoinitiator Lucirin TPO was prepared and filled into tubing connected to a T-junction (see Figures 1b and c). Droplets of the monomer mixture form at the capillary tip (orifice diameter 40 μm) and detach into the co-flowing silicone oil. Subjected to the shear flow within the microfluidic tubing, a preferred orientation of the mesogens is induced in the droplets. When permanently fixing the imposed orientation by UV-initiated polymerization, it is important to conduct the crosslinking within the nematic phase of the material. Otherwise the increasing viscosity at lower temperatures or the reduced order parameter at higher temperatures decreases the director alignment and thus reduces the actuation properties.[29] Since the phase transition temperatures of the monomer are expected to change in the presence of the non-mesogenic components[35], a mixture **M1** of 95 mol% **LC1**, 2.5 mol% PETMP, 2.5 mol% GBDA and 3 wt% photoinitator Lucirin TPO was prepared and the phase transition temperatures of the mixture were analyzed with a polarized light microscope equipped with a hot stage. We observed the expected decrease of the phase transition temperatures, with a nematic phase present on heating between 59°C (melting) and 80°C (isotropization) for the neat monomer and 38°C and 52°C for the mixture **M1** (Figure 2).

Interestingly, we did not observe a reappearance of the nematic phase when cooling the mixture from the isotropic melt, whereas the phase reappeared for the pure monomer. A potential rearrangement of the mesogens from a planar to a homeotropic alignment was ruled out by observation of the monomer mixture with a polarization microscope equipped with a Bertrand lens (conoscopy). Differential scanning calorimetry (DSC) did also not indicate a transition to a liquid crystalline phase on cooling. We assume that heating of the monomer mixture causes side-reactions, which lead to a mixture of "branched" structures from the crosslinkers. Even at a scarce amount, these impurities may inhibit the reappearance of the liquid crystalline phase on cooling. Additional experiments on the phase behavior of the monomer mixture are presented in the Supplementary Information.

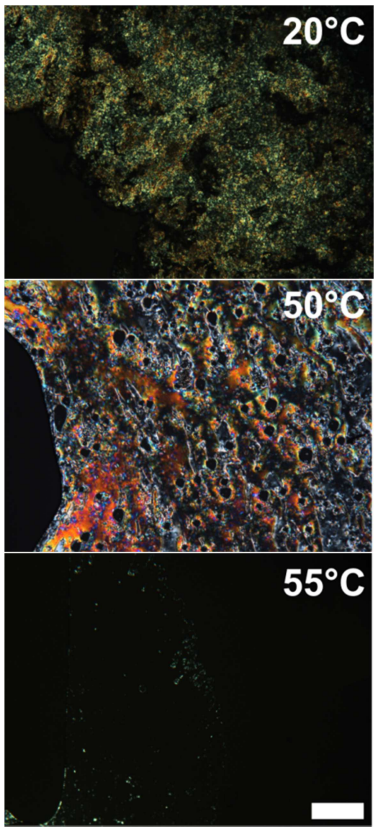

Figure 2. *Polarizing microscopy images taken from the mixture* ***M1*** *(95 mol%* ***LC1****, 2.5 mol% PETMP, 2.5 mol% GBDA and 3 wt.% Lucitin TPO). A nematic liquid crystalline phase is observed between 38°C and 52°C. The scale bar corresponds to 100 μm.*

Due to the absence of a liquid crystalline phase upon cooling, the mixture should not be heated above its clearing temperature during its preparation and processing in the microfluidic device, to avoid the risk of losing the nematic order while polymerizing. Because of the higher viscosity of the nematic phase compared to the isotropic melt, it proved impossible to handle the neat monomer mixture in its nematic state inside the microfluidic device, since it would clog the thin glass capillary (diameter 100 μm). We addressed the problem by adding a solvent to the monomer mixture. The solvent reduces the viscosity of the mixture to allow droplet formation in the isotropic state and subsequently diffuses into the surrounding silicone oil. We chose chlorobenzene due to its high boiling point of 131°C and its miscibility with silicone oil. Preliminary test showed, that the addition of 10 wt.% chlorobenzene to the mixture did not lower the viscosity enough for an easy handling, while 20 wt.% chlorobenzene made the mixture too runny for a stable droplet formation. Diluted with 15 wt.% chlorobenzene, however,

droplets from the monomer mixture could be produced at a temperature of T_1 = 45°C. We monitored the droplet formation with a stereo microscope and observed that the chlorobenzene quickly diffuses into the silicone oil. Shortly after detachment from the capillary tip, the size of the droplets decreases slightly due to the loss of chlorobenzene. Concomitantly, the contrast of the droplets increases, indicating that the diluted monomer mixture becomes nematic again.

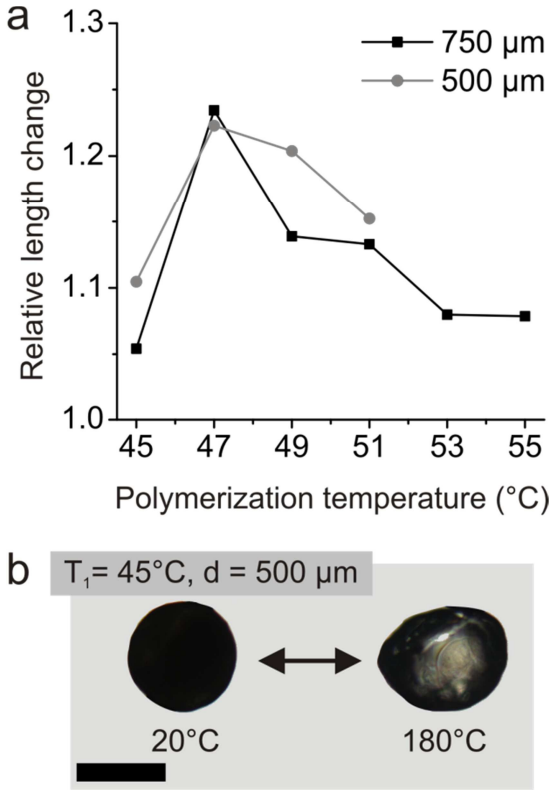

Figure 3. a *The actuation properties of the LCE particles strongly depend on T_2, the polymerization temperature of the droplets. Maximal shape changes are observed at T_2 = 47°C. Decreasing the diameter of the polymerization tube from 750 µm to 500 µm leads to an increased relative shape change.* ***b*** *LCE particles formed at T_1 = 45°C and polymerized at T_2 = 47°C, within the nematic phase of the mixture* ***M1,*** *exhibit the most pronounced shape changes. The scale bar corresponds to 200 µm.*

Induced by the microtubular shear flow, the director pattern within the droplets was permanently fixed by UV initiated polymerization. With the chosen microfluidic parameters (see Experimental Section) the "on the fly" fabrication process allowed only 1.9 s (for the 500 µm-tube) and 4.2 s (for the 750 µm-tube) for a successful thiol-ene crosslinking reaction. Swelling experiments verify, however, that the polymerization was successful. LC-elastomer particles were swollen in chloroform and did not dissolve over

several days. Mechanical measurements of the particles are presented below and also demonstrate the formation of a well crosslinked elastomer network.

Since the degree of nematic order during crosslinking influences the actuation properties of the LCE particles, we varied the polymerization temperature (T_2) between 45°C and 55°C in steps of 2°C. We kept the flow rates constant at 0.06 mL/h for the monomer phase and 1.50 mL/h for the silicone oil in a polymerization tube with an inner diameter of 750 μm to ensure the results to be comparable. 20 particles from every batch of LCE actuators were evaluated by light microscopy. The particles were of spherical shape at room temperature with an aspect ratio of 1.00 (± 1%). Heating the particles to 180°C, well above the nematic-isotropic transition temperature, results in a shape change for all particles. We plotted the relative length change (aspect ratio at 180°C/aspect ratio at 20°C) in dependence of the polymerization temperature T_2 in Figure 3a. While the relative length change at T_2 = 45°C is only 5%, it reaches a maximum of 23% at T_2 = 47°C (see black graph in Figure 3a). Further increasing the polymerization temperature leads to a gradual decline of the extent of actuation. At 55°C, the actuation subsides to 8%. This is in accordance with previous results, which demonstrated that two effects lower the induced orientation: An increased viscosity at low temperatures and a low order parameter close to the isotropic phase.[29] The results demonstrate that actuating LC-elastomer particles of the main chain type can be prepared with a microfluidic devices.

In order to obtain particles that actuate to a larger extent, we attempted to increase the shear flow within the microfluidic device by decreasing the inner diameter of the polymerization tube. Instead of 750 μm, a 500 μm-diameter tube was connected to the T-junction. As can be seen in Figure 3a (grey graph), higher shear rate enhances the relative length change of particles prepared at a given polymerization temperature. The maximum actuation is again observed at a polymerization temperature of 47°C. Further details on dimensions and actuation properties of the LCE particles can be found in the Supplementary Information.

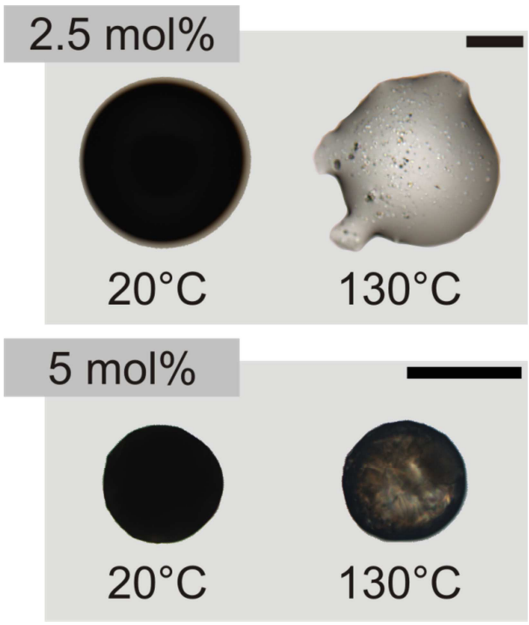

Figure 4. *Particles made with a total amount of 2.5 mol% crosslinker (1.25 mol% PETMP and 1.25 mol% GBDA) melt when heated to the isotropic phase. Increasing the crosslinker amount to 5 mol% (2.5 mol% PETMP and 2.5 mol% GBDA) results in dimensionally stable particles. The scale bars correspond to 200 μm.*

Besides the degree of confinement, the actuation of LCE particles can also be controlled by regulating the crosslinking density of the elastomer network.[36] A reduction of the crosslinker concentration may lead to a more pronounced shape change due to the reduced stiffness of the elastomer network. However this might come at the cost of losing the reversibility of the shape change. We prepared a monomer mixture **M2** with a reduced amount of 2.5 mol% crosslinker (1.25 mol% PETMP and 1.25 mol% GBDA). Particles were produced in the microfluidic device with flow rates of 0.02 mL/h for the monomer phase and 1.0 mL/h for the silicone oil. Due to the decreased amount of non-mesogenic components in the mixture, the phase transition temperatures for **M2** are slightly higher than for mixture **M1**. The operating temperatures were adjusted accordingly and set to T_1 = 50°C and T_2 = 52°C. As can be seen in Figure 4, the resulting particles are not dimensionally stable on heating, but melt at 130°C and form a liquid droplet of polymer. The amount of crosslinker in the mixture is not sufficient for the formation of an elastomer network. The margin between 2.5 mol% and 5 mol% crosslinker leaves, however, little scope for further adjustment of the crosslinker

concentration, ensuring a larger shape change while at the same time keeping the particles dimensionally stable and the shape change fully reversible.

Microactuators made from a comparable thiol-ene elastomer exhibited contractions of up to 400%.[18] In this case, the uniform director configuration was achieved by the cooperative effect of spatial confinement and the application of a magnetic field and the monomer was slowly polymerized without flow. Our elastomer particles, oriented by the shear flow in the microfluidic capillary, showed a less pronounced change of shape. We assume that this is a direct result from the fabrication process in the microfluidic setup, where the induced orientation in a mixture of LC monomer and oligomers is locked by subsequent crosslinking. As demonstrated in previous works, the orientation of the mesogens, and hence the quality of director alignment determines the magnitude of actuation. The director configuration is highly dependent on the flow conditions in the microfluidic setup[27] and both bipolar and concentric configurations can be obtained.[27,31] This makes it possible to obtain LC-elastomer particles from the same monomer mixture which either expand, contract or hardly actuate at all, just by changing the parameters of the microfluidic device.[27,29] Since the poly-addition kinetics of the thiol-ene polymerization is different from vinyl-polymerization it is possible that an "intermediate" alignment occurs, which explains the smaller shape change observed for our main-chain elastomer particles. In this manuscript we focus on establishing the fabrication process of thiol-ene microactuators. Further evaluation of the orientational order of the director and the polymerization kinetics of the thiol-ene elastomer will be addressed in more detail in another essay. We performed, however, preliminary analyses of the monomer conversion and the polymerization degree by GPC measurements. These results are presented in the Supporting Information.

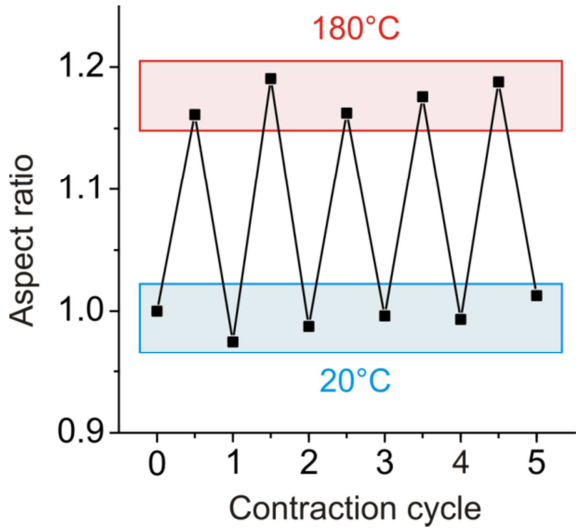

Figure 5. *Contraction recovery cycle of a LCE particle made with the following parameters: droplet formation at T_1 = 45°C, polymerization temperature at T_2 = 47°C within a 500 µm polymerization tube. The particle was repeatedly heated to 180°C and cooled back to room temperature and exhibited an overall reversible shape change.*

When used as part of an active device, for example in lab-on-chip or micro(electro)mechanical systems, an important quality for microactuators, besides the degree of actuation, is their mechanical robustness and reversibility of their actuation. We studied the robustness of the thermo-mechanical response of the thiol-ene elastomer particles, polymerized with a total amount of 5 wt.% crosslinker, by conducting heating and cooling cycles between 20°C and 180°C. Figure 5 shows the contraction-recovery behavior of a microactuator, an LCE particle polymerized at T_2 = 47°C in a 500 µm tube. The response of the particle to the repeated changes in temperature remains nearly constant, with an average aspect ratio at room temperature (non-actuated state) of 0.99 (± 1%) and 1.18 (± 1%) in the actuated state at 180°C. The standard deviation of ± 1% for both aspect ratios confirms the reproducibility of the shape change for this type of microactuators.

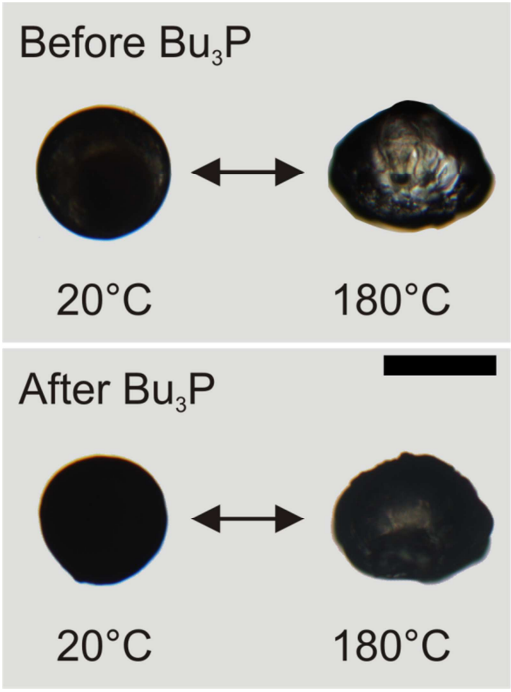

Figure 6. *LCE particles were swollen in tributylphosphine Bu_3P for 24 h. Shape and actuation properties remain unchanged after the treatment, indicating that crosslinking is achieved by "click chemistry" between thiol and ene groups, with only marginal formation of disulfide bonding between two thiol groups. The scale bar corresponds to 200 μm.*

Another desirable property of microactuators is chemical durability. A common and competing side reaction in thiol-ene chemistry is the formation of disulfide bonds by thiyl-thiyl radical coupling.[37] Such disulfide bonds are easily cleavable with an reducing agent. As part of the elastomer network, however, reduction of the disulfide bonds would reduce the number of crosslinking points in the network. Consequently this would lead to a degradation of the elastomer and negatively affect the shape changing properties of the microactuators, since a reduced crosslinking density deteriorates the reversibility of the shape change. In order to examine the robustness of the elastomer network, we treated three LCE particles (polymerized at T_2 = 47°C in a 500 μm tube) with tributylphosphine Bu_3P (see Figure 6). Before treatment, the particles' aspect ratios at room temperature abd at 180°C were determined as 1.02 (± 1%) and 1.22 (± 5%), respectively. This corresponds to a relative length change of 1.21 (± 6%). The particles were then swollen in tributylphosphine under oxygen exclusion for 24 hours. After this treatment the aspect ratio was found to be 0.99 (± 1%) at room temperature and 1.22 (± 2%) in the isotropic phase at 180°C. The relative length change slightly increased to 1.23

(± 3%). While the aspect ratio at 180°C remains constant before and after the treatment with tributylphosphine, the aspect ratio at room temperature slighty decreases by 3%. This might be due to an incomplete conversion of the monomer in the short UV-mediated polymerization. Unreacted monomer might be washed out when the particle is swollen in tributylphosphine. We attempted to characterize the quality of the crosslinking by swelling the particles in chloroform. However, due to the small size of the particles and as a consequence thereof, their low weight (between 1-2 mg) gravimetric analysis gave insignificant results within the error margin. Since shape and actuation properties remain unchanged after the treatment with tributlyphophine, crosslinking is primarily achieved by "click chemistry" between thiol and ene groups, with only marginal formation of disulfide bonding between two thiol moieties.

3.5.3 Experimental Section

Materials and reagents

Silicone oil (100 cSt and 1000 cSt), dichloromethane, photoinitiator Lucirin TPO (2,4,6-trimethylbenzoyldiphenylphosphine oxide), pentaerythritol tetrakis(3-mercaptopropionate) (PETMP) and glyoxal bis(diallyl acetal) (GBDA) were purchased from Sigma-Aldrich. Tri-*n*-butylphosphine (95%) and chlorobenzene (99%) were purchased from Acros Organics. The liquid crystalline monomer **LC1** (4-(4-pentenyloxy)phenyl 4-(6-mercaptohexyloxy)-benzoate) was synthesized according to the literature.[16,18] Components for the microfluidic device were obtained from Postnova Analytics GmbH (fused silica capillary, T-junction, nuts and ferrules) and WICOM (PTFE tubings). The tapered glass capillary was prepared with a micropipette puller (Sutter Instrument P97, USA) and cut to an orifice diameter of 40 μm with a microforge (Narishige MF830, Japan)

Processing in the microfluidic device

The monomer mixture used in the microfluidic setup was prepared by mixing the monomer **LC1**, the crosslinkers PETMP and GBDA and 3 wt% photoinitiator Lucirin

TPO in dichloromethane. After evaporation of the solvent, 15 wt.% of chlorobenzene were added to adjust the viscosity of the mixture, which was then heated to 45 °C and filled into a PTFE tube (ID 1.59 mm). The tube was mounted between two PTFE tubes (OD 1.59 mm). One tube was filled with silicone oil (100 cSt) and connected to the syringe pump (Harvard 33), the second tube was connected to a T-junction. The monomer phase was pumped through a fused silica capillary (ID: 100 μm, OD: 165 μm, tip orifice: 40 μm) leading into the polymerization tube (PTFE tube, ID: 500 μm and 750 μm, respectively). The continuous phase silicone oil (1000 cSt) was injected into the T-junction through the second inlet. Droplets were formed at the capillary tip at a constant temperature of 45 °C, while the polymerization was conducted at varying temperatures. Initiation of the polymerization was done with a LOT Oriel LSH302 500 W UV lamp equipped with a 365 nm line filter and a waveguide. The diameter of the waveguides' light beam was 4 mm.

Characterization

The formation of monomer droplets within the microfluidic device was observed with a Zeiss stereo microscope Stemi 2000-C equipped with an Olympus XM10 camera. For optical characterizations, the light microscope Olympus BX51 equipped with a hot-stage (Linkam TMS 94) and a camera (Olympus ColorView II) was used. The actuation properties were evaluated with the imaging software Cell^D. Differential scanning calorimetry (DSC) measurements were carried out on a Perkin-Elmer DSC 7 calibrated with lead and indium standards with heating/cooling rates of 10 °C min^{-1}. The molecular weight of non-crosslinked particles and of the sol content of crosslinked particles was determined by gel permeation chromatography (GPC) in THF with polystyrene as external standard.

3.5.4 Conclusion

Concluding, we showed that the microfluidic technique is a versatile tool not only for processing acrylate and methacrylate monomers, but also for monomers which react in a thiol-ene click mechanism to form an elastomer network. By choosing a

thermotropic liquid crystalline monomer, the resulting elastomer particles exhibit a temperature-driven change of shape. The LCE microparticles presented here are comprised of a thiol-ene monomer and tetra-functional thiol- and ene-crosslinkers. The monomer droplets generated within the microfluidic device are exposed to the shear flow of the surrounding co-flowing silicone oil. The induced orientation of the LC mesogen within the droplet is frozen by the thiol-ene click reaction between monomer and crosslinkers and initiated by UV-irradiation. With irradiation times of less than 2 seconds, the conversion is sufficient for the formation of an elastomer network, which exhibits a fully reversible contraction upon heating. Furthermore we could tune the extent of the shape change by controlling the temperature during polymerization and by varying the degree of confinement inside the microfluidic device. Main-chain LCE actuators are known to contract strongly on losing their liquid crystalline order and we are confident that the here reported values for the shape changes can be considerably increased by further optimizing the preparation parameters.

Acknowledgements

We thank Maria Müller for the DSC measurement and Hsin-Ling Liang for the preparation of the tapered glass capillaries. This work was financially supported by the Deutsche Forschungsgemeinschaft (DFG: Ze 230/19).

3.5.5 References

1 J. H. Wendorff, *Angew. Chem. Int. Ed. Engl.*, 1991, **30**, 405.

2 a) R. Zentel, *Angew. Chem.*, 1989, **101**, 1437–1445. b) Y. Yu and T. Ikeda, *Angew. Chem. Int. Ed.*, 2006, **45**, 5416. c) C. Ohm, M. Brehmer and R. Zentel, *Adv. Mater.*, 2010, **22**, 3366.

3 a) E. M. Terentjev, *J. Phys.: Condens. Matter*, 1999, **11**, R239. b) H. R. Brand and H. Finkelmann, *Handbook of Liquid Crystals*, Wiley-VCH, Weinheim, Germany, 1998.

4 a) P.-G. de Gennes, *C. R. Acad. Sci. Paris, Ser. B*, 1975, **281**, 101. b) P.-G. de Gennes, *C. R. Acad. Sci. II B*, 1997, **324**, 343.

5 H. Finkelmann and G. Rehage, *Makromol. Chem., Rapid Commun.*, 1980, **1**, 31.

6 J. Küpfer and H. Finkelmann, *Makromol. Chem., Rapid Commun.*, 1991, **12**, 717.

7 D. L. Thomsen, P. Keller, J. Naciri, R. Pink, H. Jeon, D. Shenoy and B. R. Ratna, *Macromolecules*, 2001, **34**, 5868.

8 M.-H. Li, P. Auroy and P. Keller, *Liq. Cryst.*, 2000, **27**, 1497.

9 a) R. Zentel and M. Benalia, *Makromol. Chem.*, 1987, **188**, 665. b) J. Naciri, A. Srinivasan, H. Jeon, N. Nikolov, P. Keller and B. R. Ratna, *Macromolecules*, 2003, **36**, 8499.

10 Y. Xia, R. Verduzco, R. H. Grubbs and J. A. Kornfield, *J. Am. Chem. Soc.*, 2008, **130**, 1735.

11 S. V. Ahir, A. R. Tajbakhsh and E. M. Terentjev, *Adv. Funct. Mater.*, 2006, **16**, 556.

12 a) G. H. F. Bergmann, H. Finkelmann, V. Percec and M. Zhao, *Macromol. Rapid Commun.*, 1997, **18**, 353. b) I. A. Rousseau and P. T. Mather, *J. Am. Chem. Soc.*, 2003, **125**, 15300.

13 a) K.-H. Hanus, W. Pechhold, F. Soergel, B. Stoll and R. Zentel, *Colloid Polym. Sci.*, 1990, **268**, 222. b) C. Ortiz, M. Wagner, N. Bhargava, C. K. Ober and E. J. Kramer, *Macromolecules*, 1998, **31**, 8531. c) P. Beyer, L. Braun and R. Zentel, *Macromol. Chem. Phys.*, 2007, **208**, 2439.

14 a) C. E. Hoyle and C. N. Bowman, *Angew. Chem. Int. Ed.*, 2010, **49**, 1540. b) C. E. Hoyle, T. Y. Lee and T. Roper, *J. Polym. Sci. A Polym. Chem.*, 2004, **42**, 5301.

15 a) J. Lub, D. J. Broer and N. van den Broek, *Liebigs Ann./Recl.*, 1997, **1997**, 2281. b) J. Lub, D. J. Broer, M. E. M. Antonio and G. N. Mol, *Liq. Cryst.*, 1998, **24**, 375. c) H. T. A. Wilderbeek, J. G. P. Goossens, C. W. M. Bastiaansen and D. J. Broer, *Macromolecules*, 2002, **35**, 8962. d) H. T. A. Wilderbeek, M. G. M. van der Meer, C. W. M. Bastiaansen and D. J. Broer, *J. Phys. Chem. B*, 2002, **106**, 12874. e) H. Yang, L. Wang, R. Shao, N. A. Clark, J. Ortega, J. Etxebarria, P.-A. Albouy, D. M. Walba and P. Keller, *J. Mater. Chem*, 2009, **19**, 7208. f) H. Yang, J. M. Richardson, D. M. Walba, C. Zhu, R. Shao, N. A. Clark, J. Ortega, J. Etxebarria and P. Keller, *Liq. Cryst.*, 2010, **37**, 325.

16 H. T. A. Wilderbeek, M. G. M. van der Meer, M. A. G. Jansen, L. Nelissen, H. R. Fischer, J. J. G. S. van Es, C. W. M. Bastiaansen, J. Lub and D. J. Broer, *Liquid Crystals*, 2003, **30**, 93.

17 a) R. Zentel and J. Wu, *Makromol. Chem.*, 1986, **187**, 1727. b) P. Martinoty, P. Stein, H. Finkelmann, H. Pleiner and H. R. Brand, *Eur. Phys. J. E*, 2004, **14**, 311.

18 H. Yang, A. Buguin, J.-M. Taulemesse, K. Kaneko, S. Méry, A. Bergeret and P. Keller, *J. Am. Chem. Soc*, 2009, **131**, 15000.

19 T. Ikeda, M. Nakano, Y. Yu, O. Tsutsumi and A. Kanazawa, *Adv. Mater.*, 2003, **15**, 201.

20 H. Ringsdorf and R. Zentel, *Makromol. Chem.*, 1982, **183**, 1245.

21 M.-H. Li, P. Keller, J. Yang and P.-A. Albouy, *Adv. Mater.*, 2004, **16**, 1922.

22 H. Yang, G. Ye, X. Wang and P. Keller, *Soft Matter*, 2011, **7**, 815.

23 a) A. Buguin, M.-H. Li, P. Silberzan, B. Ladoux and P. Keller, *J. Am. Chem. Soc.*, 2006, **128**, 1088. b) C. Ohm, N. Haberkorn, P. Theato and R. Zentel, *Small*, 2011, **7**, 194.

24 C. L. van Oosten, C. W. M. Bastiaansen and D. J. Broer, *Nat. Mater.*, 2009, **8**, 677.

25 C. Ohm, C. Serra and R. Zentel, *Adv. Mater.*, 2009, **21**, 4859.

26 A. S. Utada, L.-Y. Chu, A. Fernandez-Nieves, D. R. Link, C. Holtze and D. A. Weitz, *MRS Bull.*, 2007, **32**, 702.

27 C. Ohm, N. Kapernaum, D. Nonnenmacher, F. Giesselmann, C. Serra and R. Zentel, *J. Am. Chem. Soc.*, 2011, **133**, 5305.

28 M. Bouquey, C. Serra, N. Berton, L. Prat and G. Hadziioannou, *Chem. Eng. J.*, 2008, **135**, S93.

29 C. Ohm, E.-K. Fleischmann, I. Kraus, C. Serra and R. Zentel, *Adv. Funct. Mater.*, 2010, **20**, 4314.

30 C. Ohm, M. Morys, F. R. Forst, L. Braun, A. Eremin, C. Serra, R. Stannarius and R. Zentel, *Soft Matter*, 2011, **7**, 3730.

31 E.-K. Fleischmann, H.-L. Liang, N. Kapernaum, F. Giesselmann, J. Lagerwall and R. Zentel, *Nat Commun*, 2012, **3**, 1178.

32 R. A. Prasath, M. T. Gokmen, P. Espeel and F. E. Du Prez, *Polym. Chem*, 2010, **1**, 685.

33 T. Rossow, J. A. Heyman, A. J. Ehrlicher, A. Langhoff, D. A. Weitz, R. Haag and S. Seiffert, *J. Am. Chem. Soc*, 2012, **134**, 4983.

34 T. Ikeda, M. Nakano, Y. Yu, O. Tsutsumi and A. Kanazawa, *Adv. Mater.*, 2003, **15**, 201.

35 R. A. Vora and S. J. Rajput, *Mol. Cryst. Liquid Cryst.*, 1991, **209**, 265.

36 E.-K. Fleischmann, C. Ohm, C. Serra and R. Zentel, *Macromol. Chem. Phys.*, 2012, **213**, 1871.

37 S. P. S. Koo, M. M. Stamenović, R. A. Prasath, A. J. Inglis, F. E. Du Prez, C. Barner-Kowollik, W. van Camp and T. Junkers, *J. Polym. Sci. A Polym. Chem.*, 2010, **48**, 1699.

3.5.6 Supplementary Information

Table S1. *Dimensions and actuation properties of the LCE particles prepared in a 750 µm polymerization tube.*

Droplet formation	Polymerization temperature	Particle diameter / µm	Aspect ratio at 20°C	Aspect ratio at 180°C	Relative length change
45°C	**45°C**	284 (± 6%)	1.00 (± 3%)	1.05 (± 4%)	1.05 (± 5%)
45°C	**47°C**	200 (± 2%)	0.99 (± 2%)	1.23 (± 5%)	1.23 (± 6%)
45°C	**49°C**	166 (± 6%)	0.99 (± 3%)	1.13 (± 9%)	1.14 (± 10%)
45°C	**51°C**	170 (± 4%)	1.00 (± 1%)	1.13 (± 9%)	1.13 (± 9%)
45°C	**53°C**	136 (± 4%)	1.01 (± 3%)	1.09 (± 6%)	1.08 (± 6%)
45°C	**55°C**	133 (± 5%)	1.01 (± 4%)	1.09 (± 6%)	1.08 (± 7%)
70°C	**47°C**	308 (± 3%)	1.02 (± 3%)	1.04 (± 2%)	1.01 (± 4%)

Table S2. *Dimensions and actuation properties of the LCE particles prepared in a 500 µm polymerization tube.*

Droplet formation	Polymerization temperature	Particle diameter / µm	Aspect ratio at 20°C	Aspect ratio at 180°C	Relative length change
45°C	**45°C**	130 (± 8%)	1.01 (± 2%)	1.11 (± 8%)	1.10 (± 9%)
45°C	**47°C**	232 (± 4%)	1.00 (± 2%)	1.22 (± 5%)	1.22 (± 6%)
45°C	**49°C**	242 (± 3%)	0.98 (± 2%)	1.18 (± 6%)	1.20 (± 6%)
45°C	**51°C**	121 (± 2%)	1.00 (± 2%)	1.15 (± 7%)	1.15 (± 7%)

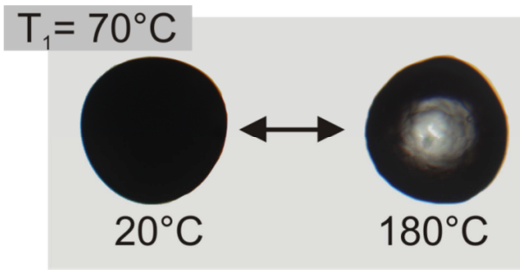

Figure S3. *Droplet formation in the isotropic phase (70°C) and its effect on the actuation behavior of the elastomer particles.*

To support our observation of a non-existent nematic phase on cooling, we prepared particles from the monomer mixture **M1** (95 mol% LC1, 2.5 mol% PETMP, 2.5 mol% GBDA and 3 wt% photoinitator Lucirin TPO). The droplet formation was conducted in the isotropic melt at T_1 = 70°C and followed by photo-polymerization of the droplets at T_2 = 47°C, well within the temperature region where a nematic phase was observed upon heating. The flow rates of the microfluidic device were set to 0.06 mL/h for the monomer phase and 1.5 mL/h for the silicone oil. The resulting elastomer particles were of spherical shape with an aspect ratio of 1.02 (± 3%) at room temperature. If the particles' mesogens were oriented along one common axis, heating the LC elastomer to its isotropic phase would result in a change of shape. When heating the particles to 180°C – well within the isotropic phase of the elastomer – the aspect ratio changes to 1.04 (± 2%) without any directed change of shape (see Figure 3 below). This confirms that the mixture was still in its isotropic phase and the mesogens randomly oriented while crosslinking. The scale bar corresponds to 200 μm.

Supplementary Discussion S4. S*tandard deviation of the particles' aspect ratios at varying temperatures.*

We note that while the standard deviation for the particles' aspect ratios at room temperature is ± 1-3%, the value increases to ± 4-9% for aspect ratios measured at 180°C. The higher uncertainty values at 180°C are mainly due to the fact that the spherical shape of the particles at room temperature makes it difficult to predict the direction of actuation. When heating the particles to their isotropic state, the shape change is not necessarily along an even plane but can be tilted towards the viewing angle. The extent of actuation in the latter direction remains unnoted. This does not only lead to an increase of the standard deviation but also causes the aspect ratio to be slightly underestimated. The values for the relative shape change given here can therefore be seen as a lower threshold of the particles' actuation.

Supplementary Discussion S5. *Degree of polymerization and sol-content of the elastomer particles.*

The degree of polymerization of the thiol-ene polymer was determined by preparation of non-crosslinked LC particles in the microfluidic device. To accommodate for the omitted crosslinkers, the amount of solvent chlorobenzene had to be increased to 17.5 wt.%. Processed with standard parameters, the monomer droplets were irradiated with UV light for several seconds. The number average molecular weight of the resulting polymer particles is 3400 g/mol, corresponding to a degree of polymerization of 8, as determined by gel permeation chromatography (GPC) in THF.

Crosslinked particles (parameters: T_1 = 45°C; T_2 = 47°C, d = 500 μm) were swollen in THF for 18 h and the excess solvent analyzed by GPC. Polymeric traces with a number average of 6400 g/mol were detected (degree of polymerization = 15), indicating that some fragments are not covalently bound to the LC elastomer. The conversion of the polymerization and crosslinking reactions are, however, sufficient for the formation of elastomer particles which exhibit a fully reversible actuation.

4 Conclusion

Today's advanced technology depends more and more on micro- and nanometer-sized components. As a result, new fabrication techniques have to be developed for the preparation of components that can act as sensors, controls or actuators. In this context, liquid crystalline elastomers have emerged as an interesting class of soft materials. They react upon an external stimulus with a macroscopic motion and can be used as actuators. Methods for the preparation of macro-sized LCEs have been established for quite some time, but processing of micrometer-sized LCEs remains challenging. This thesis demonstrates that microfluidic devices are versatile tools for the preparation of microactuators made from liquid crystalline elastomers. The liquid crystalline precursors are injected through a capillary into a co-flowing medium. The shear flow induces a uniform orientation of the liquid crystalline moieties, which is then locked up by photo-crosslinking to yield the LC elastomer.

The thiol-ene "click" reaction was used for the polymerization and crosslinking of a main-chain elastomer in the microfluidic setup (**Chapter 3.5**). Even with short UV-irradiation times, the conversion was sufficient for the production of microactuators, which exhibited a fully reversible contraction upon heating. The shape change of these particles could be controlled by adjusting the temperature and the confinement during the crosslinking step. The thermo-mechanical response of the particles underlines their feasibility as microactuating components.

The crosslinking density provides another means to influence the properties of LCE microactuators. Liquid crystalline side-chain polymers were synthesized with an adjustable amount of crosslinkable moieties. In combination with a side-chain monomer, LCE microparticles were prepared with emphasis either on strong actuation (low crosslinking density) or mechanical robustness (high crosslinking density). The liquid crystalline polymer crosslinker further stabilized the nematic phase of the monomer, which simplified the preparation process and allowed the isothermal fabrication of microactuators in the microfluidic setup (**Chapter 3.3**).

By judicious modifications of the microfluidic parameters, the design of the LCE actuators can be altered from bulk particles to LCE fibers (**Chapter 3.4**). Fibers become accessible, when the hydrophobic continuous phase PDMS is replaced with a hydrophilic silicone fluid. The change in polarity obviously lowers the interfacial tension between the dispersed liquid crystalline phase and the ambient fluid. This effect favors the extrusion of a jet at the capillary tip against the formation of droplets. The jet, consisting of a solution of crosslinkable side-chain polymers **CrP**, can be photo-crosslinked to yield LCE fibers. Depending on their crosslinking density, these fibers exhibit volume contractions of several hundred percent.

Technically the most sophisticated setup presented in this thesis, a microfluidic double emulsion process allowed the preparation of actuating LC core-shell particles (**Chapters 3.1 and 3.2**). In this process, a liquid core of glycerol was encapsulated by a shell of an LC side-chain monomer. Dispersed in a continuous phase of silicone oil, the LC shell was photo-polymerized to yield the corresponding elastomer. WAXS analyses of the elastomer shell revealed a bipolar orientation of the director, which resulted in a temperature-driven shape change upon the nematic-isotropic phase transition. Pierced with a thin capillary, the temperature-induced deformation of the elastomer shell lead to a reversible change of the volume of the core, causing the liquid to be reversibly expelled from and sucked into the particle. The core-shell particles have the potential to be integrated into a microfluidic system as micropumps for flow regulation that do not require additional components except passive channel connectors and a source of actuation.

In conclusion, the microfluidic setup allows the preparation of micrometer-sized LCE actuators with customized properties and design. The possibility to handle monomer as well as polymer precursors, to polymerize and crosslink monomers following as diverse polymerization mechanisms as (meth)acrylic chain and thiol-ene step reactions, and to change the actuators design by modification of the microfluidic parameters demonstrates the versatility of the fabrication method. Future advancements will certainly focus on the integration of the LCE microactuators into micromechanical devices. Here, the development of light-responsive microactuators in the microfluidic

setup will be of major importance, since the shape change for these actuators can be triggered without heating. Their preparation, however, presents a major challenge, since UV light cannot be used to initiate the polymerization reaction and other pathways for crosslinking have to be explored.

5 List of Publications

Publications in Peer-Reviewed Journals

- Liquid crystalline ordering as a concept in materials science: From semiconductors to stimuli-responsive devices

E.-K. Fleischmann, R. Zentel

Angew. Chem. Int. Ed. **2013**, *accepted*, DOI: 10.1002/anie.201300371

- Liquid crystalline elastomer fibers exhibiting ultralarge length contractions

E.-K. Fleischmann, F. R. Forst, R. Zentel

2013, *in preparation*

- Microactuators from a main-chain liquid crystalline elastomer via thiol-ene "click" chemistry

E.-K. Fleischmann, F. R. Forst, K. Köder, R. Zentel

J. Mater. Chem. C, **2013**, *under revision*

- One-piece micropumps from liquid crystalline core-shell particles

E.-K. Fleischmann‡, H.-L. Liang‡, N. Kapernaum, F. Giesselmann, J. Lagerwall, R. Zentel

Nat. Commun. **2012**, *3*, 1178

‡ These authors contributed equally.

- Preparation of soft microactuators in a continuous flow synthesis using a liquid-crystalline polymer crosslinker

E.-K. Fleischmann, C. Ohm, C. Serra, R. Zentel

Macromol. Chem. Phys. **2012**, *213*, 1871

- Towards micrometer sized core-shell actuators from liquid crystalline elastomers by a continuous flow synthesis

E.-K. Fleischmann‡, H.-L. Liang‡, J. Lagerwall, R. Zentel

Proc. of SPIE **2012**, *8279*, 82790M-1

‡ These authors contributed equally.

- Control of the properties of micrometer sized actuators from liquid crystalline elastomers prepared in a microfluidic setup

C. Ohm, **E.-K. Fleischmann**, I. Kraus, C. Serra, R. Zentel

Adv. Funct. Mater. 20, 4314 (2010)

Contributed Talks

- Towards micrometer sized core-shell actuators from liquid crystalline elastomers by a continuous flow synthesis (*Invited talk*)

SPIE Photonics West 2012

San Francisco, USA (2012)

- Designing LCE microactuators using microfluidics

24th International Liquid Crystal Conference

Mainz, Germany (2012)

- Core-shell actuators from liquid crystalline elastomers by a continuous flow synthesis

Materials Science and Engineering Congress

Darmstadt, Germany (2012)

Poster Contributions

- A flow-synthesis of microactuators from liquid crystalline elastomers

1st Frontiers in Polymer Science Symposium

Mainz, Germany (2009)

- Fabricating and designing micrometer sized actuators from liquid crystalline elastomers in a microfluidic device

38th Topical Meeting on Liquid Crystals

Mainz, Germany (2010)

- Liquid crystalline elastomers as stimuli-responsive microactuators

Winner of the Macro Award 2013 for Best Poster Presentation

Makromolekulares Kolloquium 2013

Freiburg im Breisgau, Germany (2013)

6 Acknowledgments

[redacted]

[redacted]